Natural Left-Handed Behavior and Electromagnetic Responses of Relativistic Quantum Gases

Daniel Medeiros Reis

PhD Thesis

Advisor:

Carlos Alberto Aragão de Carvalho Filho

Rio de Janeiro, RJ

2021

Daniel Medeiros Reis

Natural Left-Handed Behavior and Electromagnetic Responses of Relativistic Quantum Gases

PhD Thesis

Thesis submitted to the Graduate Program at the Centro Brasileiro de Pesquisas Físicas in partial fulfillment of the requirements for the degree of Doctor in Science (Physics).

Advisor:

Carlos Alberto Aragão de Carvalho Filho

Rio de Janeiro, RJ

2021

"NATURAL LEFT-HANDED BEHAVIOR AND ELECTROMAGNETIC RESPONSES OF RELATIVISTIC QUANTUM GASES"

DANIEL MEDEIROS REIS

Tese de Doutorado em Física apresentada no Centro Brasileiro de Pesquisas Físicas do Ministério da Ciência Tecnologia e Inovação. Fazendo parte da banca examinadora os seguintes professores:

Carlos Alberto Aragão de Carvalho Filho – Presidente/Orientador/CBPF

Carlos Farina de Souza

Carlos Farina de Souza - UFRJ

Eduardo Souza Fraga– UFRJ

José Abdala Helayel Neto - CBPF

Tobias Micklitz – CBPF

Rio de Janeiro, 06 de dezembro de 2021.

RESUMO

Nesta tese, calculamos as respostas eletromagnéticas de gases relativísticos de elétrons e de bósons e mostramos que a permissividade elétrica e permeabilidade magnética desses meios podem assumir valores simultaneamente negativos dentro de uma região de frequência limitada pelas frequências das oscilações coletivas de plasmon. A partir da lei de Snell, mostramos que, quando ambos ϵ e μ são negativos, os gases têm índice de refração $n = -1$. Esse comportamento ocorre em sistemas relativísticos, presentes em vários exemplos na física, como em estrelas compactas de nêutrons. Para o gás de bósons carregados, obtivemos estruturas tipo *rotons*, similares às que são observadas em um superfluido, na relação de dispersão do gás. Essa excitação de *rotons* surge apenas na fase condensada, desaparecendo para temperaturas acima da temperatura crítica de transição do condensado de Bose - Einstein. Também obtivemos correções à pressão, temperatura crítica e densidade de carga do condensado, causadas pela interação corrente-corrente induzida por flutuações quânticas eletromagnéticas tratadas via eletrodinâmica quântica escalar.

Palavras chave: Gás de eletrons relativístico; gás de bósons relativistico; índice de refração negativo; eletrodinâmica quântica

Abstract

In this thesis, we calculated the electromagnetic responses of relativistic gases of electrons and bosons, and showed that the electric permittivities and magnetic permeabilities can be simultaneously negative in a certain frequency region limited by the frequencies of collective oscillations of plasmon modes. From Snell's law, we showed that when both ϵ and μ are negative, the gases have index of refraction $n = -1$. This behavior will occur in relativistic systems, present in several examples in Physics, as in compact neutron stars. In addition, we obtained roton structures, similar to those in superfluid systems, in the dispersion relation of the charged relativistic Bose gas, which disappear above the critical temperature of Bose-Einstein condensation. We also obtained corrections for the pressure, critical temperature, and condensed charged density caused by the current-current interaction induced by electromagnetic quantum fluctuations treated via Scalar Quantum Electrodynamics.

Keywords: Relativististic electron gas; relativistic Bose gas; negative index of refraction; Quantum Electrodynamics

Agradecimentos

Sempre imaginei a pesquisa científica como uma grande partida de xadrez - os primeiros passos são sempre os mais difíceis pelas inúmeras possibilidades de atacar o problema, porém quando o jogo avança e toma sua forma, as coisas começam a tornar-se mais interessantes, as estratégias abordadas são mais objetivas, mas sacrifícios acabam sendo necessários para alcançar o xeque-mate. Quando o jogo é bem jogado, ao final da partida vemos que na verdade o jogo nunca acabou, apenas mudamos de tabuleiro para um muito maior, mais difícil e muito mais empolgante. Nesse grande xadrez da pesquisa científica, ninguém vence o jogo sozinho e por isso sinto-me na obrigação de oferecer meus profundos agradecimentos a todos os que se aventuraram nessa partida comigo.

Aos pilares da minha vida que são a minha família, *tal como as torres no xadrez, sempre na defensiva e decisivos no final do jogo*, apoiando-me em todas as minhas decisões: minha mãe Geni, meu pai Valfredo e meus irmãos Leandro e Tarcísio.

Ao meu orientador, Carlos Alberto Aragão de Carvalho Filho, ou simplesmente professor Aragão, agradeço imensamente pela confiança depositada em mim desde o início do doutorado, pelas inúmeras discussões e conselhos, tanto na vida acadêmica quanto na vida pessoal, que tiveram papel fundamental para o desenvolvimento desta tese, *tal como o cavalo no xadrez, pulando os obstáculos e abrindo o caminho para o pleno andamento do jogo.*

Para completar o grupo dos *quatro mosqueteiros*, agradeço ao prof. Ernesto Reyes-Gómez e ao prof. Luiz Oliveira, com sua motivação peculiar, que tiveram participação fundamental no resultado desta tese; à Daniela Szilard, que colaborou conosco e com quem pude aprender muitas coisas; e à profa. Solange Cavalcanti, cuja participação aos 45 do segundo tempo foi muito significativa. Por fim, ao professor Itzhak Roditi, que me recebeu no

CBPF e me apresentou ao prof. Aragão.

Não podendo também esquecer dos eternos companheiros da melhor sala do CBPF, a sala 515-D - Rubem, Francisco, Edher e Erick, e seus esporádicos visitantes, Saulo, Erich e Samir; certamente os cafés à tarde na sala e os eventuais chopps e caipirinhas fortaleceram essa amizade. Vocês tiveram imensa contribuição para que eu pudesse passar por todos os percalços da vida acadêmica.

Agradeço a Louyze, minha esposa, principalmente por toda a paciência nesse *trisal* (eu, ela e o doutorado), seu suporte ao meu lado em todos os momentos foi essencial na minha trajetória.

Para todos aqueles que estiveram envolvidos direta ou indiretamente, mas não foram citados, meus sinceros agradecimentos.

Por fim, agradeço às instituições que possibilitaram tal feito: o CBPF e a CAPES, pelo apoio financeiro.

And then one day you find

Ten years have got behind you

No one told you when to run

You missed the starting gun

– TIME, PINK FLOYD

List of Figures

Contents

Chapter 1

Introduction

1.1 The concept of metamaterial and historical remarks

The challenge of manipulating electromagnetic fields inside matter has led, over the years, to the pursuit and development of novel materials. A not-so distant example is that of photonic crystals, which consist of a periodic dieletric arrangement artificially manufactured to create a band structure that allows the propagation of electromagnetic waves in a specific frequency range [1]. Another example of customized internal structures of materials to obtain a specific electromagnetic response is given by the so-called *metamaterials*[1] .

The first mention of "*metamaterial*" appeared in the literature in the year 2000 [2], when it was demonstrated that a periodic array of conducting elements behaves as an effective medium for an electromagnetic wave whenever the wavelength is much longer than the lattice spacing. The propagating wave sees the periodic array as a continuum where the electromagnetic responses can be expressed in terms of effective parameters.

Such periodic arrays are made up of geometric arrangements of nanostructures called Split-Ring Resonators (SRR) [3, 4, 5], whose effective electric permittivity $\epsilon_{\text{eff}}(\omega)$ and magnetic permeability $\mu_{\text{eff}}(\omega)$ may assume values not observed in ordinary materials. A definition of metamaterial may be quite defying because of the wide range of applications involved. Originally, the concept applied to media with simultaneously negative permittivity

[1] The prefix *meta* ($\mu\epsilon\tau\alpha$ from Greek) means *beyond*

and permeability. Nowadays, however, it denotes artificially structured composite materials engineered to have desired responses to wave propagation. Indeed, besides electromagnetic metamaterials, there exist, for instance, acoustic ones, where sound (rather than electromagnetic) propagation is of interest [6].

Historically, the concept of electromagnetic metamaterial goes back to the work of Viktor Veselago [7], who described the electrodynamics of a hypothetical material with simultaneously negative values of electric permittivity ϵ and magnetic permeability μ. The electric permittivity and magnetic permeability are essential parameters in the description of a medium's response to electric and magnetic fields. Also known as constitutive parameters, they are related to the absorption and dispersion of light in materials.

The first consequence for a material with those characteristics is that, when we look at Maxwell's equations for a plane monochromatic wave, in which all quantities are proportional to $e^{i(\vec{k}\cdot\vec{z}-\omega t)}$, then

$$\begin{aligned} \vec{k}\times\vec{E} &= \frac{\omega}{c}\mu\vec{H}, \\ \vec{k}\times\vec{H} &= -\frac{\omega}{c}\epsilon\vec{E}, \end{aligned} \tag{1.1}$$

if $\epsilon < 0$ and $\mu < 0$ simultaneously, the vectors $\vec{E}$, $\vec{H}$ and $\vec{k}$ form a left-handed triplet. A medium with such a behavior is also called as *left-handed material* (LHM). Therefore, in those media energy flow and wave fronts travel in opposite directions, i.e, the Poynting vector $\vec{S} \propto \vec{E}\times\vec{H}$ and the wave vector $\vec{k}$ are antiparallel, as depicted in Fig. (1.1), and the phase velocity of light is also opposite to the energy flow.

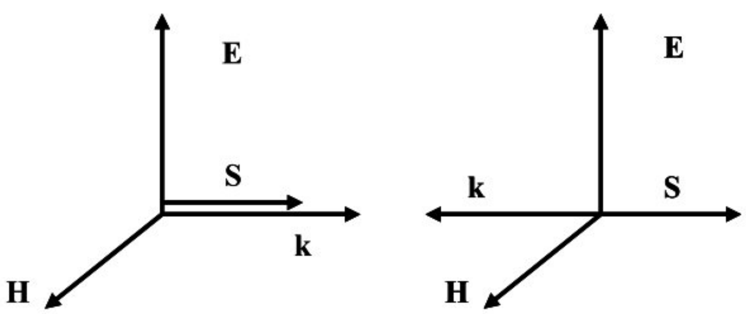

Figure 1.1: Right-handed orientation and left-handed orientation of the field vectors.

New phenomena arise in a left-handed material: as Veselago pointed out, since the index of refraction may be taken as $n \equiv c\sqrt{\epsilon}\sqrt{\mu}$, in a LHM one obtains a negative value ($n < 0$). Thanks to this, when light rays refract into a LHM, the refracted angle is reversed ($\theta_r \to -\theta_r$), which allows for the development of super-lenses that go beyond the diffraction limit [8, 9]. Other reversals in fundamental phenomena also take place, such as backward wave propagation, inverse Cherenkov radiation, and inverse Doppler effect [10].

Regarding the two effective parameters, ϵ and μ, most materials found in nature have positive values of the electric permittivity and magnetic permeability, that is, $\epsilon > 0$ and $\mu > 0$. Negative permittivity ($\epsilon < 0$) can be found in a dispersive medium, where the electric permittivity $\epsilon(\omega)$ depends on the frequency of radiation, such as a homogeneous isotropic electric plasma. At low frequencies, the permittivity may be approximated by $\epsilon(\omega) = 1 - (\omega_p^2/\omega^2)$ [11], where $\omega_p^2 = e^2 N/m$ is the plasmon frequency. When $\omega < \omega_p$, the permittivity $\epsilon(\omega)$ is clearly negative, indicating that the direction of the electric field induced in matter is opposite to the direction of the external electric field.

On the other hand, modulating the permeability $\mu(\omega)$ presents a challenge, since at optical frequencies, due to molecular currents, the magnetic permeability tends to the value in free space $\mu = 1$ [12]. However, an environment such as a magnetic plasma could have a dispersive magnetic response $\mu(\omega)$. The combination of the forbidden and allowed values of ϵ and μ may be summarized in an electromagnetic parametric space (Fig.1.2).

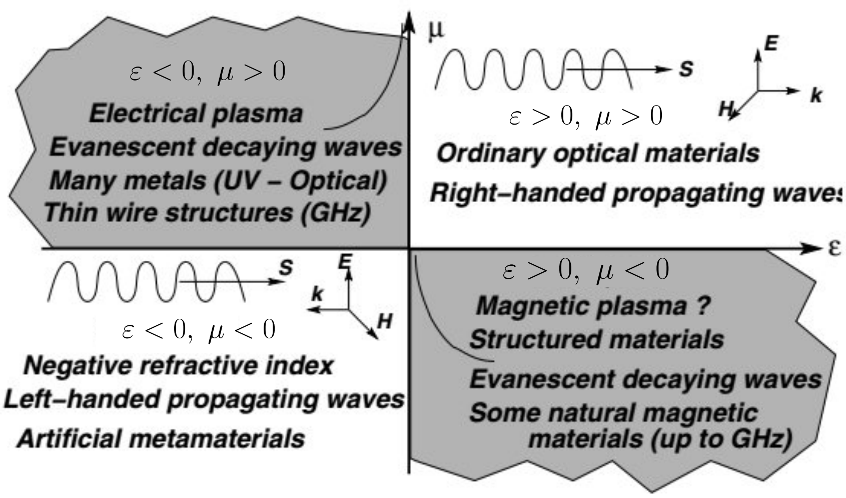

Figure 1.2: Parametric space for ϵ and μ, extracted from reference [15].

No one has ever found a material in nature exhibiting simultaneously negative values of ϵ and μ. Consequently, this restriction imposes a limitation on the propagation of light in matter. Also, it was believed that the refractive index could not take negative values ($n < 0$). Nevertheless, there seems to be no physical reason why materials with negative refractive index could not exist in nature.

In fact, the discussion began with Sir Arthur Schuster and Sir Horace Lamb, in 1904 [13]: because the dielectric function is dispersive, they believed that the signs of the group velocity and energy-flow could be anti-parallel whenever the frequency of the EM wave was close to the absorption resonance frequency. Similar conclusions were drawn by Mandelstham in 1945 [14], who presented an example of negative group velocity in spatially periodic media. That is a direct consequence of the signs of the electric permittivity and magnetic permeability.

It is not immediately obvious that simultaneously $\epsilon < 0$ and $\mu < 0$ imply a negative index of refraction $n < 0$. The appropriate choice of sign of n is a consequence of the reversal of the wave vector in a LHM. Considering an isotropic medium, the index of refraction may be obtained from Snell's law: the wave vector $\vec{k}$ in a LHM is opposite to the propagation of the wave; then, the continuity of the electromagnetic fields at the interface of two media, one with $n_1 = 1$ (RHM) and incidence angle θ_1, and the other a LHM with index of refraction n and transmission angle θ_2, imply [16]

$$\sin\theta_1 = n\sin\theta_2. \tag{1.2}$$

With $n < 0$, $\sin\theta_2 < 0$, and the transmitted rays make a *negative* angle with respect to the normal to the interface (fig.1.3).

One may derive the same conclusion about the sign of n by noting that ϵ, μ and n are complex numbers, which may be written as

$$n = \sqrt{|\epsilon||\mu|}e^{\frac{i}{2}(\theta+\phi)}. \tag{1.3}$$

If one imposes that the imaginary part of n should be positive (energy loss), this implies that the phase is limited to $0 < \frac{1}{2}(\theta+\phi) < \pi$. If the real parts of ϵ and μ are both negative, ($\cos\theta < 0$ and $\cos\phi < 0$), we must have, $\frac{\pi}{2} < \frac{1}{2}(\theta+\phi) < \pi$, i.e., a negative real part of the refractive index

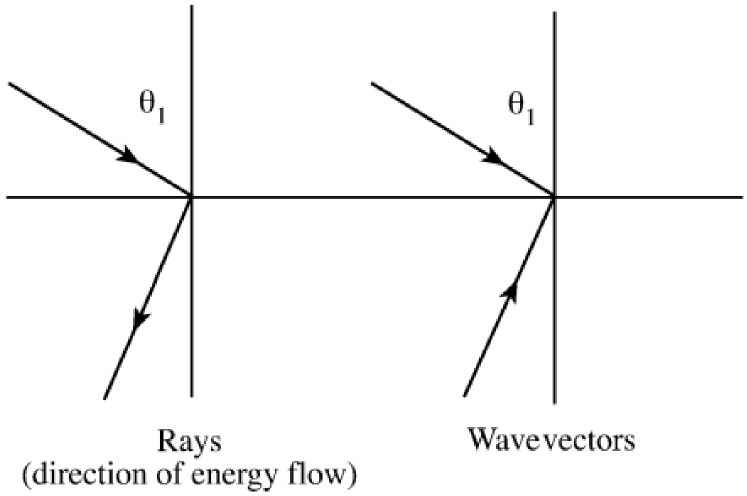

Figure 1.3: Rays and wave vectors when an incident radiation from vacuum passes through a LHM with refractive index $n < 0$. The direction of the wave vector is opposite to the direction of energy flow. Figure extracted from reference [16].

$$n_R \equiv \mathrm{Re}[n] = \sqrt{|\epsilon||\mu|}\cos\frac{1}{2}(\theta+\phi) < 0. \tag{1.4}$$

Therefore, demanding that n has a positive imaginary part leads to the conclusion that if ϵ and μ have negative real parts, the real part of n must be also be negative.

1.2 A natural candidate for a system with left-handed behavior

Despite the fact that artificial metamaterials are a physical reality today, the existence of natural metamaterials remains a mystery. The question of the existence of natural metamaterials was recently treated by de Carvalho [17], who obtained simultaneously negative electric permittivity and magnetic permeability in a natural physical system with fast moving electrons of velocity $v \sim c$, a relativistic electron gas (REG) at finite temperature and density. As the sources of magnetic fields are current densities, in relativistic systems one obtains magnetic responses comparable to electric ones, in opposition to nonrelativistic ($v \ll c$), where the magnetic responses are much smaller than electric ones.

In fact, it was shown that, in the long wavelength limit, a finite density of relativistic electrons exhibits Drude-type responses for both ϵ and μ^{-1} at temperature $T = 0$, implying that they can be simultaneously negative for frequencies that are low when compared to the electric plasmon frequency. In addition, the validity of the model has been tested in the non-relativistic limit by successfully [18] describing the experimental behavior of the plasmon energy, as a function of both temperature and wave vector, in low energy condensed- matter systems such as graphite and tin oxide [19, 20].

The REG is a plasma of electrons which, in the absence of interactions, obeys a Fermi-Dirac distribution at very high densities, or very high temperatures, or both. Under those circumstances, either the Fermi energy of the system, or its thermal energy, or both, will be much greater than the electron rest mass, so that many electrons will have relativistic speeds. The appropriate formalism to treat the REG is that of Quantum Electrodynamics (QED) [21]. It describes the interaction of electrons and positrons with photons, the quanta of EM fields, and was initially proposed at zero temperature and zero average densities, i.e., for equal number of electrons and positrons, characteristic of a vacuum state. QED was soon generalized for finite values of temperature and average charge which characterize the REG (more electrons than positrons) [22, 23, 24]. We will be interested in the interaction of this REG with an EM field composed of a classical background part plus quantum (photonic) fluctuations around it. Our main concern is to show how this medium reacts to the classical EM field in order to establish that it is a *natural* example of a left-handed material.

In order to accomplish our goal, in chapter 2 we discuss in detail the work of de Carvalho [17]. We start from the partition function of QED at finite temperature and charge density, and perform a semiclassical expansion around the classical EM background by integrating over quantum fluctuations of the EM field, as well as over the fermionic fields of electrons and positrons. In leading order in the fine structure constant α, we may neglect the fermion-fermion interactions obtained from the integration over EM fluctuations, and restrict our attention to the interaction of the fermions with the EM classical background. Then, integrating over fermions yields a determinant that may be functionally expanded in the EM background. If the background is weak, we need not go beyond the quadratic term, which leads to a linear response to the external field (this is the familiar RPA approximation). The procedure just described allows for the computation of an effective action for the classical EM field. Extremizing that action yields Maxwell's equations, with the polarization and magnetization that result from quantum fluctuations of the fermions around the classical background. From those quantities, we extract the responses of both medium and vacuum to an external classical background.

Thanks to the QED treatment, we were able to estabilish that: (i) all responses depend on three scalar functions (one for the vacuum; two for the medium); (ii) polarizations depend on both the electric and magnetic fields, just as magnetizations depend on both magnetic and electric fields; and (iii) many aspects of the analysis of the electric responses carry over to the magnetic ones, due to the analogies between permittivities ϵ and inverse permeabilities $\nu \equiv \mu^{-1}$, among them the fact that both ϵ and ν exhibit Drude-like responses at low frequencies in the long wavelength limit.

In chapter 3, we calculate the real and imaginary parts of the electromagnetic responses of the relativistic electrons [25]. At temperature $T \neq 0$, the problem is reduced to one-dimensional (1-D) integrals which involve the Fermi-Dirac occupation numbers for electrons and positrons. At $T = 0$, however, as the occupation numbers become step functions, we obtain analytic expressions for the medium contributions. The real part of the longitudinal responses may be used to obtain dispersion relations for plasmon modes that propagate as the external electromagnetic fields induce resonant charge density collective oscillations in the electron gas. Such modes are present even if we neglect electron-electron-interactions, as is well established in the Condensed Matter [26, 27, 28] and Finite Temperature Field Theory literatures [29, 22]. The imaginary parts of the longitudinal responses are useful to calculate regions of instability for plasmon propagation. The appearance of non zero imaginary parts is associated with the creation of electron-hole (low energies) or electron-positron (high energies) pairs.

Analytic results for the response functions of the REG at $T = 0$ have already appeared in the literature in the context of plasma physics [30, 31, 32, 33, 34, 35, 36], but only expressions for the longitudinal and transverse parts of the electric permittivity, ϵ_L and ϵ_T, were derived. It is worth noting that, in the non-relativistic case, electromagnetic responses may be completely obtained from ϵ_L and ϵ_T. In the relativistic case, however, responses depend on three independent functions, one of which accounts for the vacuum contribution, as mentioned before. It turns out that the vacuum contribution is negligible at low frequencies for typical electron densities, so one can obtain magnetic responses from electric ones. Nonetheless, one might envisage situations of extremely low densities, in which the vacuum may contribute at low frequencies. The chapter presents analytic results at $T = 0$, and numerical ones at $T \neq 0$, for electric permittivities and for magnetic permeabilities.

It should also be noted that finite temperature and density QED has been used by several authors to compute electromagnetic responses [37, 38, 39, 40, 41, 42]. Nevertheless, those articles do not obtain analytic expressions at $T = 0$, and concentrate on some limiting cases for $T \neq 0$.

We finish chapter 3 with a general discussion of the collective modes of oscillation in the REG [43]. Rewriting the propagator for the electromagnetic field in terms of the electric and magnetic responses, the modes that propagate in the gas are identified. As expected, the usual collective excitations are obtained, i.e., a longitudinal electric and two transverse magnetic plasmonic modes. In addition, a purely photonic mode is found, which satisfies the wave equation in vacuum, for which the electron gas is transparent.

In chapter 4, we show that a gas of relativistic electrons is a left-handed material at low frequencies by computing the effective electric permittivity and effective magnetic permeability that appear in Maxwell's equations in terms of the responses appearing in the constitutive relations, and showing that the effective responses are both negative below the same frequency, which coincides with the zero-momentum frequency of longitudinal plasmons. We also show, by explicit computation, that the photonic mode of the electromagnetic radiation does not dissipate energy, confirming that it propagates in the gas with the speed of light in vacuum, and that the medium is transparent to it. We then combine those results to show that the gas has a negative effective index of refraction $n_{\mathrm{eff}} = -1$. We illustrate the consequences of this fact for Snell's law, and for the reflection and transmission coefficients of the gas [44].

In chapters 5 and 6, we investigate the Relativistic Bose gas (RBG) [45, 46]. The RBG is an ideal gas of charged bosons and antibosons whose dispersion relation is $E_{\pm}(\vec{p}) =$

$\pm\sqrt{\vec{p}^2c^2+m^2c^4}$ (+ bosons, − antibosons). A chemical potential $-mc^2 \leq \xi \leq +mc^2$ is used to fix the conserved charge, proportional to the number of bosons minus antibosons. The system undergoes a phase transition, forming a Bose-Einstein condensate below a critical temperature T_c [47, 48, 49].

In the nonrelativistic limit, the ideal charged Bose gas is used to describe a superconducting system. Schafroth [50], for instance, has shown that it exhibits the Meissner effect, the total expulsion of an external magnetic field. It is also used to describe the phenomenon of superfluidity in liquid Helium at low temperatures, where a microscopic field-theoretic description is formulated in terms of the complex charged Bose gas [51]. The superfluid state emerges when the $U(1)$ symmetry of the Lagrangian is spontaneously broken. The main physical ingredient to obtain a superfluid is a Bose-Einstein condensate, which is responsible for frictionless flow [52].

In the relativistic limit, it is useful to investigate the Bose plasma, a charged gas of bosons and antibosons, which may be found in astrophysical scenarios such as neutron stars [53]. This environment provides ideal conditions for the creation of charged pion pairs, allowing for the phenomenon of pion condensation [54, 55, 56].

As a result of the investigation: i) we establish the gas as a left-handed material below the transverse plasmon frequency; ii) we show that it supports longitudinal and transverse plasmons, and a photonic mode that propagates without loss with the velocity of light in vacuum, which we use to characterize it as a medium with negative effective index of refraction $n_{\text{eff}} = -1$ below the transverse plasmon frequency; iii) we check for signatures of the condensed phase in the dispersion relations of the electromagnetic propagation modes.

Besides the search for left-handed behavior through the electromagnetic responses of the RBG, the other motivation of the study was the search for structures in the condensed phase of the gas, inspired by the physics of superfluids such as liquid ^{4}He, described by self-interacting charged scalars. There, the observation via neutron scattering [57] of collective phonon-roton modes in the (condensed) superfluid phase was a major discovery. Such collective excitations were ultimately responsible for superfluidity, according to the seminal work of Landau [58].

We have found structures similar to superfluid rotons in the dispersion relation of the longitudinal plasmon mode of the RBG, which exhibits a roton type local minimum that disappears at the critical temperature, and whose gap energy vanishes at T_c. This strongly suggests that we are seeing rotons in the charge density oscillations that disorder the system, and drive it into the normal phase.

In chapter 6, we compute deviations from ideal gas behavior of the pressure, density, and Bose-Einstein condensation temperature of a relativistic gas of charged scalar bosons caused by the current-current interaction induced by electromagnetic quantum fluctuations treated via scalar quantum electrodynamics. We obtain expressions for those quantities in the ultra-relativistic and nonrelativistic limits, and present numerical results for the relativistic case.

Most of the calculations in this thesis use Euclidean metric. Euclidean and Minkowski coordinates are related by $x_4 = ix^0$ and $x_j = x^j$. For gauge fields, $A_4 = iA^0$ and $A_j = A^j$. For Dirac matrices, $\gamma_4 = i\gamma^0$ and $\gamma_j = \gamma^j$. The Minkowski metric is $\eta_{\mu\nu} = (+,-)$. In appendix A, we discuss aspects of the Euclidean and Minkowski metric in Maxwell and Dirac Lagrangians. We mostly use natural (Heaviside) units, $k_B = \hbar = c = 1$, so that $\beta = 1/T$ is the inverse of temperature, and $\alpha = e^2/4\pi = 1/137$ is the fine-structure constant.

1.3 List of publications

The following papers are associated with the content of this thesis:

1. D. M. Reis, E. Reyes-Gómez, L. E. Oliveira, and C. A. A. de Carvalho, Electromagnetic propagation in a relativistic electron gas at finite temperatures, Annalen der Physik **530**, 1700443 (2018)

2. C. A. A. de Carvalho and D. M. Reis, Electromagnetic responses of relativistic electrons, Journal of Plasma Physics **84**, 905840112 (2018).

3. C. A. A. de Carvalho, D. M. Reis, and D. Szilard, Negative refraction in relativistic electron gas, J. Opt. Soc. Am. B **37**, 3542 (2020).

4. D. M. Reis, S. B. Cavalcanti, and C. A. A. de Carvalho, Negative refraction and rotons in the relativistic Bose gas. Physics Letters B, **812**, 136003 (2021).

5. D. M. Reis and C. A. A. de Carvalho, Electromagnetic quantum shifts in relativistic Bose-Einstein condensation. Physics Letters B, **823**, 136715 (2021).

Chapter 2

Electromagnetic responses of the relativistic electron gas

2.1 Introduction

In this chapter, we derive a general strategy to compute the electric permittivity, ϵ, and the magnetic permeability, μ, of a gas of charged particles. These two quantities account for the polarization and magnetization in a material under an external electromagnetic (EM) field. From Maxwell's equations, their values determine how waves propagate in the medium. We shall concentrate on systems with magnetic responses comparable to electric ones. Since current densities are the sources of magnetic fields, a system with fast-moving electrons ($v \approx c$) such as the Relativistic Electron Gas (REG) satisfies this condition, so that it will be our first object of study.

2.2 Field theory treatment

Let us consider a gas of fast moving electrons under the action of an electromagnetic external field A_ν. We may treat this system by using QED at finite temperature and density, whose grand partition function is given by $\Xi = \mathrm{Tr} e^{-\beta(\hat{H}-\xi\Delta\hat{N})}$, and which describes an electron gas, with fixed $\Delta N = N_e - N_p$ (N_e is the number of electrons; N_p is the number of positrons) at temperature $T = \beta^{-1}$ (Boltzmann constant $k_B = 1$), and chemical potential ξ, coupled to the EM field A_ν. The grand partition function Ξ may be expressed as a functional integral over gauge and fermion fields

$$\Xi = \oint [dA_\mu]\mathcal{M}[A]e^{-S_A[A]}\Xi_e[A], \tag{2.1}$$

where

$$\Xi_e[A] = \oint [id\psi^\dagger][d\psi]e^{-S_e[\psi^\dagger,\psi,A]}, \tag{2.2}$$

$\mathcal{M}[A] = \delta(\mathcal{F}[A])\det\left(\frac{\partial\mathcal{F}}{\partial\lambda}\right)$, and the determinant is the Jacobian of the gauge transformation $A_\nu \to A_\nu - \partial_\nu\lambda$, the Faddeev-Popov determinant. The delta function $\delta(\mathcal{F}[A])$, with $\mathcal{F}[A] = \partial_\nu A_\nu$, imposes the Lorentz gauge condition. The Euclidean action is $S_A[A] = \int d^4x \frac{1}{4} F_{\mu\nu}F_{\mu\nu}$, with $F_{\mu\nu} = \partial_\mu A_\nu - \partial_\nu A_\mu$, the field strength tensor, and $S_e[A,\psi^\dagger,\psi] = \int d^4x \left[\bar{\psi}(i\not{D} - m - i\xi\gamma_4)\psi\right]$, where $\not{D} \equiv \gamma\cdot(\partial - ieA)$; e and m are the electron charge and mass, and $\bar{\psi} = \psi^\dagger\gamma_4$. The chemical potential ξ was introduced in the Dirac grand partition function as a consequence of its invariance under a global symmetry $U(1)$, with a Noether conserved current $j_\mu = \bar{\psi}\gamma_\mu\psi$, for which the total conserved fermion number is $\Delta N = \int d^3x\, \psi^\dagger\psi$.

The integral in (2.1) is over gauge fields obeying the condition $A_\nu(0,\vec{x}) = A_\nu(\beta,\vec{x})$, whereas the electron fields obey $\psi(0,\vec{x}) = -\psi(\beta,\vec{x})$. A semiclassical approximation can be performed by writing $A_\mu = A_\mu^{(c)} + \hbar a_\mu$ (Appendix B), where $A_\mu = A_\mu^{(c)}$ is a classical solution of the sourceless equation of motion for A_μ, which we identify with the external classical field incident on the electron gas. In the lowest order of the semiclassical approximation, the functional integral is given by

$$\Xi^{(sc)} = e^{-S_A^{(c)}}\oint [id\psi^\dagger][d\psi]\exp\left[\oint d^4x\bar{\psi}(i\not{D}^{(c)} - m - i\xi\gamma_4)\psi\right], \tag{2.3}$$

where $\not{D}^{(c)} = \not{D}(A^{(c)})$ and $F_{\mu\nu}^{(c)} = F_{\mu\nu}(A^{(c)})$.

For the integration over the fermion fields, it is most convenient to work in $(\vec{p},\omega_n)$ space in the imaginary time formalism,

$$\psi_\alpha(\vec{x},t) = \frac{1}{\sqrt{V}}\sum_n\sum_{\vec{p}} e^{i(\vec{p}\cdot\vec{x}+\omega_n\tau)}\tilde{\psi}_{\alpha;n}(\vec{p}), \tag{2.4}$$

where $\tau = it$ is the imaginary time defined over the interval $0 \le \tau \le \beta$, and the discrete frequencies are $\omega_n = \frac{(2n+1)\pi}{\beta}$ for fermions. Thus, if we integrate over Grassman variables, we obtain the fermion determinant

$$\Xi_e[A] = \det\left[-\beta\gamma_4(i\not{D}^{(c)} - m - i\xi\gamma_4)\right]. \tag{2.5}$$

Using $\det[\Gamma] = e^{\mathrm{Tr}\ln\Gamma}$, we obtain an effective action with the quantum contribution of the electrons in interaction with the external classical field $A_\mu = A_\mu^{(c)}$. Thus,

$$\Xi^{(sc)} = e^{-S_{\mathrm{eff}}}, \tag{2.6}$$

where

$$S_{\mathrm{eff}} = \oint d^4x \left[\frac{1}{4}F_{\mu\nu}^{(c)}F_{\mu\nu}^{(c)} + \frac{1}{2\lambda}(\partial_\mu A_\mu^{(c)})^2 - (\partial_\mu \bar{C})(\partial_\mu C)\right] + \mathrm{Tr}\ln[-\beta\gamma_4(i\not{D}^{(c)} - m - i\xi\gamma_4)], \tag{2.7}$$

with $\bar{C}$ and C the auxiliary ghost fields due to the Fadeev-Poppov procedure on the functional integral, and λ the gauge parameter. The equation of motion for the external classical eletromagnetic field in interaction with the electron gas can be obtained by extremizing (2.7)

$$\frac{\delta S_{\mathrm{eff}}}{\delta A_\nu} = 0. \tag{2.8}$$

We obtain Maxwell's equations,

$$\partial_\mu F_{\mu\nu} = -\mathrm{Tr}[e\gamma_\nu G_F[A]] = J_\nu, \tag{2.9}$$

where $G_F[A] \equiv (i\not{D} - m - i\xi\gamma_4)^{-1}$ is the fermion propagator in the presence of the external classical gauge field A_ν. We dropped the superscript c with the understanding, from now on, that A is just the classical field.

The current density in eq.(2.9) has the contribution of the free, $J_\nu^{(0)}$ (for $A = 0$), and induced current, J_ν^I, so the total density current is $J_\nu = J_\nu^0 + J_\nu^I$. We may write the equation of motion for the induced current as,

$$\begin{aligned} J_\nu^I &= J_\nu - J_\nu^0 \\ &= -\mathrm{Tr}[e\gamma_\nu G_F(A)] + \mathrm{Tr}[e\gamma_\nu G_F(0)], \end{aligned} \tag{2.10}$$

In the presence of a medium, we rewrite Maxwell's equations in (2.9) to account for the polarization as

$$\partial_\mu F_{\mu\nu}^{\mathrm{eff}} = \partial_\mu(F_{\mu\nu} + P_{\mu\nu}) = j_\nu^0. \tag{2.11}$$

From that, we identify the medium contribution for the induced current

$$\begin{aligned} \partial_\mu P_{\mu\nu} &= -J^I_\nu, \\ \partial_\mu P_{\mu\nu} &= -\mathrm{Tr}[e\gamma_\nu G_F(0)] + \mathrm{Tr}[e\gamma_\nu G_F(A)]. \end{aligned} \tag{2.12}$$

The tensor $P_{\mu\nu}$ defines the polarization $\vec{P}(P_{4j} = iP^j)$ and magnetization $\vec{M}(P_{ij} = -\epsilon_{ijk}M^k)$ vectors. Eq. (2.9) is the Maxwell equation for the total current in the REG, obtained from an effective action for the electromagnetic field. The induced current accounts for the quantum contribution of the electrons in interaction with the gauge field, obtained from the fermion integration in eq. (2.7).

We may perform an expansion in the field A_ν in the fermion propagator appearing in $\mathrm{Tr}[e\gamma_\nu G_F(A)]$. This type of expansion leads to an infinite sum of one-loop graphs in the effective action, which is equivalent to the random phase approximation [17] in condensed matter physics. We write the fermion propagator as

$$\begin{aligned} G(A) &= (i\not{D} - m - i\xi\gamma_4)^{-1} \\ &= (G_0^{-1} + e\not{A})^{-1} \\ &= G_0(\mathbb{I} + e\not{A}G_0)^{-1}, \end{aligned} \tag{2.13}$$

where $G_0 \equiv G_F(A=0) = (i\not{\partial} - m - i\xi\gamma_4)^{-1}$. The propagator can be expanded in the background field A_ν, Fig.2.1, to yield

$$G_F(A) = G_0 - eG_0\not{A}G_0 + e^2 G_0\not{A}G_0\not{A}G_0 + \mathcal{O}(e^3) + \ldots \tag{2.14}$$

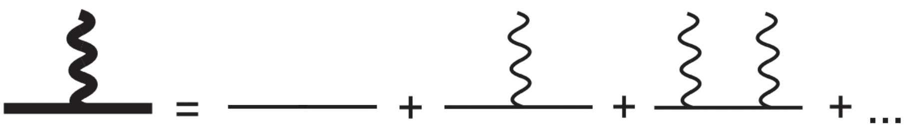

Figure 2.1: Expansion of the electron propagator in the external field, represented by wiggly lines.

Substituting (2.14) into (2.12), and only retaining the linear term, which corresponds to the linear response approximation, we obtain

$$\partial_\mu P_{\mu\nu} = -\mathrm{Tr}[e^2\gamma_\nu G_0\gamma_\sigma A_\sigma G_0]. \tag{2.15}$$

The equation above may be written in momentum space as

$$iq_\mu P_{\mu\nu}(q) = \Pi_{\nu\sigma} A_\sigma(q), \tag{2.16}$$

where $\Pi_{\nu\sigma}$ is the polarization tensor of QED,

$$\Pi_{\nu\sigma} = -\frac{e^2}{\beta}\sum_{n=-\infty}^{+\infty}\int \frac{d^3p}{(2\pi)^3}\mathrm{Sp}[\gamma_\nu G_0(p)\gamma_\sigma G_0(p-q)], \tag{2.17}$$

and $G_0(p) = -(\not{p} + m + i\xi\gamma_4)^{-1}$ is the fermion propagator in momentum space. The sum in (2.17) is over Matsubara frequencies $p_4 = (2n+1)\pi T$, with Sp denoting the trace over Dirac matrices. The field theory treatment allows us to obtain the induced current $J^I_\nu = -\Pi_{\nu\sigma}(q)A_\sigma(q)$ in the gas, the result of a fully quantum description of the relativistic electrons, through the QED polarization tensor $\Pi_{\nu\sigma}$ at one loop, and linear response in the external classical EM field A_σ.

The current conservation law, $q_\nu J^I_\nu = 0$, is associated to the gauge invariance of the polarization tensor, $q_\nu \Pi_{\nu\sigma} = 0$. Thus, we can solve eq. (2.12) by noting that $P_{\mu\nu}$ may be written as

$$P_{\mu\nu} = -i\left(\frac{q_\mu}{q^2}\Pi_{\nu\sigma}A_\sigma - \Pi_{\mu\sigma}A_\sigma\frac{q_\nu}{q^2}\right), \tag{2.18}$$

where from $iq_\mu P_{\mu\nu}$ we recover the one-loop, linear response result, since $q_\mu \Pi_{\mu\nu} = 0$. So, using the fact that the electromagnetic tensor in momentum space is $F_{\nu\sigma} = iq_\nu A_\sigma - iq_\sigma A_\nu$, eq. (2.18) becomes

$$P_{\mu\nu} = \left(\frac{\Pi_{\mu\sigma}}{q^2}F_{\nu\sigma} - \frac{\Pi_{\nu\sigma}}{q^2}F_{\mu\sigma}\right). \tag{2.19}$$

The polarization tensor involves vacuum ($T = \xi = 0$) and medium contributions. To investigate the solution of (2.17), one may write $\Pi_{\nu\sigma} = \Pi^{(v)}_{\nu\sigma} + \Pi^{(m)}_{\nu\sigma}$, where the vacuum contribution $\Pi^{(v)}_{\nu\sigma}$ may be written in a fully covariant form

$$-\frac{\Pi^{(v)}_{\nu\sigma}}{q^2} = \left(\delta_{\sigma\nu} - \frac{q_\nu q_\sigma}{q^2}\right)\mathscr{C}(q^2). \tag{2.20}$$

The scalar function $\mathscr{C}(q^2)$ may be obtained from the standard calculation at $T = \xi = 0$ [21]. However, one cannot write the medium contribution tensor $\Pi^{(m)}_{\nu\sigma}$ in a fully covariant form due to the fact that the center of mass frame of the medium introduces a preferred reference frame. The symmetry is then reduced to three-dimensional rotation and gauge invariance, leading to (Appendix C)

$$-\frac{\Pi_{ij}^{(m)}}{q^2} = \left(\delta_{ij} - \frac{q_i q_j}{|\vec{q}|^2}\right)\mathscr{A} + \delta_{ij}\frac{q_4^2}{|\vec{q}|^2}\mathscr{B}. \tag{2.21}$$

$$-\frac{\Pi_{44}^{(m)}}{q^2} = \mathscr{B}, \quad -\frac{\Pi_{4i}^{(m)}}{q^2} = \frac{q_4 q_i}{|\vec{q}|^2}\mathscr{B}, \tag{2.22}$$

where $\mathscr{A}(q_4,\vec{q})$ and $\mathscr{B}(q_4,\vec{q})$ are scalar functions determined from the Feynman graph in eq. (2.17) at finite temperature and density. The Matsubara sums of $\Pi_{\mu\mu}^{(m)}$ and $\Pi_{44}^{(m)}$, are calculated in detail in Appendix D. Once we subtract the vaccum contribution, the functions $\mathscr{A}(q_4,\vec{q})$ and $\mathscr{B}(q_4,\vec{q})$ read

$$\mathscr{A} = \frac{-e^2}{2\pi^3 q^2}\mathrm{Re}\int \frac{d^3p}{\omega_p} n_F(p)\frac{p\cdot(p+q)}{q^2-2p\cdot q} + \left(1-\frac{3q^2}{2|\vec{q}|^2}\right)\mathscr{B}, \tag{2.23}$$

$$\mathscr{B} = \frac{-e^2}{2\pi^3 q^2}\mathrm{Re}\int \frac{d^3p}{\omega_p} n_F(p)\frac{p\cdot q - 2p_4(q_4-p_4)}{q^2-2p\cdot q}, \tag{2.24}$$

where $p_4 = i\omega_p = i\sqrt{|\vec{p}|^2+m^2}$, and $n_F(p)$ is the Fermi-Dirac distribution for particles and antiparticles,

$$n_F(p) = \frac{1}{e^{\beta(\omega_p-\xi)}+1} + \frac{1}{e^{\beta(\omega_p+\xi)}+1}. \tag{2.25}$$

Expressions (2.23) and (2.24) may be integrated over angles (Appendix E). The final result with the functions analytically continued to Minkowski metric, $\mathscr{A}\to\mathscr{A}^*$ and $\mathscr{B}\to\mathscr{B}^*$, may be obtained by changing, $q_4 \to i\omega$ and $q^2 \to -q_M^2$, with $q_M^2 = \omega^2 - |\vec{q}|^2$,

$$\mathscr{A}^* - \left(1+\frac{3q_M^2}{2|\vec{q}|^2}\right)\mathscr{B}^* = -\frac{e^2}{\pi^2 q_M^2}\int_0^\infty \frac{p^2dp}{\omega_p} n_F(p)\left[1+\frac{2m^2+q_M^2}{8p|\vec{q}|}f_1\right], \tag{2.26}$$

$$\mathscr{B}^* = -\frac{e^2}{\pi^2 q_M^2}\int_0^\infty \frac{p^2dp}{\omega_p} n_F(p)\left[1+\frac{4\omega_p^2+q_M^2}{8p|\vec{q}|}f_1 - \frac{\omega_p\omega}{2p|\vec{q}|}f_2\right], \tag{2.27}$$

where,

$$f_1 = \ln\left(\frac{(q_M^2 - 2p|\vec{q}|)^2 - 4\omega_p^2\omega^2}{(q_M^2 + 2p|\vec{q}|)^2 - 4\omega_p^2\omega^2}\right), \tag{2.28}$$

$$f_2 = \ln\left(\frac{q_M^4 - 4(p|\vec{q}| + \omega_p\omega)^2}{q_M^4 - 4(p|\vec{q}| - \omega_p\omega)^2}\right). \tag{2.29}$$

The next step is to derive ϵ and μ as function of $\mathscr{A}^*(\omega,\vec{q})$ and $\mathscr{B}^*(\omega,\vec{q})$.

2.3 Constitutive equations

We may obtain the constitutive equations which relate the fields induced in the gas, the polarization $\vec{P}$ and the magnetization $\vec{M}$, with the external fields $\vec{E}$ and $\vec{B}$. Eq.(2.19) relates polarization and magnetization to the fields $\vec{E}(F_{4j} = iE^J)$ and $\vec{B}(F_{ij} = \epsilon_{ijk}B^k)$, thus yielding electric and magnetic susceptibilities and, ultimately, electric permittivities and magnetic permeabilities. From eq. (2.19), the components, P_{4j} and P_{ij}, may be written as

$$P_{4j} = \frac{\Pi_{44}}{q^2}F_{j4} + \frac{\Pi_{4k}}{q^2}F_{jk} - \frac{\Pi_{jk}}{q^2}F_{4k}, \tag{2.30}$$

$$P_{ij} = \frac{\Pi_{i4}}{q^2}F_{j4} + \frac{\Pi_{ik}}{q^2}F_{jk} - \frac{\Pi_{j4}}{q^2}F_{i4} - \frac{\Pi_{jk}}{q^2}F_{ik}. \tag{2.31}$$

The components of the EM tensor in the Euclidean metric are related to the electromagnetic fields ($\vec{E}$ and $\vec{B}$) in Minkowski metric via $F_{4j} = iE^j$ and $F_{ij} = \epsilon_{ijk}B^k$. The field equations in the medium [12], are $\vec{D} = \vec{E} + \vec{P}$ and $\vec{H} = \vec{B} - \vec{M}$. They relate to the induced charge and current as $\vec{\nabla}\cdot\vec{P} = -\rho_{ind}$ and $\vec{\nabla}\times\vec{M} = \vec{J}_{ind}$. This leads us to define, in the Euclidean metric, $P_{4j} = iP^j$ and $P_{ij} = -\epsilon_{ijk}M^k$. Thus, the polarization component vector P^j is written from eq. (2.30) as

$$P^j = \left(-\frac{\Pi_{44}}{q^2}\right)E^j + \left(-\frac{\Pi_{jk}}{q^2}\right)E^k + \left(-i\epsilon_{jkl}\frac{\Pi_{4k}}{q^2}\right)B^l, \tag{2.32}$$

and the magnetization M^k from eq. (2.31) as

$$M^k = i\epsilon_{kij}\frac{\Pi_{i4}}{q^2}E^j + \frac{\Pi_{jj}}{q^2}B^k - \frac{\Pi_{lk}}{q^2}B^l. \tag{2.33}$$

If we split the polarization tensor into vacuum and medium contributions, and using the relations (2.20-2.22) in P^j and M^j in eqs. (2.32) and (2.33), we obtain for D^j and H^j

$$\begin{aligned} D^j &= \left\{\left[1+\mathscr{A}+\left(1+\frac{q_4^2}{|\vec{q}|^2}\right)\mathscr{B}+\left(2-\frac{q_4^2}{q^2}\right)\mathscr{C}\right]\delta_{jk}+\left(-\mathscr{A}-\frac{|\vec{q}|^2}{q^2}\mathscr{C}\right)\hat{q}_j\hat{q}_k\right\}E^k \\ &+ \epsilon_{jkl}\hat{q}_l\frac{(iq_4)}{|\vec{q}|}\left(\mathscr{B}+\frac{|\vec{q}|^2}{q^2}\mathscr{C}\right)B^k, \end{aligned} \tag{2.34}$$

and

$$\begin{aligned} H^j &= \left\{\left[1+\mathscr{A}+2\frac{q_4^2}{|\vec{q}|^2}\mathscr{B}+\left(2-\frac{|\vec{q}|^2}{q^2}\right)\mathscr{C}\right]\delta_{jk}+\left(\mathscr{A}+\frac{|\vec{q}|^2}{q^2}\mathscr{C}\right)\hat{q}_j\hat{q}_k\right\}B^k \\ &+ \epsilon_{jlk}\hat{q}_l\frac{(iq_4)}{|\vec{q}|}\left(\mathscr{B}+\frac{|\vec{q}|^2}{q^2}\mathscr{C}\right)E^k. \end{aligned} \tag{2.35}$$

Here, we have used $\hat{q}^i \equiv q^i/|\vec{q}|$. Expressions for D^j and H^j may be simplified, and going to Minkoswki metric $q_4 \to i\omega$, we have

$$D^j = \epsilon_{jk}E^k+\tau_{jk}B^k, \tag{2.36}$$

$$H^j = \nu_{jk}B^k+\tau_{jk}E^k, \tag{2.37}$$

where we have used the notation $\nu_{jk} \equiv (\mu^{-1})_{jk}$ for the inverse of the magnetic permeability tensor. The linear-response tensors are

$$\epsilon_{jk} = \epsilon\delta_{jk}+\epsilon'\hat{q}_j\hat{q}_k, \tag{2.38}$$

$$\nu_{jk} = \nu\delta_{jk}+\nu'\hat{q}_j\hat{q}_k, \tag{2.39}$$

$$\tau_{jk} = \tau\epsilon_{jkl}\hat{q}_l. \tag{2.40}$$

Again, $\nu \equiv \mu^{-1}$ and $\nu' \equiv \mu'^{-1}$. For ϵ_{jk}, the eigenvalues λ satisfy $\det(\epsilon_{jk}-\lambda\delta_{jk})=0$, leading to $(\epsilon-\lambda)^2(\epsilon+\epsilon'-\lambda)=0$. The eigenvector associated with $\epsilon+\epsilon'$ is along $\hat{q}_k$, thus longitudinal, whereas the two eigenvectors corresponding to the eigenvalues ϵ are in directions transverse to $\hat{q}_k$. The same occurs for ν_{jk}, with eigenvalues $\nu+\nu'$ and ν, while τ_{jk} is clearly transverse.

One should stress that there are contributions to $(\vec{D},\vec{H})$ along the directions of the fields $(\vec{E},\vec{B})$, of the wave vector $\vec{q}$, and of $(\vec{q}\times\vec{B},\vec{q}\times\vec{E})$. This is a characteristic of a bian-isotropic medium, because the electromagnetic responses described by the general relations ϵ_{jk}, ν_{jk} and τ_{jk} are tensors, and they depend on the wave vector in the material. Different from an isotropic medium, where electric field $\vec{E}$ and electric displacement $\vec{D}=\epsilon\vec{E}$, as well as magnetic field $\vec{B}$ and induced magnetic field $\vec{H}=\mu^{-1}\vec{B}$, are parallel to one another. Materials with bi-isotropic and bianisotropic properties have found many potential applications, from microwave to optical frequencies, including bianisotropic crystals [84, 85], and the so-called split-ring resonators.

The set of parameters in (2.38-2.40) defines the electric permittivities and inverse magnetic permeabilities,

$$\begin{aligned}
\epsilon &= 1+\mathscr{A}^*+\left(1-\frac{\omega^2}{|\vec{q}|^2}\right)\mathscr{B}^*+\left(2-\frac{\omega^2}{q^2}\right)\mathscr{C}^*, &(2.41)\\
\nu &= 1+\mathscr{A}^*-2\frac{\omega^2}{|\vec{q}|^2}\mathscr{B}^*+\left(2+\frac{|\vec{q}|^2}{q^2}\right)\mathscr{C}^*, &(2.42)\\
\epsilon' &= -\nu'=\frac{|\vec{q}|^2}{q^2}\mathscr{C}^*-\mathscr{A}^*, &(2.43)\\
\tau &= \frac{\omega}{|\vec{q}|}\left(\frac{|\vec{q}|^2}{q^2}\mathscr{C}^*-\mathscr{B}^*\right), &(2.44)
\end{aligned}$$

where here the asterisk means $q_4\to i\omega$. $\mathscr{C}^*$ may be obtained from the standard calculation at $T=\xi=0$,

$$\mathscr{C}^*=\frac{-e^2}{12\pi^2}\left\{\frac{1}{3}+2\left(1+\frac{2m^2}{q^2}\right)[h\times\operatorname{arccot}(h)-1]\right\} \tag{2.45}$$

with $q^2=\omega^2-\vec{q}^2$, $h=\sqrt{(4m^2/q^2)-1}$, and the renormalization condition is $e^2/(4\pi)=1/137$, with $e^2=e^2(\omega=0,\vec{q}=0)$.

The vacuum contributions to permittivities and permeabilities are obtained by setting $\mathscr{A}^*=\mathscr{B}^*=0$. On the other hand, medium susceptibilities may be obtained by taking $\mathscr{C}^*=0$. Thus, for the longitudinal responses, one obtains

$$\epsilon_L \equiv \epsilon + \epsilon' = 1 + \mathscr{C}^* + \left(1 - \frac{\omega^2}{|\vec{q}|^2}\right)\mathscr{B}^*, \tag{2.46}$$

$$\nu_L \equiv \nu + \nu' = 1 + 2\mathscr{C}^* + 2\mathscr{A}^* - 2\frac{\omega^2}{|\vec{q}|^2}\mathscr{B}^*. \tag{2.47}$$

Whenever $\mathscr{C}^*$ is negligible with respect to $\mathscr{A}^*$ and $\mathscr{B}^*$, the longitudinal ϵ_L and transverse $\epsilon_T \equiv \epsilon$ electric permittivities may be used to compute $\mathscr{A}^*$ and $\mathscr{B}^*$. Indeed, $\mathscr{A}^* = \epsilon_T - \epsilon_L$ and $\mathscr{B}^* = (|\vec{q}|^2/q^2)(1-\epsilon_L)$. In this case, we will have $\nu_L = \nu_L(\epsilon_L, \epsilon_T)$ and $\nu_T = \nu_T(\epsilon_L, \epsilon_T)$, as in a non-relativistic system. However, Fig. 2.2 exhibits situations where the vacuum makes a relevant contribution to the longitudinal permittivity ϵ_L.

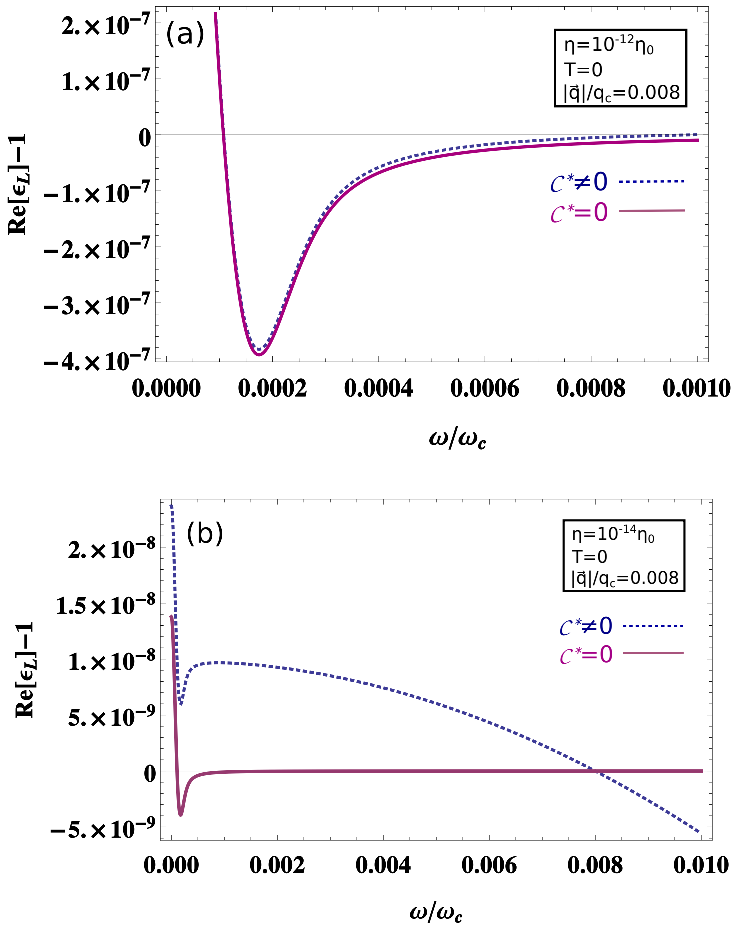

Figure 2.2: Plot of (Re $\epsilon_L - 1$) for low densities of the electron gas at $T = 0$. The dashed line has the vacuum contribution ($\mathscr{C}^* \neq 0$), whereas the full line only has the medium contribution ($\mathscr{C}^* = 0$). (a) Electron density $\eta = 10^{-12}\eta_0$ and (b) $\eta = 10^{-14}\eta_0$, where $\eta_0 \approx 1.76 \times 10^{30}$ cm^{-3}. Both the frequency and wave vector are given in units of $\omega_c = mc^2/\hbar$, the Compton frequency, and $q_c = mc/\hbar$, the Compton wave vector.

We have obtained relativistic expressions for the longitudinal responses of the relativistic Fermi gas at finite temperature and density. It is useful to analyze the long-wavelength limity, $|\vec{q}| \to 0$, where the wavelength of the radiation is much larger than the Compton wavelength of the electrons. In particular, for $T = 0$, the electric permittivity ϵ and the inverse of magnetic permeability μ^{-1} have Drude-type responses in the relativistic case for $|\vec{q}| \to 0$ (Appendix F).

$$\epsilon = 1 - \frac{\omega_e^2}{\omega^2} + \frac{e^2}{3\pi^2} g_e(\zeta) + \mathcal{O}\left(\frac{\omega^2}{4m^2}\right), \tag{2.48}$$

$$\mu^{-1} = 1 - \frac{\omega_m^2}{\omega^2} + \frac{5e^2}{6\pi^2} g_m(\zeta) + \mathcal{O}\left(\frac{\omega^2}{4m^2}\right), \tag{2.49}$$

where $\zeta \equiv \xi/m$. We note that there is a relation between ω_m and ω_e, i.e, $\omega_m = \sqrt{2}\omega_e$, and the vacuum contribution is $\mathcal{O}(\omega^2/4m^2)$. These Drude-type expressions imply that the electric and magnetic responses may be simultaneously negative for small frequencies ω. This is only due to the medium contribution, since the vacuum contribution is of order $(\omega^2/4m^2)$, and does not exhibit any such behavior. However, as we will show, taking the long-wavelength limit after the nonrelativistic limit of the system yields a Drude expression only for ϵ, but not for μ^{-1}.

2.4 Nonrelativistic limit

Nonrelativistic expressions for the dielectric functions [27, 61] will follow whenever $|\xi - m| \ll m$ and $\beta m \gg 1 (m \gg T)$. The total energy of each fermion, for $|\vec{p}| \ll m$, is

$$\omega_p = \sqrt{m^2 + |\vec{p}|^2} \approx m + \frac{|\vec{p}|^2}{2m}. \tag{2.50}$$

Looking at the Fermi-Dirac distribution, we have

$$\omega_p - \xi \approx \frac{|\vec{p}|^2}{2m} - \xi' \ll m \tag{2.51}$$

$$\omega_p + \xi \approx m + \xi + |\vec{p}|^2/2m \geq 2m \tag{2.52}$$

where $\xi' = \xi - m$. The expression in (2.52) implies that $\beta(\omega_p + \xi) \gg 1$, so the Fermi-Dirac distribution in the nonrelativistic limit becomes

$$
\begin{aligned}
n_F(p) \to n(p) &= \frac{1}{e^{\beta(\omega_p-\xi)}+1} + \mathcal{O}(e^{-2\beta m}) \\
&\approx \frac{1}{e^{\beta(\varepsilon_{\vec{p}}-\xi')}+1},
\end{aligned} \tag{2.53}
$$

where we have defined $\varepsilon_{\vec{p}} \equiv \frac{|\vec{p}|^2}{2m}$. With that in mind, we will calculate the nonrelativistic limit of the scalar functions $\mathscr{A}(q_4,\vec{q})$ and $\mathscr{B}(q_4,\vec{q})$ defined in Euclidean space. Taking the limit of $\omega_P \approx m \to p_4 \approx im$, we write (2.23) as

$$
\mathscr{A} - \left(1 - \frac{3q^2}{2|\vec{q}|^2}\right)\mathscr{B} = \frac{-e^2}{4\pi^3(|\vec{q}|^2+q_4^2)}\mathrm{Re}\int d^3p\, n(p)\frac{-1+\frac{\vec{p}\cdot\vec{q}}{m^2}+i\frac{q_4}{m}}{\frac{|\vec{q}|^2-2\vec{p}\cdot\vec{q}}{2m} - iq_4 + \frac{q_4^2}{2m}}. \tag{2.54}
$$

Since $q_4 = 2\pi nT$, this leads to $q_4/m \sim T/m \ll 1$, and $q_4 \sim |\vec{q}|^2/2m$, with $q_4^2 \ll \vec{q}^2$. Then, we obtain

$$
\mathscr{A} - \left(1 - \frac{3}{2}\right)\mathscr{B} = \frac{e^2}{4\pi^3}\mathrm{Re}\int d^3p\, n(p)\frac{1}{\varepsilon_{\vec{p}+\vec{q}} - \varepsilon_{\vec{p}} - iq_4}. \tag{2.55}
$$

If we perform the same steps for $\mathscr{B}(q_4,\vec{q})$ in eq.(2.24), we also obtain

$$
\frac{1}{2}\mathscr{B}(q_4,\vec{q}) = \frac{e^2}{4\pi^3}\mathrm{Re}\int d^3p\, n(p)\frac{1}{\varepsilon_{\vec{p}+\vec{q}} - \varepsilon_{\vec{p}} - iq_4}, \tag{2.56}
$$

which is the same result obtained in (2.55). So we conclude that $\mathscr{A}(q_4,\vec{q}) = 0$ in the nonrelativistic limit. Taking the vaccum contribution $\mathscr{C}^* = 0$, we have $\epsilon' = \nu' = 0$, and the longitudinal response $\epsilon_L \equiv \epsilon \approx 1 + \mathscr{B}$. Letting $q_4 \to i\omega + \gamma$ and performing a change of variables $\vec{p} - \vec{q} = \vec{p}'$ in (2.56), we may convert the expression of the electric permittivity to the well known Lindhard [62] formula of the dielectric function at finite temperature

$$
\epsilon(\omega,\vec{q}) = 1 - \frac{e^2}{4\pi^3|\vec{q}|^2}\mathrm{Re}\int d^3p\frac{n(\vec{p}+\vec{q}) - n(\vec{p})}{\varepsilon_{\vec{p}+\vec{q}} - \varepsilon_{\vec{p}} - \omega - i\gamma}. \tag{2.57}
$$

Let us analyze the long-wavelength of the nonrelativistic limit expression in (2.56). By taking the real part and integrating over angles, we obtain

$$
\mathscr{B}^*(\omega,\vec{q}) = \frac{e^2 m}{2\pi|\vec{q}|^3}\int_0^\infty dp\; p\; n(p)\ln\frac{\left(|\vec{q}|^2 + 2p\vec{q}\right)^2 - 4m^2\omega^2}{\left(|\vec{q}|^2 + 2p\vec{q}\right)^2 - 4m^2\omega^2}. \tag{2.58}
$$

At $T = 0$, the Fermi-Dirac distribution becomes $n(p) \to \Theta(p_F - \xi')$, where $\Theta(x)$ is the Heaviside step function, and $p_F = \sqrt{2m\xi'}$ is the Fermi momentum. Expanding the equation above in the limit of $|\vec{q}| \to 0$, and integrating over p, we obtain

$$\mathscr{B}^*(\omega, \vec{q}) = -\frac{e^2}{3\pi^2 m}\frac{p_F^3}{\omega^2}, \tag{2.59}$$

so the electric permittivity $\epsilon = 1 + \mathscr{B}^*$ becomes

$$\epsilon = 1 - \frac{\omega_e^2}{\omega^2}, \tag{2.60}$$

where $\omega_e^2 = \eta e^2/m$ is the plasmon frequency, with electron density $\eta = p_F^3/(3\pi^2)$ $(\hbar = 1)$. So, in the nonrelativistic limit we also obtained a Drude-type expression in the long-wavelength limit, which implies negative values when the frequency $\omega < \omega_e$. Therefore, if we make the same analysis for $\mu^{-1} = 1 - 2(\omega^2/|\vec{q}|^2)\mathscr{B}^*$, in the limit of $|\vec{q}| \to 0$ of the nonrelativistic expression, we obtain $\mu^{-1} \approx 1$. In addition, the term $\tau = -(\omega/|\vec{q}|)\mathscr{B}^* \to 0$ in the long-wavelength limit, and we recover the usual isotropy of the vector $\vec{D} = \epsilon\vec{E}$ and $\vec{H} = \mu^{-1}\vec{B}$. Thus, we may conclude that the only way to obtain both ϵ and μ negative, is in a relativistic system as we have showed.

2.5 The chemical potential

To compute the electromagnetic responses of the REG through equations (2.41) - (2.44), one needs to obtain the chemical potential ξ, which depends on the temperature and carrier density. The carrier density is $\eta = \Delta N/V$, where $\Delta N = N^- - N^+$ is the difference between the N^- number of particles and the N^+ number of antiparticles in the system. Then, one needs to solve the transcedental equation [17]

$$\Delta N = N^- - N^+ = \sum_{\vec{p}} g f(p, \beta, \xi), \tag{2.61}$$

where

$$f(p, \beta, \xi) = \frac{1}{e^{\beta(\Omega_p - \xi)} + 1} - \frac{1}{e^{\beta(\Omega_p + \xi)} + 1} \tag{2.62}$$

is the distribution function accouting for the presence of both particles and antiparticles, $\Omega_p = \sqrt{p^2c^2 + m^2c^4}$ is the relativistic energy of a carrier with momentum p, and $g = 2$ is the degeneracy factor of the electron gas. Equation (2.61) reduces to

$$\tilde{\eta} = \frac{\eta}{\eta_0} = \int_0^\infty dy\, y^2 f(y, \tilde{\beta}, \tilde{\xi}). \tag{2.63}$$

where $\eta_0 = g q_c^3/(2\pi^2) \approx 1.76 \times 10^{30} cm^{-3}$. Here, we have defined the dimensionless variables $y = p/mc$, $\tilde{\beta} = \beta mc^2$ and $\tilde{\xi} = \xi/mc^2$, and $q_c = mc/\hbar$. The term η_0 only depends on universal constants and may therefore be used as a natural unit to measure the effective carrier density η of the *REG*. It should be noted from (2.62) that $f(y, \tilde{\beta}, \tilde{\xi}) = -f(y, \tilde{\beta}, -\tilde{\xi})$, i.e., $f = f(y, \tilde{\beta}, \tilde{\xi})$ is an odd function of the chemical potential. Eq. (2.63) implicitly defines the function $\tilde{\xi} = \tilde{\xi}(\tilde{\beta}, \tilde{\eta})$. One sees that $\tilde{\eta} = 0$ leads to $\eta/\eta_0 = 0$, a case with corresponds to the vacuum.

The chemical potential as a function of $\tilde{\beta}$ is is displayed in fig. 2.3. Calculations were performed for three different values of the density expressed in units of η_0. The numerical results suggest a weak temperature dependence of the chemical potential, if compared with $mc^2 \approx 0.511$MeV, in the low-temperature limit ($\tilde{\beta} \to \infty$). Actually, the chemical potential exhibits variations of a few eV in the low-temperature limit, a fact which agrees with the non-relativistic theory of the electron gas (see below).

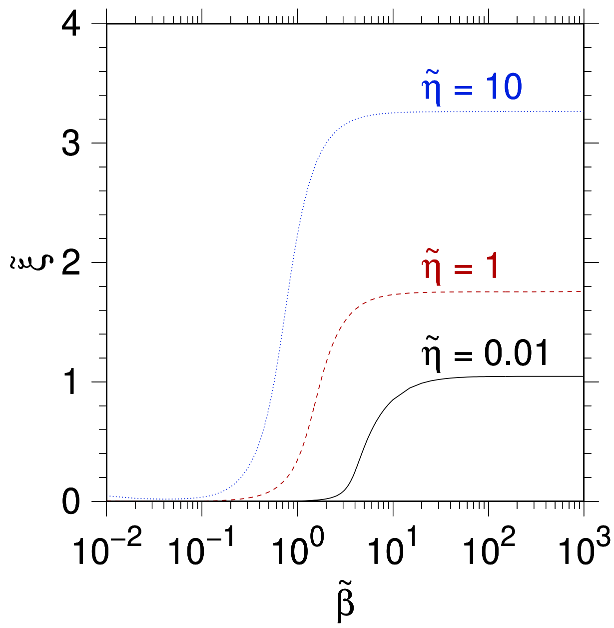

Figure 2.3: Chemical potential as a function of the gas temperature. Solid, dashed, and dotted lines correspond to $\tilde{\eta} = 0.01$, $\tilde{\eta} = 1$, and $\tilde{\eta} = 10$, respectively.

The chemical potential is displayed in Figure 2.4 as a function of the density expressed in units of η_0. Numerical results were obtained for three different values of the gas temperature. The chemical potential is a growing monotomic function of $\tilde{\eta}$. One may note that the chemical pontetials for $\tilde{\beta} = 10$ and $\tilde{\beta} = 100$ essentially coincide in the scale of the figure [cf. dashed and doted lines in Figure 2.4]. The ratio $\rho = N^+/N^-$, as a function of $\tilde{\beta}$ is

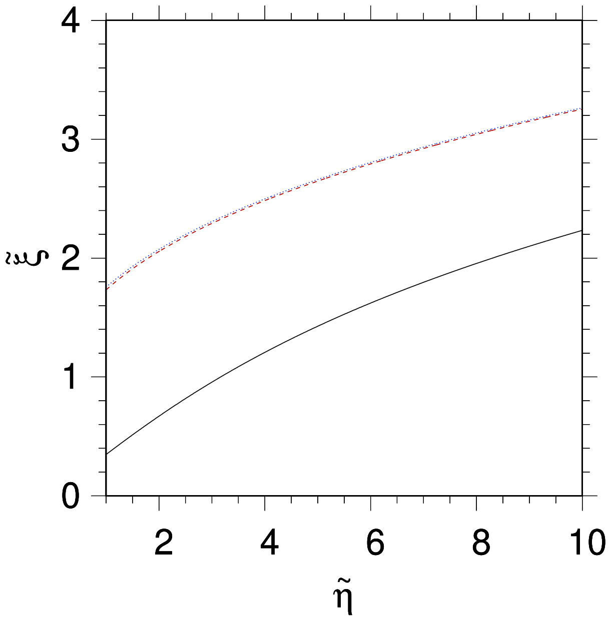

Figure 2.4: Chemical potential as a function of the gas density. Solid, dashed, and dotted lines correspond to $\tilde{\beta} = 1$, $\tilde{\beta} = 10$, and $\tilde{\beta} = 100$, respectively.

displayed in Figure 2.5 for various values of the density, where

$$\rho = \frac{N^+}{N^-} = \frac{\int_0^\infty dy \frac{y^2}{e^{\tilde{\beta}\left(\sqrt{y^2+1}+\tilde{\xi}\right)}+1}}{\int_0^\infty dy \frac{y^2}{e^{\tilde{\beta}\left(\sqrt{y^2+1}-\tilde{\xi}\right)}+1}}. \tag{2.64}$$

For a given temperature, it is apparent that the number of particles exceeds the number of antiparticles in all cases, and the ratio $\rho = N^+/N^-$ decreases as the density of particles in the electron gas is increased, as expected. One may also note that $\rho \to 0$ as $\tilde{\beta} \to \infty$, since in the low-temperature limit one has $N^+ \ll N^-$. In other words, in the limit of $\tilde{\beta} \to \infty$, the term corresponding to the occupation factor of antiparticles in the Fermi-Dirac distribution function [cf. the second term in the RHS of Equation 2.62] may essentially be neglected ($N^+ \ll N^-$), and the non-relativistic limit of the Fermi-Dirac distribution function is eventually recovered.

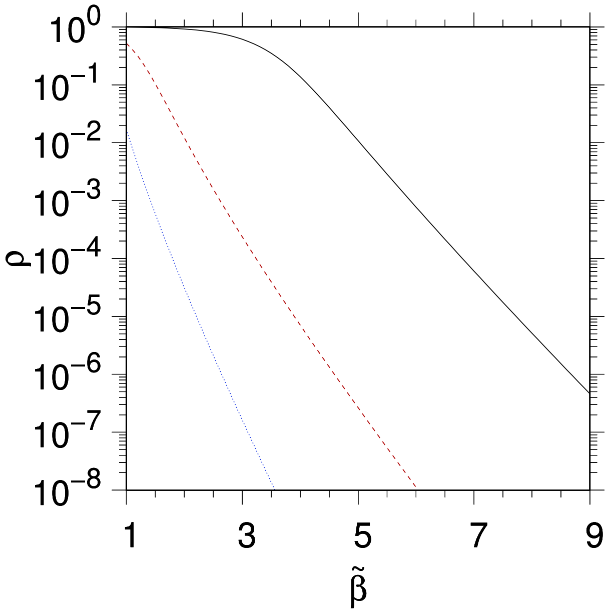

Figure 2.5: The ration $\rho = N^+/N^-$ [cf. Equation (2.64)] as a function of of $\tilde{\beta}$. Solid, dashed, and dotted lines correspond to $\tilde{\eta} = 0.01$, $\tilde{\eta} = 1$, and $\tilde{\eta} = 10$, respectively.

We have also explored the behavior of the chemical potential for density and temperature values appropriate for solid-state materials. In this respect, we have defined

$$\xi_e(T) = \xi(T) - mc^2 \tag{2.65}$$

as the non-relativistic chemical potential. According to the non-relativistic theory of the free-electron gas, it is well known that [28]

$$\xi_e(T) \approx E_F \left[1 - \frac{\pi^2}{12} \left(\frac{T}{T_F} \right)^2 \right], \tag{2.66}$$

where

$$E_F = \left(\frac{6\pi^2}{g} \eta \right)^{2/3} \frac{\hbar^2}{2m} \tag{2.67}$$

is the Fermi-Energy and $T_F = E_F / k_B$ is the Fermi temperature. The chemical potential ξ_e is depicted in Figure 2.6 as a function of the gas temperature. Calculations in Figure 2.6a were performed for three different values of η varying within the range exhibited by most of the solid-state materials. In Figure 2.6b, we have assumed $\eta \approx 2.0 \times 10^{23} \text{cm}^{-3}$, corresponding to the electron density in silicon. The solid line corresponds to the result computed by combining Equations (2.63) and (2.65), whereas the dashed line was obtained from Equation (2.66). The Fermi energy computed from the non-relativistic electron-gas model [cf. full dot in the vertical axis of Figure 2.6b and Equation (2.67)] essentially coincides with the numerical result obtained from Equations (2.63) and (2.65) in the limit $T \to 0$. Low-temperature results obtained from the non-relativistic model agree with those derived from the relativistic theory, as expected.

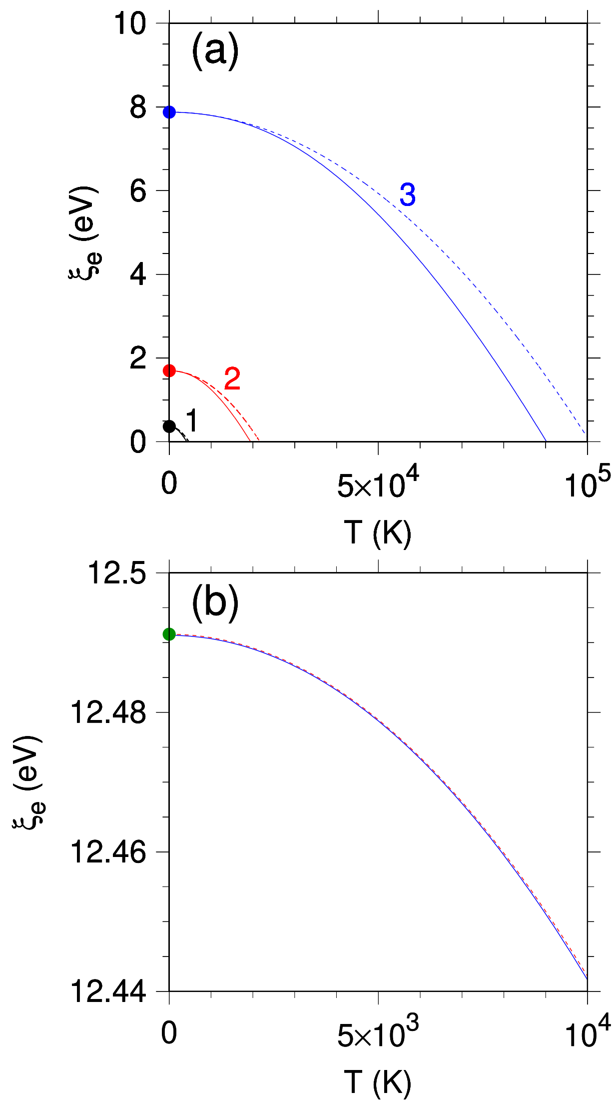

Figure 2.6: Chemical potential measured with respect to the mc^2 rest energy [cf. Equation (2.65)], as a function of the gas temperature for different values of the η gas density. Solid and dashed lines corresponds to numerical results obtained from Equations (2.63) and (2.66), respectively. The set of curves 1, 2, and 3 in (a) correspond to $\eta = 10^{21}\mathrm{cm}^{-3}$, $\eta = 10^{22}\mathrm{cm}^{-3}$, and $\eta = 10^{23}\mathrm{cm}^{-3}$, respectively. In (b), calculations were performed for η corresponding to the electron density in silicon. The full dot in the left vertical axis corresponds to the Fermi energy obtained from Equation (2.67)

Chapter 3

Propagation in the relativistic electron gas

3.1 Introduction

We compute the real and imaginary parts of the electric permittivities and magnetic permeabilities of relativistic electrons from quantum electrodynamics at finite temperatures and densities, for weak fields, neglecting electron–electron interactions. For non-zero temperatures, electromagnetic responses are reduced to one-dimensional integrals computed numerically. For zero temperature, we find analytic expressions for both their real/dispersive and imaginary/absorptive parts. As an application of our results, we obtain the dispersion relation for longitudinal electric plasmons. Present calculations support our recent claim that, at low frequencies and long wavelengths, the system will exhibit simultaneously negative electric and magnetic response

Dispersion relations for the plasmon modes at zero and finite temperatures are presented and the intervals of frequency and wavelength where both electric and magnetic responses are simultaneously negative are identified, a behavior previously thought not to occur in natural systems. The investigation of the electromagnetic responses of a relativistic electron gas shows that, apart from the usual longitudinal electric plasmon mode and the two transverse magnetic plasmon modes, there is also a pure photonic mode that propagates with the speed of light, as if the medium were transparent.

3.2 Real and imaginary parts of longitudinal responses ϵ_L and ν_L

Let us write the functions (2.23) and (2.24) as

$$\mathscr{B}^* = -\frac{e^2}{\pi^2 q^2}\int_0^\infty \frac{p^2 dp}{\omega_p} n_F(p)\left[1+\frac{4\omega_p^2+q^2}{8p|\vec{q}|}L_1+\frac{\omega_p\omega}{p|\vec{q}|}L_2\right], \tag{3.1}$$

$$\mathscr{D}^* = -\frac{e^2}{\pi^2 q^2}\int_0^\infty \frac{p^2 dp}{\omega_p} n_F(p)\left[1+\frac{2m^2+q^2}{8p|\vec{q}|}L_1\right], \tag{3.2}$$

where $\mathscr{D}^* = \mathscr{A}^* - \left[1+3q^2/(2|\vec{q}|^2)\mathscr{B}^*\right]$, and the functions L_1 and L_2 are given by

$$L_1 = \ln\left\{\frac{(\chi^2-by)^2-a^2x^2}{(\chi^2+by)^2-a^2x^2}\right\}, \tag{3.3}$$

$$L_2 = \ln\left|\frac{\chi^2-by+ax}{\chi^2+by+ax}\right| - \frac{L_1}{2}, \tag{3.4}$$

where we have used dimensionless variables $x \equiv \omega_p/m$, $y \equiv p/m = \sqrt{x^2-1}$, $a \equiv \omega/2m$, $b \equiv |\vec{q}|/2m$, and $\chi^2 \equiv a^2 - b^2 = q^2/4m^2$.

Real parts at $T \neq 0$

The real parts of $\mathscr{B}^*$ and $\mathscr{D}^*$ reduce to 1-D integrals. We write them as

$$\mathrm{Re}\mathscr{B}^* = \frac{-e^2}{4\pi^2\chi^2}\left(\int_1^\infty dx\, n_F\sqrt{x^2-1}+\frac{1}{4b}\int_1^\infty dx\, n_F\left[(x^2+\chi^2R_1+4axR_2)\right]\right), \tag{3.5}$$

$$\mathrm{Re}\mathscr{D}^* = \frac{-e^2}{4\pi^2\chi^2}\left(\int_1^\infty dx\, n_F\sqrt{x^2-1}+\frac{1}{8b}\int_1^\infty dx\, n_F\left[1+2\chi^2\right]R_1\right), \tag{3.6}$$

with $R_1 \equiv \mathrm{Re}L_1$ and $R_2 \equiv \mathrm{Re}L_2$. Since $\mathscr{C}^*$ is real, we obtain

$$\mathrm{Re}\,\epsilon_L = 1+\mathscr{C}^*-\frac{\chi^2}{b^2}\mathrm{Re}\mathscr{B}^*, \tag{3.7}$$

$$\mathrm{Re}\,\nu_L = 1+2\mathscr{C}^*+2\mathrm{Re}\mathscr{D}^*+\frac{\chi^2}{b^2}\mathrm{Re}\mathscr{B}^*. \tag{3.8}$$

The result above allows for the calculation of plasmon dispersion relations, as we will show later on.

Imaginary parts at $T \neq 0$

The vacuum contribution does not have an imaginary part. On the other hand, imaginary parts for $\mathscr{B}^*$ and $\mathscr{D}^*$ will appear whenever the argument in L_1 becomes negative (note that $\mathrm{Im}L_2 = -\mathrm{Im}L_1/2$). For that to occur, the product of the numerator $\mathfrak{N}$ times the denominator $\mathfrak{D}$ of the argument must satisfy,

$$\mathfrak{N}\mathfrak{D} = [(\chi^2 - by)^2 - a^2x^2][(\chi^2 + by)^2 - a^2x^2] < 0. \tag{3.9}$$

The roots of the related biquadratic equation in x (≥ 0) are $x_\pm = a \pm b\eta$, where $\eta^2 \equiv 1 - (1/\chi^2)$, leading to the condition $(a - b\eta)^2 < x^2 < (a + b\eta)^2$. Three cases have to be considered:

(i) $\chi^2 < 0$ $(\eta > 1; a < b < b\eta) : -a + b\eta < x < a + b\eta$;

(ii) $0 < \chi^2 < 1$ (η pure imaginary): the condition is never satisfied and $\mathrm{Im}L_1 = 0$;

(iii) $\chi^2 > 1$ $(\eta < 1; a > b > b\eta)$: $a - b\eta < x < a + b\eta$.

The difference between numerator $\mathfrak{N}$ and denominator $\mathfrak{D}$ is given by $-\chi^2 by$. For case (i), this implies $\mathfrak{N} > 0$, $\mathfrak{D} < 0$, whereas for case (iii) $\mathfrak{N} < 0$, $\mathfrak{D} > 0$. For case (ii), $0 < \chi^2 < 1$, corresponding to the same sign for $\mathfrak{N}$ and $\mathfrak{D}$, $\mathrm{Im}\mathscr{B}^* = \mathrm{Im}\mathscr{D}^* = 0$. For cases (i) and (iii), we take $\mathrm{Im}L_1 = \mathrm{sign}(\mathfrak{N})\pi$. The choice of sign corresponds to the continuation $q_4 \to i\omega - 0^+$. For the longitudinal responses, we have

$$\mathrm{Im}\,\epsilon_L = -\frac{\mathrm{sign}(\chi^2)e^2}{16\pi b^3}\int_{x_l}^{a+b\eta} dx\, n_F\left[(x-a)^2 - b^2\right], \tag{3.10}$$

$$\mathrm{Im}\,\nu_L = \frac{\mathrm{sign}(\chi^2)e^2}{16\pi b\chi^2}\int_{x_l}^{a+b\eta} dx\, n_F\left((1+2\chi^2)\right) - \mathrm{Im}\,\epsilon_L. \tag{3.11}$$

The regions where imaginary parts are non-vanishing are shown in figure 3.1. $\mathrm{Im}\,\epsilon_L$ and $\mathrm{Im}\,\nu_L$ vanish in region (ii) of the (a,b) plane. In region (i) $x_l = -a + b\eta$ and in region (iii) $x_l = a - b\eta$. Using expressions for the imaginary parts in regions (i) and (iii), we may see how their values evolve from $T = 0$ to non-zero temperatures. This is shown in figure 3.2. One should note that the appearance of non-zero imaginary parts is associated with the creation of electron-hole (lower energies) or electron-positron (higher energies) pairs.

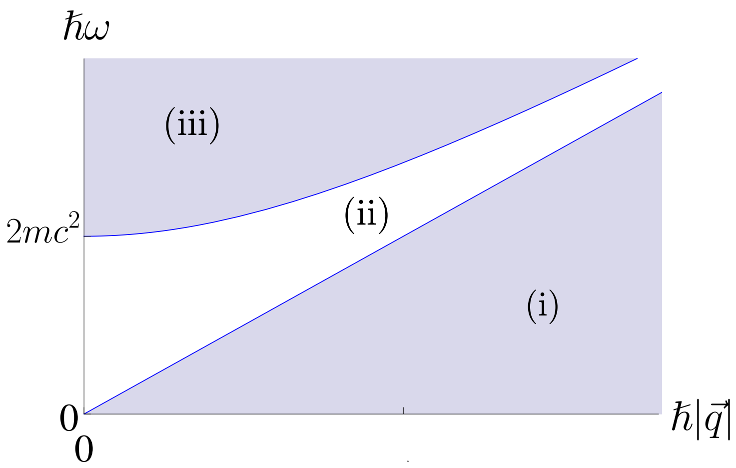

Figure 3.1: Regions of the $(a,b) \sim (\hbar\omega, \hbar|\vec{q}|)$ plane where the imaginary parts of the responses are given by different expressions. In region (ii), they always vanish, whereas in regions (i) and (iii) they are given by (3.10) and (3.11).

We have thus derived electromagnetic responses as functions of a, b, T/m, and ξ/m, the two latter ones coming from the Fermi-Dirac distribution function.

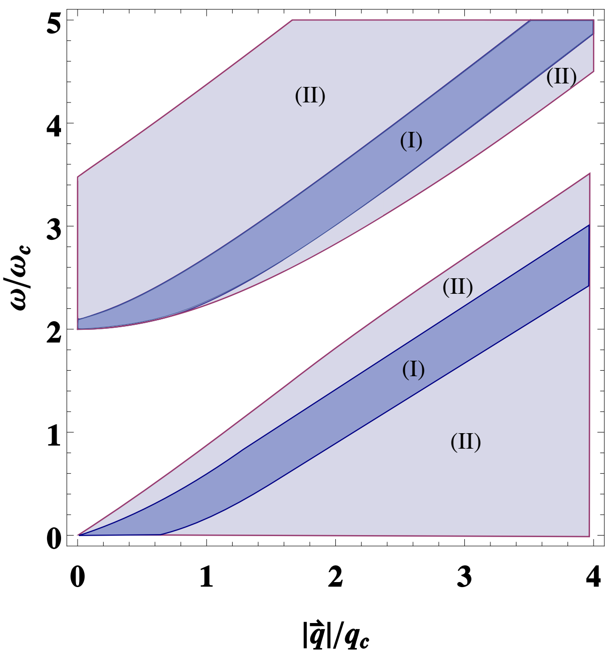

Figure 3.2: Evolution with temperature of the regions of the $(a,b) \sim (\hbar\omega, \hbar|\vec{q}|)$ plane with non-vanishing imaginary parts. As $\tilde{\beta}$ decreases, the two $T = 0$ regions (labeled I) expand. For a value of $\tilde{\beta} = 10^3$, imaginary parts appear in all regions labelled I and II. Eventually, as $T \to \infty$, only the unshaded region of figure 3.1 will have vanishing imaginary parts.

Imaginary parts at $T = 0$

At $T = 0$, we have $n_F(x) \to \Theta(x_F - x)$, with $x_F \equiv \varepsilon_F/m = \xi/m$ and $y = (1/m)\sqrt{\varepsilon_F^2 - m^2}$, where ε_F is the Fermi energy. We may analytically perform the integrals for both imaginary and real parts of the response functions. Additional restrictions come into play because of the integration limit x_F imposed by the function $\Theta(x_F - x)$.

From calculations in 3.2, we identify four regions in the (a, b) plane where longitudinal responses will have different values. We use $[f(x)]_{x_l}^{x_u} \equiv f(x_u) - f(x_l)$ and refer the reader to the appendix G for the calculation of $b_\pm$, $\bar{b}_\pm$, $b'_\pm$ and $\bar{b}'_\pm$. The regions are

Region (A): for $0 < a < (x_F - 1)/2$ **and** $(x_F + 1)/2 < a < x_F$**,** $\bar{b}_- < b < \bar{b}_+$**,** $x_L = -a + b\eta$**,** $x_u = a + b\eta$**,**

$$\mathrm{Im}\,\epsilon_L = \frac{e^2}{48\pi b^3}\left[(x-a)^3 - 3b^2 x\right]_{-a+b\eta}^{a+b\eta}, \tag{3.12}$$

$$\mathrm{Im}\,\nu_L = -\frac{e^2}{16\pi b\chi^2}\left[2a(1+2\chi^2)\right] - \mathrm{Im}\,\epsilon_L. \tag{3.13}$$

Region (B): for $(x_F - 1)/2 < a < (x_F + 1)/2$ **and** $a > x_F$**,** $b_- < b < b_+$**,** $x_L = -a + b\eta$**,** $x_u = x_F$**,**

$$\mathrm{Im}\,\epsilon_L = \frac{e^2}{48\pi b^3}\left[(x-a)^3 - 3b^2 x\right]_{-a+b\eta}^{x_F}, \tag{3.14}$$

$$\mathrm{Im}\,\nu_L = -\frac{e^2}{16\pi b\chi^2}\left[(x_F + a - b\eta)(1+2\chi^2)\right] - \mathrm{Im}\,\epsilon_L. \tag{3.15}$$

Outside regions (A) and (B), for $\chi^2 < 0$ the imaginary parts of ϵ_L and ν_L vanish.

Region (C): for $0 < a < (x_F - 1)/2$ **and** $(x_F + 1)/2 < a < x_F$**,** $\bar{b}'_- < b < \bar{b}'_+$**,** $x_L = -a + b\eta$**,** $x_u = a + b\eta$**,**

$$\mathrm{Im}\,\epsilon_L = -\frac{e^2}{48\pi b^3}\left[(x-a)^3 - 3b^2 x\right]_{a-b\eta}^{a+b\eta}, \tag{3.16}$$

$$\mathrm{Im}\, \nu_L = \frac{e^2}{16\pi b\chi^2}\left[2b\eta(1+2\chi^2)\right] - \mathrm{Im}\,\epsilon_L. \tag{3.17}$$

Region (D): for $(x_F-1)/2 < a < (x_F+1)/2$ **and** $a > x_F$**,** $b'_- < b < b'_+$**,** $x_L = a - b\eta$**,** $x_u = x_F$**,**

$$\mathrm{Im}\,\epsilon_L = -\frac{e^2}{48\pi b^3}\left[(x-a)^3 - 3b^2x\right]_{a-b\eta}^{x_F}, \tag{3.18}$$

$$\mathrm{Im}\, \nu_L = \frac{e^2}{16\pi b\chi^2}\left[(x_F - a + b\eta)(1+2\chi^2)\right] - \mathrm{Im}\,\epsilon_L. \tag{3.19}$$

Outside regions (C) and (D), for $\chi^2 > 1$ the imaginary parts of ϵ_L and ν_L vanish.

Finally, in case (ii), $0 < \chi^2 < 1$, one has $\mathrm{Im}\,\epsilon_L = \mathrm{Im}\,\nu_L = 0$. The various regions of the (a,b) plane that correspond to the different expressions discussed above are depicted in Fig. 3.3

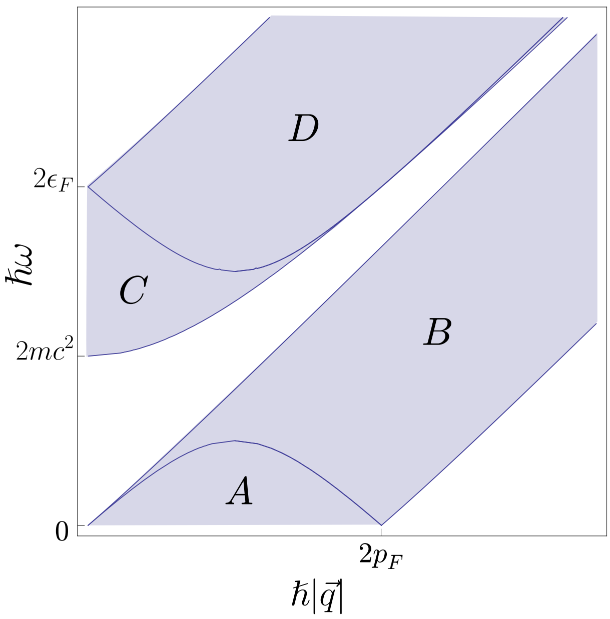

Figure 3.3: Regions in the $(a,b) \sim (\hbar\omega, \hbar|\vec{q}|)$ plane where the imaginary parts are non vanishing for $T=0$. The limits of regions A, B, C, D and the values of the longitudinal responses in each of them are shown in 3.2

Real parts at $T = 0$

For the real parts at $T = 0$, we replace n_F with $\Theta(x_F - x)$ in (3.5) and (3.6). The calculations detailed in G.2 lead to

$$\mathrm{Re}\,\mathscr{B}^* = \frac{-e^2}{4\pi\chi^2}\,[X_B + Y_B + Z_B]\,, \tag{3.20}$$

$$\mathrm{Re}\,\mathscr{D}^* = \frac{-e^2}{4\pi\chi^2}\,[X_D + Y_D + Z_D]\,, \tag{3.21}$$

where X_B, X_D, Y_B and Y_D are given by ($R_i = \mathrm{Re}L_i$)

$$X_B = \frac{x_F}{12b}[(x_F^2 + 3\chi^2)R_1(x_F) + 6ax_F R_2(x_F)], \tag{3.22}$$

$$X_D = \frac{x_F}{8b}(1 + 2\chi^2)R_1(x_F), \tag{3.23}$$

$$Y_B = \frac{2}{3}[x_F y_F - b^2 \ln(x_F + y_F)], \tag{3.24}$$

$$Y_D = \frac{1}{2}[x_F y_F + 2\chi^2 \ln(x_F + y_F)], \tag{3.25}$$

whereas Z_B and Z_D are given by

$$Z_{B,D} = C_{B,D}[(M_{B,D} + N_{B,D})\mathfrak{I}_0 - N_{B,D}\mathfrak{I}_2]. \tag{3.26}$$

$C_{B,D}(a,b)$, $M_{B,D}(a,b)$, $N_{B,D}(a,b)$, and the integrals $\mathfrak{I}_0(a,b,x_F)$ and $\mathfrak{I}_2(a,b,x_F)$ are defined and calculated in G.15. The longitudinal responses (2.46) and (2.47) are given by

$$\mathrm{Re}\,\epsilon_L = 1 + \mathscr{C}^* + \frac{e^2}{4\pi^2 b^2}[X_B + Y_B + Z_B], \tag{3.27}$$

$$\mathrm{Re}\,\nu_L = 1 + 2\mathscr{C}^* - \frac{e^2}{2\pi^2\chi^2}[X_D + Y_D + Z_D] - \frac{e^2}{4\pi^2 b^2}[X_B + Y_B + Z_B]. \tag{3.28}$$

3.3 Plasmon excitations

Electromagnetic responses may be used to obtain the dispersion relations for plasmon modes that propagate when external electromagnetic fields induce resonant charge density collective oscillations in the electron gas. The dispersion relation for longitudinal electric plasmons, for instance, is obtained from the well-known condition $\epsilon_L = 0$ [26, 28, 63, 64, 65]. As an application of our formulae, we will use our expressions for $\mathrm{Re}\,\epsilon_L$ and $\mathrm{Im}\,\epsilon_L$ to obtain it.

The solutions to $\mathrm{Re}\,\epsilon_L = 0$ are plotted in Fig. 3.4, for $T = 0$. Since we must have $\epsilon_L = 0$, the full curve in the figure is the physical one, because most of it lies in the unshaded region, where we also have $\mathrm{Im}\,\epsilon_L = 0$. The dashed curve lies completely in the region where there is an imaginary part, so that it never satisfies $\epsilon_L = 0$. The shaded region in Fig.3.4 is the same as the lower region of Fig. 3.3, where $\mathrm{Im}\,\epsilon_L \neq 0$. The dashed curve is fully within that region and thus a decaying mode, whereas the full curve lies mostly in the region where $\mathrm{Im}\,\epsilon_L = 0$. Thus, it describes a plasmon mode. As the curve enters the region where there is an imaginary part, the plasmon mode becomes unstable to the decay into electron-hole pairs, just as in the nonrelativistic case.

Analytic results at $T = 0$ and numerical results at $T \neq 0$ may be used to compute decay constants and dispersion relations for both longitudinal and transverse plasmons. A complete discussion of the modes that propagate in the relativistic electron gas is presented in the next section 3.4.

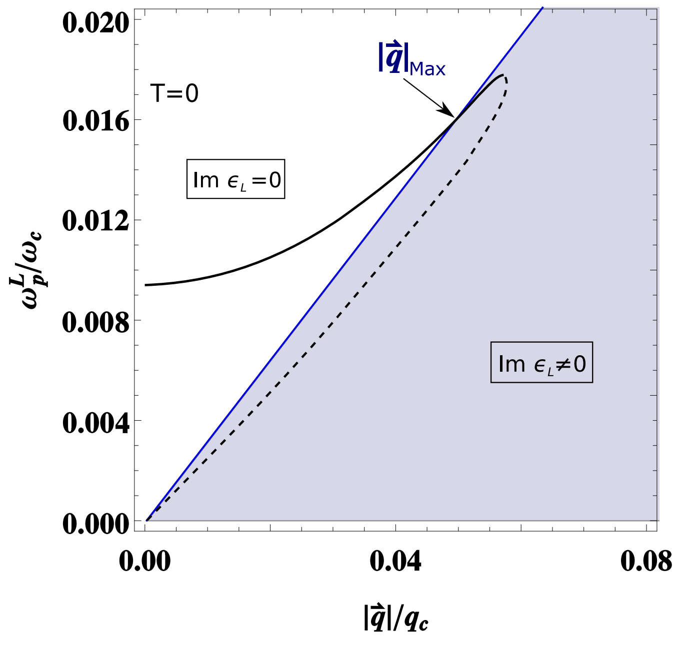

Figure 3.4: Upper (ω_p^L plasmon frequency) and lower frequency zeroes of ϵ_L (Solid and dashed lines, respectively) as functions of the $|\vec{q}|$ wave vector. Calculations were performed for $\tilde{\beta} \to \infty$ ($T = 0$) by taking the density electron gas $\eta = 10^{-2}\eta_0$, where $\eta_0 \approx 1.76 \times 10^{30}\mathrm{cm}^{-3}$. The shaded area corresponds to the region where electron-hole excitations occur. Note the maximum value of the wave vector ($|\vec{q}|_{max}$) beyond which the longitudinal plasmon decays into electron-hole pairs.

3.4 Collective excitations and plasmon modes

To obtain the collective modes of oscillation, we compute how the medium affects the photon propagator in the electron gas. We rewrite the grand partition function of QED in eq (2.6) as a quadratic functional integral

$$\Xi = \oint [dA_\mu] \det[-\partial^2] \exp\left(-\frac{1}{2\beta}\sum_{n=-\infty}^{\infty}\int \frac{d^3q}{(2\pi)^3} A_\mu \Gamma_{\mu\nu} A_\nu\right), \tag{3.29}$$

where the quadratic kernel $\Gamma_{\mu\nu}$ is

$$\Gamma_{\mu\nu} = q^2\delta_{\mu\nu} - \left(1 - \frac{1}{\lambda}\right) q_\mu q_\nu - \Pi_{\mu\nu}, \tag{3.30}$$

with $q^2 = q_4^2 + |\vec{q}|^2$The determinant comes from the Lorentz gauge condition, and λ is a gauge parameter. $\Pi_{\mu\nu} = \Pi_{\mu\nu}^{(v)} + \Pi_{\mu\nu}^{(m)}$ is the polarization tensor of QED defined in eq. (2.17). Following [22], we introduce the projector

$$\mathscr{P}_{\mu\nu} = \delta_{\mu\nu} - \frac{q_\mu q_\nu}{q^2} \tag{3.31}$$

and the transverse projector $\mathscr{P}_{ij}^T = \delta_{ij} - \hat{q}_i \hat{q}_j$, with $\mathscr{P}_{44}^T = \mathscr{P}_{4i}^T = 0$. The longitudinal projector is then $\mathscr{P}_{\mu\nu}^L \equiv \mathscr{P}_{\mu\nu} - \mathscr{P}_{\mu\nu}^T$. They obey

$$\mathscr{P}_{\mu\nu}^{(L,T)} \mathscr{P}_{\nu\sigma}^{(L,T)} = \mathscr{P}_{\mu\sigma}^{(L,T)}, \tag{3.32}$$

$$\mathscr{P}_{\mu\nu}^T \mathscr{P}_{\nu\sigma}^L = \mathscr{P}_{\mu\nu}^L \mathscr{P}_{\nu\sigma}^T = 0, \tag{3.33}$$

$$\mathscr{P}_{\mu\nu}^T q_\nu = \mathscr{P}_{\mu\nu}^L q_\nu = 0. \tag{3.34}$$

We may then write the polarization tensor with a longitudinal and transverse contribution, so that

$$\Pi_{\mu\nu} = \Pi_{\mu\nu}^{(v)} + \Pi_{\mu\nu}^{(m)} = F\mathscr{P}_{\mu\nu}^L + G\mathscr{P}_{\mu\nu}^T, \tag{3.35}$$

where F and G are scalar functions. From the vacuum and medium contributions to the polarization tensor defined in (2.20 - 2.22), and using the definition of the projectors $\mathscr{P}_{\mu\nu}$, we may write

$$\Pi_{\mu\nu}^{(v)} = -\mathscr{C} q^2 \mathscr{P}_{\mu\nu}, \tag{3.36}$$

$$\Pi_{\mu\nu}^{(m)} = -\left\{\mathscr{B}\left[\left(1 + \frac{q_4^2}{\vec{q}^2}\right)\mathscr{P}_{\mu\nu}^L + \frac{q_4^2}{\vec{q}^2}\mathscr{P}_{\mu\nu}^T\right] + \mathscr{A}\mathscr{P}_{\mu\nu}^T\right\} q^2. \tag{3.37}$$

By summing vacuum and medium contributions of $\Pi_{\mu\nu}$, we identify the functions F and G as

$$F = -q^2\left(\mathscr{C} + \mathscr{B} + \frac{q_4^2}{|\vec{q}|^2}\mathscr{B}\right), \tag{3.38}$$

$$G = -q^2\left(\mathscr{C} + \mathscr{A} + \frac{q_4^2}{|\vec{q}|^2}\mathscr{B}\right), \tag{3.39}$$

and we write the quadratic kernel as

$$\Gamma_{\mu\nu} = (q^2 - F)\mathscr{P}^L_{\mu\nu} + (q^2 - G)\mathscr{P}^T_{\mu\nu} + \frac{1}{\lambda}q_\mu q_\nu. \tag{3.40}$$

The inverse of photon propagator may be obtained from $\Gamma^{-1}_{\mu\nu}\Gamma_{\nu\sigma} = \delta_{\mu\sigma}$. If we write its inverse as

$$\Gamma^{-1}_{\mu\nu} = C_L\mathscr{P}^L_{\mu\nu} + C_T\mathscr{P}^T_{\mu\nu} + C_Q q_\mu q_\nu, \tag{3.41}$$

we obtain

$$C_L(q^2 - F)\delta_{\mu\sigma} + \left[C_T(q^2 - G) - C_L(q^2 - F)\right]\mathscr{P}^T_{\mu\sigma} + \left[\frac{C_Q}{\lambda}q^2 - \frac{C_L(q^2 - F)}{q^2}\right]q_\mu q_\nu = \delta_{\mu\sigma}. \tag{3.42}$$

We identify

$$\begin{aligned} C_L(q^2 - F) &= 1 \to C_L = \frac{1}{q^2 - F}, & (3.43)\\ C_L(q^2 - G) - C_L(q^2 - F) &= 0 \to C_L = \frac{1}{q^2 - G}, & (3.44)\\ \frac{C_Q}{\lambda}q^2 - \frac{C_L(q^2 - F)}{q^2} &= 0 \to C_Q = \frac{\lambda}{q^4}. & (3.45) \end{aligned}$$

The inverse of photon propagator reads

$$\Gamma^{-1}_{\mu\nu} = \frac{\mathscr{P}^L_{\mu\nu}}{q^2 - F} + \frac{\mathscr{P}^T_{\mu\nu}}{q^2 - G} + \frac{\lambda}{q^2}\frac{q_\mu q_\nu}{q^2}. \tag{3.46}$$

We now use Equations (3.38) and (3.39) and write the propagators in Minkowski space by letting $q_4 \to i\omega - 0^+$. We then obtain for the longitudinal and transverse propagator

$$\frac{1}{q^2 - F} \to \frac{1}{-q^2\epsilon_L}, \tag{3.47}$$

$$\frac{1}{q^2 - G} \to \frac{1}{-q^2(\nu_L + 1)}. \tag{3.48}$$

The poles of the photon propagator correspond to collective excitations, and yield their dispersion relations. In the $\mathscr{P}^L_{\mu\nu}$ longitudinal propagator in eq.(3.47), this occurs whenever the longitudinal electric permittivity is

$$\epsilon_L(\omega, \vec{q}) = 0, \tag{3.49}$$

leading to the usual Condensed Matter dispersion relation of the longitudinal plasmon collective excitation, which corresponds to an oscillation of the charge density of the gas. For $\epsilon_L(\omega, \vec{q})$ nonzero, Maxwell's equations lead to transverse fields ($\vec{q} \cdot \vec{E} = 0$), which means that the pole $q^2 = 0$ in the longitudinal propagator is not realized in this case.

The $\mathscr{P}^T_{\mu\nu}$ transverse propagator has poles whenever

$$\nu_L(\omega, \vec{q}) = -1, \tag{3.50}$$

$$q^2 = \omega^2 - |\vec{q}|^2 = 0. \tag{3.51}$$

The inverse of the magnetic permeability becomes negative $\mu_L^{-1}(\omega, \vec{q}) \equiv \nu_L(\omega, \vec{q}) = -1$. Analogous to the longitudinal case, Equation (3.50) yields the dispersion relation of the transverse plasmon collective excitations, and it corresponds to collective oscillations of the current density. Equation (3.51) shows us that we have another transverse mode of propagation in the REG whenever $q^2 = \omega^2 - |\vec{q}|^2 = 0$, yielding a photonic mode that propagates with the speed of light $c = 1$ in vacuum, something not yet accounted for in the literature.

In order to have more explicit expressions for the plasmon modes, it is useful to write the projectors as

$$\mathscr{P}_{\mu\nu} = n^{(1)}_\mu n^{(1)}_\nu + n^{(2)}_\mu n^{(2)}_\nu + n^{(3)}_\mu n^{(3)}_\nu, \tag{3.52}$$

$$\mathscr{P}^T_{\mu\nu} = n^{(1)}_\mu n^{(1)}_\nu + n^{(2)}_\mu n^{(2)}_\nu, \tag{3.53}$$

where $n^{(i)}_\mu = (0, \hat{n}^{(i)})$, $\hat{q} \cdot \hat{n} = 0$, $|\hat{n}^{(i)}| = 1$, for $i = 1, 2$, satisfying $n^{(1)}_i n^{(1)}_j + n^{(2)}_i n^{(2)}_j + \hat{q}_i \hat{q}_j = \delta_{ij}$. For $n^{(3)}_\mu$, we find

$$n^{(3)}_\mu = \left(\frac{-|\vec{q}|}{\sqrt{q^2}}, \frac{q_4 \hat{q}}{\sqrt{q^2}} \right). \tag{3.54}$$

If we demand that it must be normalized, and orthogonal to q_μ and $n^{(i)}_\mu$, $i = 1,2$, thus satisfying $n^{(1)}_\mu n^{(1)}_\nu + n^{(2)}_\mu n^{(2)}_\nu + n^{(3)}_\mu n^{(3)}_\nu + (q_\mu q_\nu / q^2) = \delta_{\mu\nu}$, then

$$\mathscr{P}^L_{\mu\nu} = n^{(3)}_\mu n^{(3)}_\nu, \tag{3.55}$$

$$\mathscr{P}^T_{\mu\nu} = n^{(1)}_\mu n^{(1)}_\nu + n^{(2)}_\mu n^{(2)}_\nu. \tag{3.56}$$

A few observations are in order:

(i) in Minkowski space, we have

$$n^{(3)}_\mu = \left(\frac{i|\vec{q}|}{\sqrt{q^2}}, \frac{\omega \hat{q}}{\sqrt{q^2}} \right), \tag{3.57}$$

which in the long-wavelength limit becomes $n^{(3)}_\mu = (0, \hat{q})$;

(ii) in that limit, one obtains Drude expressions for $\epsilon_L = 1 - (\omega_e^2/\omega^2)$ and $\nu_L = 1 - (\omega_m^2/\omega^2)$ [17]. Inserting this into (3.47) and (3.48), and using the fact that $\omega_m^2 = 2\omega_e^2$, we find $\omega_e^2 - \omega^2$ as the denominator for both longitudinal and transverse plasmon propagators.

The collective plasmon excitations correspond to charge density and current density oscillations. Indeed the collective field $A^L \equiv n^{(3)}_\mu \mathscr{P}^L_{\mu\nu} A_\nu = A_\nu n^{(3)}_\nu$, in Euclidean space, is given by

$$A^L = \frac{-i\vec{q} \cdot (-i\vec{q} A_4 + i q_4 \vec{A})}{\sqrt{q^2}|\vec{q}|} = \frac{-\vec{\nabla} \cdot \vec{E}}{\sqrt{q^2}|\vec{q}|}. \tag{3.58}$$

Since the field has a longitudinal component, we may define an effective charge density ρ_e as $\vec{\nabla} \cdot \vec{E} \equiv \rho_e(q)$. Similarly, the collective field $A^T_\mu \equiv \mathscr{P}^T_{\mu\nu} A_\nu$ is given by $(0, \vec{A}^T)$, where $\vec{A}^T = A_1 \hat{n}^{(1)} + A_2 \hat{n}^{(2)}$ and $A_i = \vec{A} \cdot \hat{n}^{(i)}$. One then obtains

$$\vec{A}^T = \frac{i\vec{q} \times (i\vec{q} \times \vec{A})}{|\vec{q}|^2} = \frac{\vec{\nabla} \times \vec{B}}{|\vec{q}|^2}. \tag{3.59}$$

We may then define an effective current density $\vec{j}_e$ through $\vec{\nabla} \times \vec{B} = \vec{j}_e$. Then, if we use (3.38), (3.39), and (3.40), and leave aside the gauge term, the plasmon Lagrangian may be written in Minkowski space as

$$\rho_e(q) \left(\frac{\epsilon_L}{|\vec{q}|^2} \right) \rho_e(q) + j^k_e(q) \left[\frac{(\nu_L + 1)\left(1 - \frac{\omega^2}{|\vec{q}|^2}\right)}{2|\vec{q}|^2} \right] j^k_e(q), \tag{3.60}$$

where $q = (\omega, \vec{q})$. The above expression physically describes the interaction of charge densities induced by the longitudinal component of the fluctuating electric fields, and current densities (loops in the plane perpendicular to $\hat{q}$) induced by the fluctuating magnetic fields. Apart from that, whenever $\epsilon_L \neq 0$ and $\nu_L \neq -1$, we just have the propagation of an electromagnetic wave with the propagator given by (3.48).

An alternative and somewhat complementary analysis may be obtained from Maxwell's equations combined with the constitutive relations written out previously. Maxwell's equation for harmonic plane waves in Fourier space are (we have now restored the speed of light c)

$$
\begin{aligned}
q_i D_i &= 0, && (3.61)\\
q_i B_i &= 0, && (3.62)\\
\epsilon_{ijk} q_j E_k &= \frac{\omega}{c} B_i, && (3.63)\\
\epsilon_{ijk} q_j H_k &= -\frac{\omega}{c} D_i. && (3.64)
\end{aligned}
$$

From equation (3.61), and the constitutive relations $D_j = \epsilon_{jk} E_K + \tau_{jk} B_k$ and $H_j = \nu_{jk} B_K + \tau_{jk} E_k$, we derive

$$(\vec{q} \cdot \vec{E}) \epsilon_L = 0. \tag{3.65}$$

If $\epsilon_L \neq 0$, then we must have $\vec{q} \cdot \vec{E} = 0$, so that Equation (3.64) and the constitutive relations give

$$\left[\tau |\vec{q}| + \epsilon \frac{\omega}{c}\right] \vec{E} + \left[\nu |\vec{q}| - \tau \frac{\omega}{c}\right] (\hat{q} \times \vec{B}) = 0, \tag{3.66}$$

which combined with Equation (3.63) yields a generalized wave equation for $\vec{E}$ (and an analogous one for $\vec{B}$)

$$\left[|\vec{q}|^2 - \mu\epsilon \frac{\omega^2}{c^2} - 2\mu\tau |\vec{q}| \frac{\omega}{c}\right] \vec{E} = 0. \tag{3.67}$$

For a plane-wave, the relation $|\vec{q}| = |\vec{q}|(\omega)$, which satisfies Eq. (3.67), leads to the index of refraction $n(\omega) = |\vec{q}|/\omega$. For $\tau = 0$, we recover the usual expression $n = \sqrt{\mu}\sqrt{\epsilon}$. Notice that, in the long-wavelength limit, one has $\tau = 0$, $n = \sqrt{\mu}\sqrt{\epsilon}$, and electric and magnetic responses may be simultaneously negative. It then follows that one may obtain *negative indices of refraction* for the relativistic regime in such a limit. In the next chapter, we will give a general description of the effective responses and of the index of refraction in the REG.

Using the Equations (2.41) to (2.44), and the equations for ϵ_L and ν_L in (2.46) and (2.47), Equation (3.66) becomes,

$$(\nu_L + 1)\left[\vec{q} \times \vec{B} + \frac{\omega}{c}\vec{E}\right] = 0, \tag{3.68}$$

whereas Equation (3.67) yields

$$(\nu_L + 1)q^2 = (\nu_L + 1)\left[\frac{\omega^2}{c^2} - |\vec{q}|^2\right] = 0. \tag{3.69}$$

We see that Maxwell's equation (3.61) will be satisfied if $\epsilon_L = 0$. This coincides with the longitudinal plasmon condition. If $\epsilon_L \neq 0$, then $\vec{E}$ is transverse, and Equation (3.69) will be satisfied if either $\nu_L = -1$ (transverse plasmons) or $q^2 = 0$ (photons). The fact that the wave equation factors out into two terms is a consequence of the specific form of the EM responses of the REG.

The plasmon modes and the photonic mode obtained from quantum responses to the electromagnetic fields will appear whenever the dispersion relation $\omega = \omega(|\vec{q}|)$ obeys one of the conditions derived in Equations (3.49)-(3.51) ($\epsilon_L = 0$; $\nu_L = -1$, and $\omega = |\vec{q}|$, respectively). Otherwise, the electromagnetic field will propagate with responses given by $\epsilon_{ij}(\omega, |\vec{q}|)$ and $\nu_{ij}(\omega, |\vec{q}|)$.

The real part of ϵ_L is depicted in Figure (3.5) as a function of ω in units of ω_c. Results were computed for $\tilde{\eta} = 0.01$, and different values of $|\vec{q}|$ expressed in units of q_c. In Figures 3.5(a) and 3.5(b), we have set $\tilde{\beta} = 1000$ and $\tilde{\beta} = 10$, respectively. The real part of the longitudinal electric permittivity exhibits two zeros for a given value of $\tilde{q}$ at a given temperature. The lower zero lies within a region where $\mathrm{Im}[\epsilon_L] \neq 0$. Therefore, in spite of the fact that $\mathrm{Re}[\epsilon_L] = 0$, it is a mode that does not propagate.

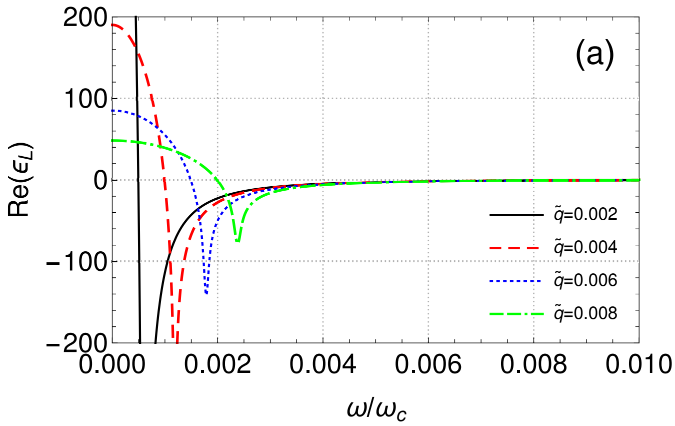

(a) $\tilde{\beta} \equiv mc^2\beta = 1000$

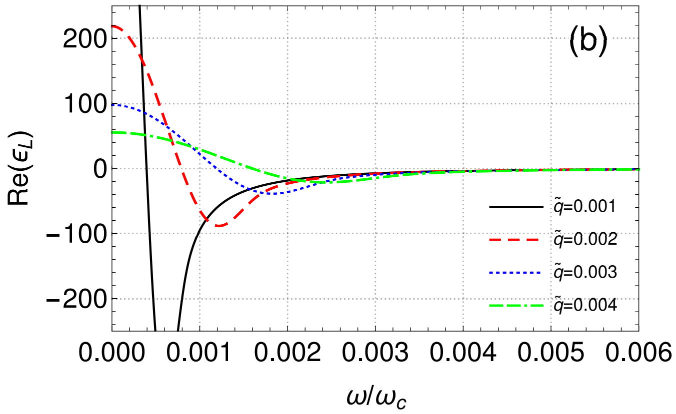

(b) $\tilde{\beta} \equiv mc^2\beta = 10$

Figure 3.5: Real part of ϵ_L as a function of frequency in units of $\omega_c = mc^2/\hbar$, for various values of the wave vector $\tilde{q} = |\vec{q}|/q_c$, with $q_c = mc/\hbar$ is the Compton wave vector. The density gas $\tilde{\eta} = 0.01$, and $\tilde{\beta} = 1000$ (fig. a), and $\tilde{\beta} = 10$ (fig. b).

We display in Figure 3.6 the upper (solid line) and lower (dashed lines) frequency zeros of the real part of ϵ_L as functions of $\tilde{q} = |\vec{q}|/q_c$. Numerical results were computed for $\tilde{\eta} = 0.01$, and different values of $\tilde{\beta}$. Figure 3.6 clearly indicates that there is a maximum value of the wave vector ($\tilde{q}_{max}$) beyond which the longitudinal plasmon decays into particle-antiparticle pairs.

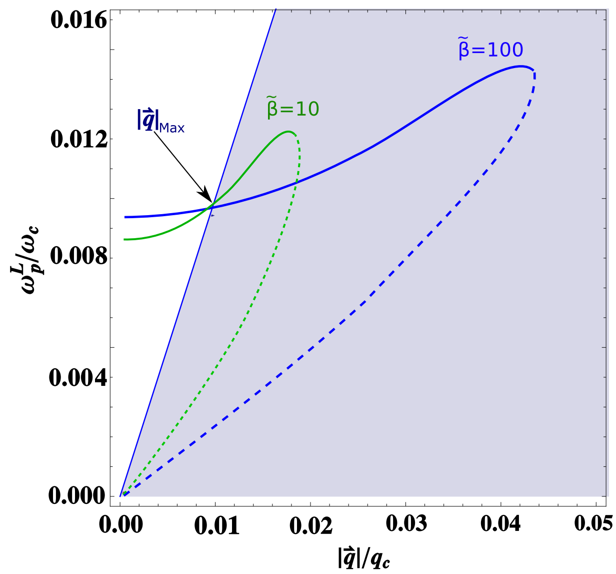

Figure 3.6: Upper (ω_p^L plasmon frequency) and lower frequency zeroes of ϵ_L (solid and dashed lines, respectively) as function of the $|\vec{q}|$ wave vector. Calculations were performed for $\tilde{\beta} = 100$ and $\tilde{\beta} = 10$ by taking $\tilde{\eta} = 0.01$. The shaded area corresponds to the region where particles-antiparticle excitation occur. Note that the maximum value of the wave vector ($\tilde{q}_{max}$) is the value beyond which the longitudinal plasmon decays into particle-antiparticle pairs. Both the frequency and wave vector are given in units of ω_c and q_c respectively.

The condition $\nu_L = -1$ [cf. (3.50)] leads to the ω_p^T frequency of the REG transverse plasmon modes. We display in Figure 3.7 the real part of ν_L as a function of the ω frequency in units of ω_c, obtained for $\tilde{\eta} = 0.01$ and different values of the wave vector $|\vec{q}|$ in unit of q_c. Results depicted in Figures 3.7(a) and 3.7(b) where computed for $\tilde{\beta} = 1000$ and $\tilde{\beta} = 10$, respectively. We would like to stress that numerical results (not shown here) indicate that Im$[\nu_L] = 0$ within the respective frequency ranges considered in both Figure 3.7(a) and 3.7(b). Therefore, in the present cases, the transverse plasmon frequencies may be obtained by solving the transcendental equation Re$[\nu_L] = -1$.

We display in Figure 3.8 the dispersion curves for the transverse and longitudinal plasmon modes at $T = 0$ [cf. Equations (3.49) and (3.50)]. The shaded area corresponds to the region where the excitation of particle–antiparticle pairs occurs. The dashed line is discarded as solution for the longitudinal plasmon dispersion as it lies entirely in the region of nonzero imaginary parts of ϵ_L. We have also shown the dispersion for the photon mode $\tilde{\omega}_\gamma = \tilde{q}$ [cf. (3.51)]. Although not shown in the figure, the straight dotted line for the photon dispersion will eventually reach the upper region where the excitation of electron-positron pairs will take place.

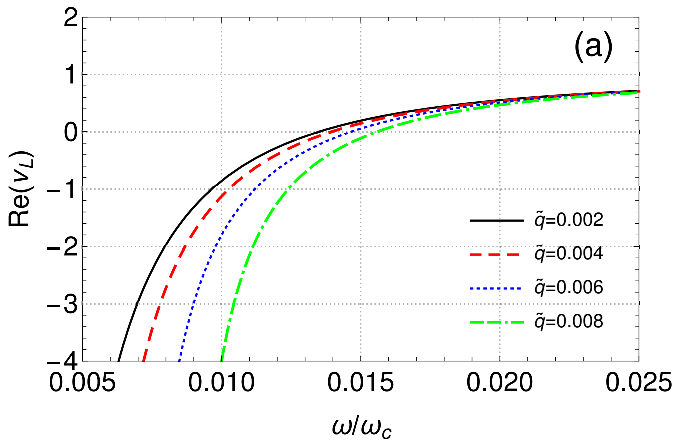

(a) $\tilde{\beta} \equiv mc^2\beta = 1000$

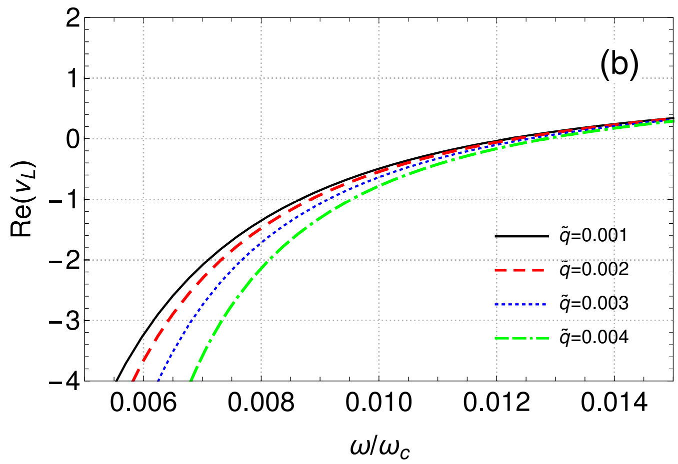

(b) $\tilde{\beta} \equiv mc^2\beta = 10$

Figure 3.7: Real part of ν_L as a function of frequency in units of $\omega_c = mc^2/\hbar$, for various values of the wave vector $\tilde{q} = |\vec{q}|/q_c$, with $q_c = mc/\hbar$ is the Compton wave vector. The density gas $\tilde{\eta} = 0.01$, and, $\tilde{\beta} = 1000$ (fig. a), and $\tilde{\beta} = 10$ (fig. b).

The model has been tested in the non-relativistic limit for some metals. Figure 3.9 shows the experimental dependence of the plasmon energy of silicon [66] at $T = 0$ as a function of wave vector parallel to the electromagnetic field that excited the plasmon mode. The numerical results show good agreement with the experimental data.

Finally, we display in Figure 3.10 the different relevant regions of the $(\tilde{q}, \tilde{\omega})$ plane where the real parts of ϵ_L and ν_L have different signs [25]. We would like to stress that there is a region where both ϵ_L and ν_L are simultaneously negative, indicating that the REG exhibits a behavior that has not been experimentally observed in natural materials. This fact was previously remarked by one of the authors [17], as mentioned.

A figure similar to Figure 3.10 can be obtained using the values of densities and tem-

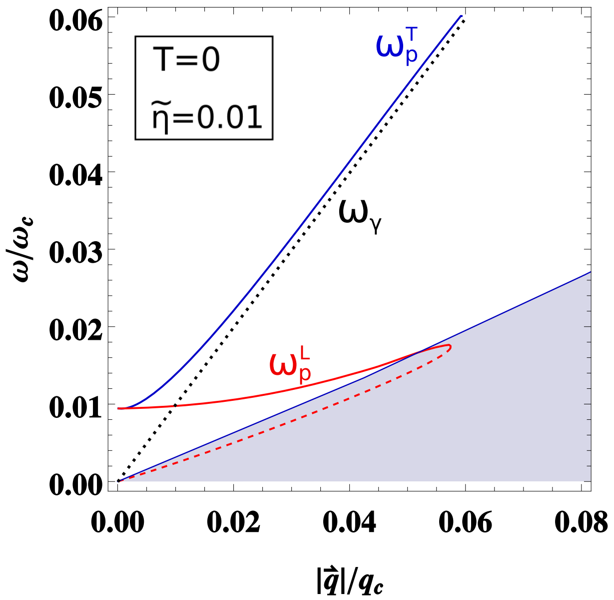

Figure 3.8: The dispersion curves for transverse and longitudinal plasmon modes at $T = 0$ and $\tilde{\eta} = 0.01$ [cf. Equations (3.49) and (3.50)]. In the shaded area, $\mathrm{Im}[\epsilon_L] = 0$, indicating decay of the longitudinal mode. The dashed line is discarded as a solution for the longitudinal dispersion as it lies entirely in the region of nonzero imaginary part of ϵ_L . We have also shown the dispersion (dotted line) for the photon mode $\tilde{\omega}_\gamma = \tilde{q}$ [see Equation (3.51)].

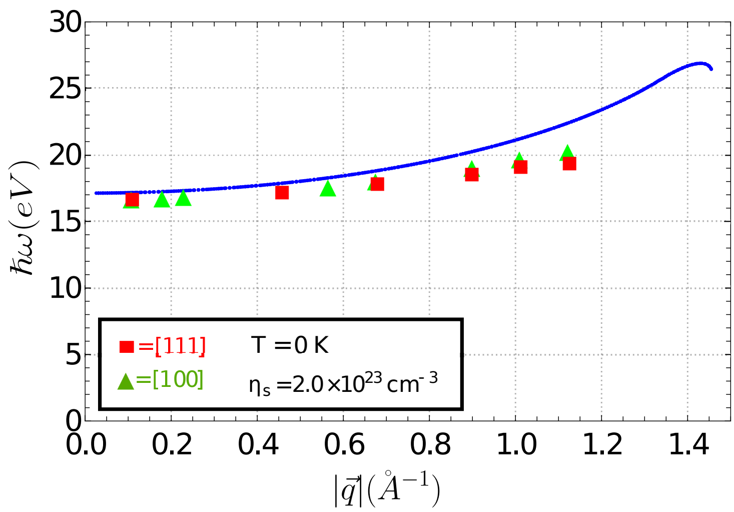

Figure 3.9: Energy loss dispersion along the [111] and [100] directions of the Silicon at $T = 0$ and silicon density $\eta_s = 2.0 \times 10^{23}\mathrm{cm}^{-3}$. Solid line correspond to the theoretical result. Squares and triangles correspond to experimental values from Stiebling [66]

.

peratures encountered in astrophysical scenarios, as in a superdense electron-plasma $(e-p)$ in gamma ray bursts (GRBs) [67, 68], where the $e-p$ density is in the range of $\eta = (10^{30} - 10^{37})\mathrm{cm}^{-3}$. According to ref. [67], in Condensed Matter, a $e-p$ plasma will eventually be produced in the laboratory with laser systems. Laser pulses with focal densities $\mathrm{I} = 10^{22}\mathrm{W\,cm}^{-2}$ incident on material targets could lead to a $e-p$ plasma with densities in the range of $(10^{23} -$

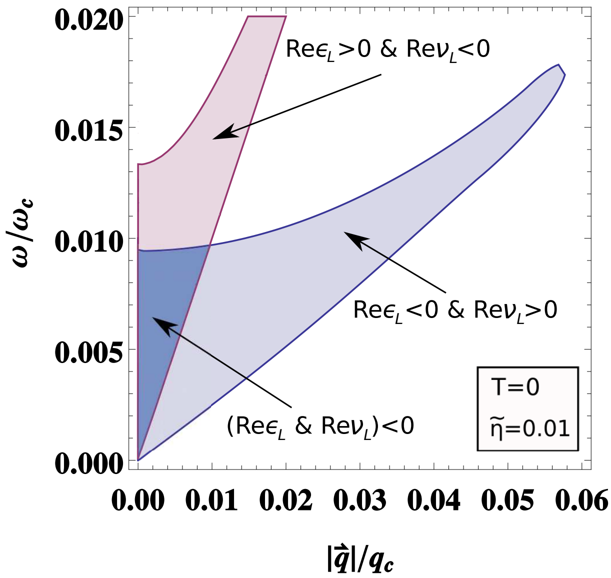

Figure 3.10: Regions of the $(\tilde{q},\tilde{\omega})$ plane according to the signs of the real parts of ϵ_L and ν_L. Outside the shaded regions the real parts of ϵ_L and ν_L are positive. Results were obtained for $T=0$ and $\tilde{\eta}=0.01$.

10^{28})cm^{-3}. We have used the upper limit of that density range in our calculations.

Summing up, we have presented a theoretical study of the EM propagation and responses of a REG for various temperatures and carrier densities. Using linear response and RPA, we have identified the propagation modes and their dispersion relations from the QED propagators, as well as from Maxwell's equations, with the added input of the constitutive relations obtained from the QED responses. We found a longitudinal plasmon mode, two transverse plasmon modes, and a photonic mode which propagates with the speed of light in vacuum, i.e., for which the medium is transparent, thanks to the specific form of its relativistic electromagnetic responses. In deriving dispersion relations, we were able to identify stable solutions and regions of instability where the plasmon modes decay. Finally, we have also identified the regions in the $(|\vec{q}|,\omega))$ plane where the longitudinal permittivity ϵ_L and longitudinal inverse permeability ν_L are both simultaneously negative.

Chapter 4

Negative refraction in the relativistic electron gas

4.1 Introduction

The quantities that Veselago assumed to be simultaneously negative were the electric permittivity and magnetic permeability appearing in Maxwell's equations. Although in nonrelativistic systems these are the same quantities that appear in the constitutive equations, this is NOT the case for the REG. In fact, we will show that what appears in Maxwell's equations for the REG are combinations of the responses present in the constitutive relations. Those combinations are to be interpreted as the effective electric permittivity and permeability that would have to be simultaneously negative in some frequency range in order to realize the Veselago system. Here, we will construct them, and show that both become negative below the *same* frequency value, which we associate with a longitudinal plasmon frequency.

From the study of the poles in the electromagnetic propagator, we have also shown that the REG supports the propagation of longitudinal and transverse plasmon modes, whose dispersion relations we have calculated, as well as that of a purely photonic mode with the speed of light in vacuum c. The photonic mode corresponds to an electromagnetic wave propagating in the gas. The fact that its speed was c implied that the *modulus* of the index of refraction was equal to one, and that there was no energy loss to the gas, something novel that we thought should be confirmed and clarified. In the present chapter, we explicitly calculate the energy dissipated to the medium by the electromagnetic wave, and show that it vanishes. Furthermore, we interpret this as a natural consequence of the absence of a dissipation mechanism in an ideal gas.

With those two ingredients well established, i.e., simultaneously negative effective permittivity and permeability, and the existence of a photonic mode for which the effective index of refraction n_{eff} has modulus one, we combine them in the discussion of refraction to show that $n_{\text{eff}} = -1$, a consequence anticipated in Veselago's work [7]. That completed our proof that the REG is indeed a LHM, something we had suggested previously, but lacked explicit demonstration. Additionally, we illustrate how this affects the reflection and transmission coefficients of the electromagnetic wave. We may now finally claim that the REG is a natural LHM.

4.2 Veselago effective responses

In order to find the exact analog of the situation proposed by Veselago [7], we need the effective electric permittivity and effective magnetic permeability that emerge in the two Maxwell equations with sources. To obtain them, we start with the polarization P_i (2.32) and magnetization M_i (2.33), and using (2.20-2.22) combined with electric and magnetic permeabilities in (2.41-2.44), we have

$$P_i = (\epsilon - 1)E_i^T + (\epsilon_L - 1)E_i^L - \tau\epsilon_{ijk}\hat{q}_j B_k^T, \tag{4.1}$$

$$M_i = (1-\nu)B_i^T + (1-\nu_L)B_i^L + \tau\epsilon_{ijk}\hat{q}_j E_k^T, \tag{4.2}$$

where the superscript refers to longitudinal and transverse. Maxwell's equations imply

$$\epsilon_{ijk} q_j E_k = \omega B_i, \tag{4.3}$$

$$\epsilon_{ijk} q_j H_k = -\omega D_i. \tag{4.4}$$

For an electromagnetic wave, the longitudinal components of the fields $B^L = E^L = 0$ vanish in Eqs. (4.1) and (4.2), so that the constitutive equations (2.36) and (2.37) read

$$D_i = \epsilon E_i^T - \tau \epsilon_{ijk} \hat{q}_j B_k^T, \tag{4.5}$$

$$H_i = \nu B_i^T - \tau \epsilon_{ijk} \hat{q}_j E_k^T. \tag{4.6}$$

Substituting them into Maxwell's equations yields

$$\vec{q} \times \vec{E}^T = \omega \left(\frac{\mu |\vec{q}|}{|\vec{q}| - \omega \mu \tau} \right) \vec{H}^T, \tag{4.7}$$

$$\vec{q} \times \vec{H}^T = -\omega \left(\epsilon + \frac{|\vec{q}|}{\omega} \tau \right) \vec{E}^T. \tag{4.8}$$

Comparing with Veselago's work [7], we identify the effective responses of the REG as

$$\mu_{\text{eff}} = \frac{\mu |\vec{q}|}{|\vec{q}| - \omega \mu \tau}, \tag{4.9}$$

$$\epsilon_{\text{eff}} = \epsilon + \frac{|\vec{q}|}{\omega} \tau. \tag{4.10}$$

Note that, when $\tau = 0$, we recover $\mu_{\text{eff}} = \mu$ and $\epsilon_{\text{eff}} = \epsilon$. Defining $|n_{\text{eff}}| \equiv |\vec{q}|/\omega$, then $n_{\text{eff}}^2 = \mu_{\text{eff}} \epsilon_{\text{eff}}$. The LHM behavior will occur whenever ϵ_{eff} and μ_{eff} are both negative.

Figure 4.1 shows the behavior of the real parts of ϵ_{eff} and μ_{eff} at $T = 0$ for $|\vec{q}| = 5.1\text{k eV}/\hbar c$. Both effective responses become negative in the shaded region, exhibiting LHM behavior. In that region, the imaginary parts $\text{Im}\epsilon_{\text{eff}} = \text{Im}\mu_{\text{eff}} = 0$ are null, so that wave propagation occurs without energy dissipation, something we will confirm by explicit calculation in the next section.

We remark that the zero temperature value used in the calculations of Fig.4.1 is a good approximation to many systems with relativistic densities. An ideal relativistic electron gas is a well-defined statistical system, whose equilibrium dynamics may be treated in the canonical ensemble, where the temperature T and the density η are independent thermodynamic variables. The gas is considered relativistic if either its Fermi energy or its thermal

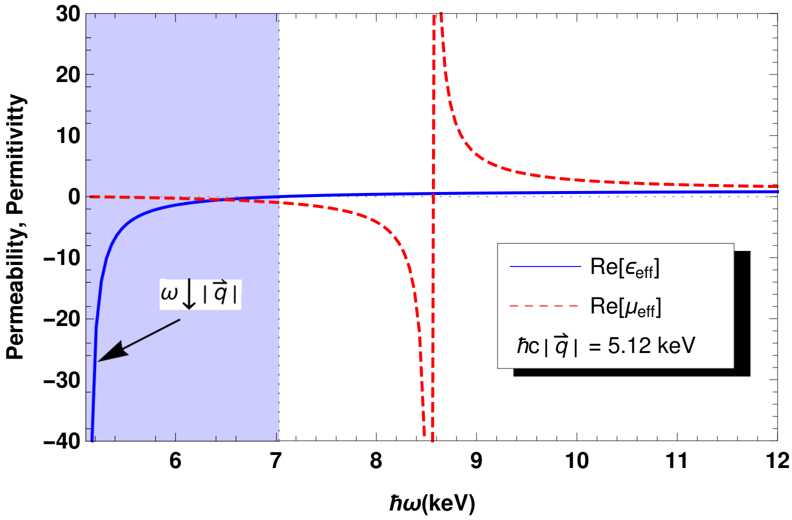

Figure 4.1: Real parts of ϵ_{eff} (solid line) and μ_{eff} (dashed line) as a function of $\hbar\omega$, and $\hbar c|\vec{q}| = 5.12$ keV, where $|\vec{q}|$ is the wave vector. When $\omega \downarrow |\vec{q}|$, $\epsilon_{\text{eff}} \to -\infty$. The shaded area corresponds to the region where both ϵ_{eff} and μ_{eff} are simultaneously negative. Results were obtained for $T = 0$ and electron gas density $\eta = 1.76 \times 10^{28}\text{cm}^{-3}$.

energy kT, or both are greater than or equal to the electron rest energy mc^2. High Fermi energy translates into high densities $\eta \geq (mc/\hbar)^3$. Thus, there is nothing to prevent a relativistic electron gas from having relativistic densities and very low (even zero) temperatures.

As an example in Plasma Physics presented in [69], high power laser pulses with intensities up to 10^{22}W/cm^2 may be used to investigate the interaction of intense laser beams with a plasma of electrons and positrons in the relativistic and quantum regimes. Such a plasma, with average temperature T_p exceeding several tens of electron volts, and extremely high number densities, in the range $10^{23} - 10^{28}\text{cm}^{-3}$, may be considered a degenerate electron gas. For density values of 10^{28}cm^{-3}, the Fermi energy $E_F = \hbar c(3\pi^2\eta)^{1/3} = 0.13\text{MeV}$, thus $kT_p \ll E_F$, validating the ZERO temperature approximation.

Using the definitions of the permittivities and permeabilities in Eqs. (2.41-2.44), we may write the effective responses (4.9) and (4.10) in terms of the scalar functions $\mathscr{A}^*$ and $\mathscr{B}^*$, neglecting the vacuum contribution $\mathscr{C}^* \ll 1$, to derive

$$\epsilon_{\text{eff}} = 1 + \mathscr{A}^* - \frac{\omega^2}{|\vec{q}|^2}\mathscr{B}^*, \tag{4.11}$$

$$\mu_{\text{eff}} = \left(1 + \mathscr{A}^* - \frac{\omega^2}{|\vec{q}|^2}\mathscr{B}^*\right)^{-1}. \tag{4.12}$$

So, we obtain $\epsilon_{\text{eff}} = \mu_{\text{eff}}^{-1} = \nu_{\text{eff}}$; thus $n_{\text{eff}}^2 = 1$. This again implies that an electromagnetic wave will propagate with the speed of light in vacuum.

From Eqs. (2.41) and (2.42), with $\mathscr{C}^* = 0$, we derive

$$\epsilon_{\text{eff}} = \nu_{\text{eff}} = \nu + \frac{\omega^2}{|\vec{q}|^2 + \omega^2}(\epsilon - \nu). \tag{4.13}$$

In the long-wavelength limit $|\vec{q}| \to 0$, we may use the Drude expressions in Eqs. (2.48) and (2.49), neglecting small corrections of $\mathscr{O}(\alpha)$, to find

$$\epsilon_{\text{eff}} = \nu_{\text{eff}} = \epsilon = \left(1 - \frac{\omega_e^2}{\omega^2}\right). \tag{4.14}$$

Therefore, in the long-wavelength limit, the effective responses will have the exact same Drude behavior, both being negative below the longitudinal electric plasmon frequency, to appear in the next section. Those simultaneously negative responses characterize the gas as a LHM, as we will show. In summary, for Fermi gases, the LHM behavior is a characteristic that appears only in a relativistic context.

4.3 Propagation without loss

A complete discussion of the modes that propagate in the REG was given in 3.4, where analytic results at $T = 0$ and numerical results for $T \neq 0$ were used to compute decay constants and dispersion relations for both longitudinal and transverse plasmons. In order to obtain the collective modes of oscillation, we computed how the medium affects the photon propagator in the REG. The inverse of the quadratic kernel $\Gamma_{\mu\nu}$ in eq.(3.46) gives the photon propagator

$$\Gamma_{\mu\nu}^{-1} = \frac{\mathscr{P}_{\mu\nu}^L}{-q^2\epsilon_L} + \frac{\mathscr{P}_{\mu\nu}^T}{-q^2(\nu_L + 1)} + \frac{\lambda}{q^2}\frac{q_\mu q_\nu}{q^2}, \tag{4.15}$$

with the projectors $\mathscr{P}_{\mu\nu} \equiv \mathscr{P}_{\mu\nu}^L + \mathscr{P}_{\mu\nu}^T = \delta_{\mu\nu} - q_\mu q_\nu / q^2$, $\mathscr{P}_{ij}^T = \delta_{ij} - \hat{q}_i \hat{q}_j$, and $\mathscr{P}_{44}^T = \mathscr{P}_{4i}^T = 0$; λ is the gauge parameter. The poles of the photon propagator correspond to collective excitations and yield their dispersion relations.

In the longitudinal propagator, there is a pole whenever the longitudinal electric permittivity vanishes $\epsilon_L(\omega, \vec{q}) = 0$, which leads to the dispersion relation of the longitudinal plasmon collective excitation. For $\epsilon_L(\omega, \vec{q})$ nonzero, Maxwell's equations lead to transverse fields,

$\vec{q}\cdot\vec{E}=0$, which means that the pole $q^2=0$ in the longitudinal propagator is not realized in this case. The transverse propagator has poles whenever the inverse of the magnetic permeability becomes $\mu_L^{-1}(\omega,\vec{q})\equiv\nu_L(\omega,\vec{q})=-1$. They correspond to collective oscillations of the current density. There is another transverse mode of propagation in the REG whenever $q^2=\omega^2-|\vec{q}|^2=0$, corresponding to a photonic mode that propagates with the speed of light c in vacuum.

Our main interest here will be the photonic mode, which corresponds to an electromagnetic wave that travels through the REG as if it were in vacuum. We will show by explicit computation that no energy is dissipated into the medium by the electromagnetic wave. We start by constructing the energy-momentum tensor $T_{\mu\lambda}$

$$T_{\mu\lambda}=F_{\mu\nu}F_{\lambda\nu}-\delta_{\mu\lambda}\frac{F^2}{4}, \tag{4.16}$$

which satisfies

$$\partial_\mu T_{\mu\lambda}=-J_\mu F_{\mu\lambda}, \tag{4.17}$$

with $T_{44}=-u$, u being the energy density , and $T_{j4}=iS_j$, $\vec{S}$ being the Poynting vector.

The total current J_μ is the sum of the free and induced current contributions, $J_\mu=J_\mu^F+J_\mu^I$. The current J_ν^I induced in the REG by the external electromagnetic field is related to the polarization $P_{\mu\nu}$ by $\partial_\mu P_{\mu\nu}=-J_\nu^I$. Since $J_4^I=i\vec{\nabla}\cdot\vec{P}$ and $J_j^I=-\partial_t P_j-(\vec{\nabla}\wedge\vec{M})_j$, eq.(4.17) may be expressed in Minkowski space, using $J_0^M=iJ_4^E$, $\vec{J}_M=-\vec{J}_E$

$$\frac{\partial u}{\partial t}+\vec{\nabla}\cdot\vec{S}=-\vec{E}\cdot\left(\vec{J}^F+\vec{\nabla}\wedge\vec{M}+\frac{\partial\vec{P}}{\partial t}\right). \tag{4.18}$$

Eq.(4.18) expresses the Poynting theorem [11, 58], with $u=(\vec{E}^2+\vec{B}^2)/2$, $\vec{S}=\vec{E}\wedge\vec{B}$, and $\vec{M}$ and $\vec{P}$ the magnetization and polarization vectors, respectively. A simple rewriting leads to

$$\left[\vec{E}\cdot\frac{\partial\vec{D}}{\partial t}+\vec{H}\cdot\frac{\partial\vec{B}}{\partial t}\right]+\nabla\cdot(\vec{E}\wedge\vec{H})=-\vec{E}\cdot\vec{J}^F. \tag{4.19}$$

The total energy dissipated may be identified as

$$\mathscr{E}=\int d^4x\left(\vec{E}\cdot\frac{\partial\vec{D}}{\partial t}+\vec{H}\cdot\frac{\partial\vec{B}}{\partial t}\right). \tag{4.20}$$

In terms of the Fourier transforms,

$$\mathscr{E}=\int\frac{d^4q}{(2\pi)^4}i\omega\left[E_j(q)D_j(-q)+H_j(q)B_j(-q)\right]. \tag{4.21}$$

Since the fields are real, $E_j(x) = E_j^*(x)$, we have $E_j(-q) = E_j^*(q)$. Inserting the constitutive equations of the REG for H and D,

$$\mathscr{E} = \int \frac{d^4q}{(2\pi)^4}(-i\omega)\left[\epsilon_L|E_L|^2 + \epsilon|E_j^T|^2 - \nu_L|B_L|^2 - \nu|B_j^T|^2 + 2\tau\epsilon_{ijk}\hat{q}_k \mathrm{Re}(E_i^* B_j)\right]. \tag{4.22}$$

From Maxwell's equations, we have $E_L = B_L = 0$, and $B_i = B_i^T = \epsilon_{ijk}q_j E_k^T/\omega$. Thus,

$$\mathscr{E} = -i\int \frac{d^4q}{(2\pi)^4}\omega\left[\epsilon(q) - \nu(q)\frac{|\vec{q}|^2}{\omega^2} + 2\tau(q)\frac{|\vec{q}|}{\omega}\right]|E_i^T(q)|^2. \tag{4.23}$$

For the photonic mode, $|\vec{q}|^2 - \omega^2 = 0$, the term inside the brackets in eq.(4.23) is $[\epsilon(q) - \nu(q) + 2\tau(q)]$. Setting $\mathscr{C}^* = 0$ in eqs.(2.41)-(2.44), we have

$$\epsilon(q) - \nu(q) + 2\tau(q) = \left(1 - \frac{\omega}{|\vec{q}|}\right)^2 \mathscr{B}^*. \tag{4.24}$$

Thus, for the electromagnetic wave, $|\vec{q}| = \omega$ implies

$$\mathscr{E} = 0 \tag{4.25}$$

No energy is dissipated.

In conclusion, the photonic mode propagates with the speed of light in vacuum, meaning that there are no losses to the medium, as explicitly verified by our calculation of the vanishing energy dissipation. Physically, this is inevitable, because there is no mechanism for dissipating energy in the REG, as it is an ideal gas. Its particles do not interact with each other, only with the photons of the external radiation, which will only change the momenta of the electrons, without losing energy (elastic collisions). Had we been dealing with atoms, the photons could induce transitions in the energy levels of the electrons, and that would lead to energy loss.

4.4 Negative index of refraction

For the photonic mode, since $|n_{\text{eff}}| = 1$, the effective responses in eqs. (4.9) and (4.10) become $\epsilon_{\text{eff}} = \epsilon + \tau$ and $\nu_{\text{eff}} = \nu - \tau$, where $\nu_{\text{eff}} = \mu_{\text{eff}}^{-1}$. Neglecting the vacuum term $\mathscr{C}^* = 0$, eqs. (2.41), (2.42), and (2.44) become

$$\epsilon = 1 + \mathscr{A}^*, \tag{4.26}$$

$$\nu = 1 + \mathscr{A}^* - 2\mathscr{B}^*, \tag{4.27}$$

$$\tau = -\mathscr{B}^*, \tag{4.28}$$

leading to

$$\epsilon_{\text{ eff}} = \nu_{\text{ eff}} = 1 + \mathscr{A}^* - \mathscr{B}^*. \tag{4.29}$$

The longitudinal responses for the photonic mode are

$$\epsilon_L = \epsilon + \epsilon' = 1, \tag{4.30}$$

$$\nu_L = \nu + \nu' = 1 + 2(\mathscr{A}^* - \mathscr{B}^*), \tag{4.31}$$

leading to

$$\epsilon_{\text{ eff}} = \nu_{\text{ eff}} = \frac{\nu_L + 1}{2}. \tag{4.32}$$

This becomes negative for $\nu_L < -1$ and, then,

$$\epsilon_{\text{ eff}} = \nu_{\text{ eff}} < 0. \tag{4.33}$$

A numerical calculation shows that, for the electromagnetic wave of the photonic mode $\omega = |\vec{q}|$, $\epsilon_{\text{ eff}} = \nu_{\text{ eff}} \to -\infty$, keeping the product $n^2_{\text{eff}} = \mu_{\text{ eff}}\epsilon_{\text{ eff}} = 1$. That can be seen by taking the limit $\omega \downarrow |\vec{q}|$ from above, since $\omega = \lim_{m_\gamma \to 0} \sqrt{\vec{q}^2 + m_\gamma^2}$, m_γ being the vanishing photon mass, as shown in Fig. 4.2. Thus, we have $\epsilon_{\text{ eff}} < 0$ and $\nu_{\text{ eff}} < 0$, for the electromagnetic wave.

Maxwell's equations provide the relative orientation of the wave unit vector ($\hat{q}$) with respect to the electric ($\hat{e}$) and magnetic ($\hat{h}$) field unit vectors. For the usual case where the medium is right-handed, we have $\hat{q} \wedge \hat{e} = +\hat{h}$ and $\hat{q} \wedge \hat{h} = -\hat{e}$. On the other hand, Maxwell's equations (4.7) and (4.8), for a LHM with $\mu_{\text{ eff}} < 0$ and $\epsilon_{\text{ eff}} < 0$, yield $\hat{q} \wedge \hat{e} = -\hat{h}$ and $\hat{q} \wedge \hat{h} = +\hat{e}$. From previous considerations, the REG is a LHM. Then,

$$\hat{e} \wedge \hat{h} = -\hat{q}. \tag{4.34}$$

From the definition of the Poynting vector, $\vec{S} \equiv \vec{E} \wedge \vec{H}$, the vector $\hat{s} = \hat{e} \wedge \hat{h}$ is opposite to its wave vector by eq.(4.34).

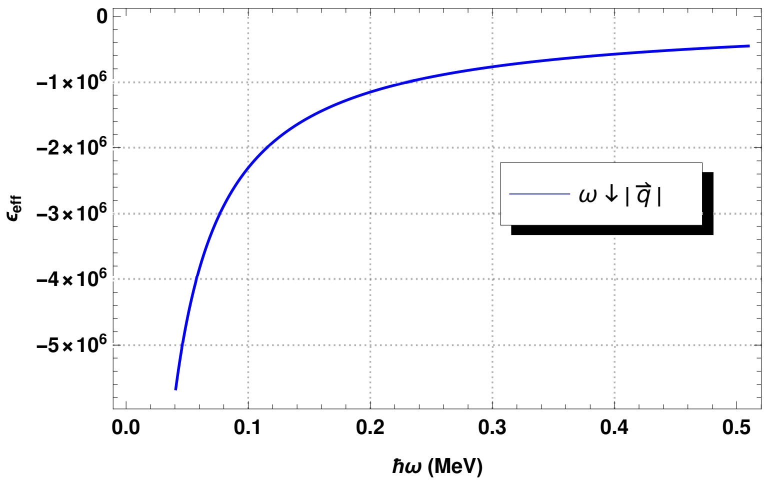

Figure 4.2: Effective permittivity for values of $\omega \downarrow |\vec{q}|$ (photonic mode). Calculations were performed at $T = 0$ and electron density $\eta = 1.76 \times 10^{28}\mathrm{cm}^{-3}$.

Let us analyze the refraction of light into a LHM. Maxwell's equations lead to boundary conditions at the interface ($z = 0$) delimited by the two media

$$E_{(xy)a} = E_{(xy)b}, \quad H_{(xy)a} = H_{(xy)b}, \tag{4.35}$$

$$\epsilon_1 E_{(z)a} = \epsilon_{\,\mathrm{eff}} E_{(z)b}, \quad \mu_1 H_{(z)a} = \mu_{\,\mathrm{eff}} H_{(z)b}, \tag{4.36}$$

where ϵ_1 and μ_1 correspond to the responses of a right-handed material (RHM). As Veselago argued, the boundary conditions must be satisfied regardless of the relative rightness of the media. Thus, because of the continuity of the tangential component of $\vec{q}$, an incident wave with Poynting vector $\vec{S}_0$ and wave vector $\vec{q}_0$ from medium (a) has two possibilities to refract into medium (b), depicted in Fig. 4.3, depending on the rightness of the vector fields. If $\epsilon_{\,\mathrm{eff}}$ and $\mu_{\,\mathrm{eff}}$ are simultaneously negative in medium (b), the only way to refract is with an angle θ_2 opposite to the one for a RHM. Since the radiation flows along the Poynting vector $\vec{S}_2$, which is antiparallel to wave vector $\vec{q}_2$, Snell's law implies that, for the pure photonic mode, $\omega = |\vec{q}|$, the index of refraction is $n_{\,\mathrm{eff}} = -1$, which completes our proof.

Indeed, let us define the wave vector of the radiation incident from the RHM as $\vec{q}_0$, that of the reflected wave as $\vec{q}_1$, and that of the wave refracted in the LHM as $\vec{q}_2$. Then, from the continuity of the tangential components, the boundary conditions on (4.35) and (4.36) lead to $q_{0y} = q_{1y} = +q_{2y}$. In the LHM, the tangential component q_{2y} has positive sign. However, its Poynting vector $\vec{S}_{2y}$ has a minus sign, $S_{0y} = -S_{2y}$. Since, $|\vec{q}_0| = |\vec{q}_1| =$

$\omega|n_1|$, where n_1 is the refractive index of medium (a), following standard calculations [58], for transparent media $\theta_0 = \theta_1$, and we obtain Snell's law

$$p_1\, n_1 \sin\theta_0 = p_2\, n_2 \sin\theta_2, \tag{4.37}$$

where for a RHM, $p_1 = +1$, and for a LHM, $p_2 = -1$, with $n_1 > 0$, and $n_2 < 0$.

We have thus shown that the only way that the electromagnetic wave propagates in the REG is with $n_{\,\mathrm{eff}} = -1$ in the photonic mode $\omega = |\vec{q}|$. This result corrects a misunderstanding in Ref.[70], which misused the concept of index of refraction for the electric plasmon oscillation. The concept of index of refraction can only be applied to a propagating electromagnetic wave, not to a plasmon excitation, which is an oscillation of the electric charge density in the medium.

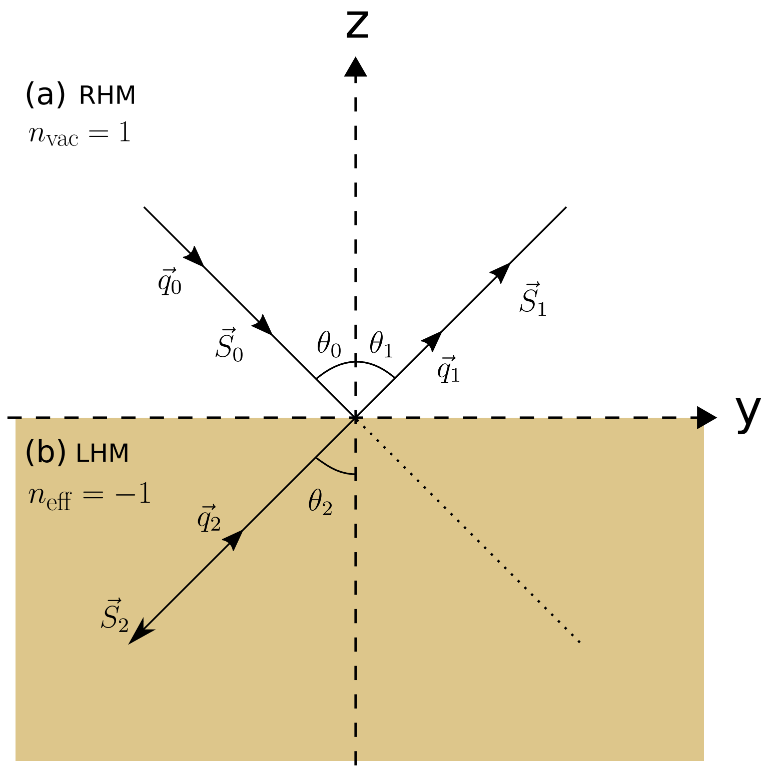

Figure 4.3: Illustration of the two media with refractive index (a) $n_{\,\mathrm{vac}} = 1$ and (b) $n_{\,\mathrm{eff}} = -1$. When the electromagnetic wave enters the LHM (b), the Poynting vector $\vec{S}_2$ is opposite to $\vec{q}_2$, and the refracted angle is θ_2.

4.5 Reflection and transmission coefficients

Although the REG may be bianisotropic, since its polarization and magnetization depend on both $\vec{E}$ and $\vec{B}$, for the EM wave characteristic of the photonic mode this is NOT the case. This is shown in detail in Appendix H. The electric and magnetic fields in a LHM may be obtained from Maxwell's equation, where

$$\vec{D} = \epsilon_{\text{eff}}\vec{E}, \tag{4.38}$$

$$\vec{H} = \nu_{\text{eff}}\vec{B}. \tag{4.39}$$

We shall use the boundary conditions given by Eqs.(4.35) and (4.36) in order to find the reflection and transmission coefficients for an incoming wave propagating from medium (a)(RHM) to medium (b) (LHM), as shown in Fig.4.3.

Let us start with the case where the electric field only has the component $\vec{E}_i = E_i\hat{x}$ (TE-mode). From (4.7) we obtain

$$H_y = \left(\frac{1}{\omega\mu_{\text{eff}}}\right) q_z E_x. \tag{4.40}$$

Therefore, continuity of tangential components of $\vec{E}$ and $\vec{H}$ leads to

$$E_0 + E_1 = E_2, \quad H_0 + H_1 = H_2, \tag{4.41}$$

where $E_{0x} = E_0$, $E_{1x} = E_1$ and $E_{2x} = E_2$. Noting that $q_{1z} = -q_{0z}$, after some algebraic manipulations and using Snell's law for transparent media [58], we find

$$E_1 = \frac{\alpha - \beta}{\alpha + \beta} E_0, \tag{4.42}$$

$$E_2 = \frac{2\alpha}{\alpha + \beta} E_0. \tag{4.43}$$

where, $\alpha = |\mu_{\text{eff}}| \sin\theta_2 \cos\theta_0$, and $\beta = \mu_1 \sin\theta_0 \cos\theta_2$. These results allow us to compute the reflection and transmission coefficients for the TE-incident wave. For that, we need to compute the Poynting vector $S_i = \epsilon_{ijk} E_j H_k$. For a LHM, using Maxwell's equations (4.7) and (4.8),

$$S_i = -\sqrt{\frac{\epsilon_{\text{eff}}}{\mu_{\text{eff}}}} E_j E_j \hat{q}_i. \tag{4.44}$$

where we identified $\hat{q}_i|\vec{q}|/\omega = -|n_{\text{eff}}|\hat{q}_i$.

The reflection coefficient $R = \langle S_1\rangle/\langle S_0\rangle$ may be computed as the ratio between the average reflected flux $\langle S_1\rangle$ and the average incident flux $\langle S_0\rangle$. For the transmission coefficient, we have $T = \langle S_2\rangle/\langle S_0\rangle$, where $\langle S_2\rangle$ is the average transmitted flux. Assuming $\langle S_1\rangle$ in the same direction as the wave vector, as we are in a right-handed medium, $\theta_0 = \theta_1$, and considering medium (a) ($n = 1$) and medium (b) ($n_{\text{eff}} = -1$) transparent, from Eqs.(4.42) and (4.43) we obtain

$$R = \frac{(\alpha-\beta)^2}{(\alpha+\beta)^2}, \tag{4.45}$$

$$T = \frac{4\alpha\beta}{(\alpha+\beta)^2}, \tag{4.46}$$

which give the reflection and transmission coefficient for a TE-incident wave. Note that $R + T = 1$ as expected, since no energy is absorbed by the LHM, as we have seen before.

Eqs.(4.45) and (4.46) can be further simplified for the photonic mode, $\omega = |\vec{q}|$, where $\theta_0 = \theta_2$, as shown in Fig.4.3. We find

$$R = \left(\frac{|\mu_{\text{eff}}| + \mu_1}{|\mu_{\text{eff}}| - \mu_1}\right)^2, \tag{4.47}$$

$$T = \frac{4|\mu_{\text{eff}}|\mu_1}{\left(|\mu_{\text{eff}}| + \mu_1\right)^2}. \tag{4.48}$$

As mentioned before, for the photonic mode $\omega = |\vec{q}|$, $\epsilon_{\text{eff}} = \nu_{\text{eff}} \to -\infty$, or $\mu_{\text{eff}} \to 0$. We then obtain the coefficients of reflection $R = 1$, and transmission $T = 0$, for that mode. This implies that, if the radiation propagates in vacuum ($n = 1$), and the external medium is a LHM ($n_{\text{eff}} = -1$), we obtain total reflection at the interface for any angle of incidence, suggesting that a LHM can be used as a waveguide with no energy dissipation.

Chapter 5

Electromagnetic responses of a charged relativistic Bose gas

5.1 Introduction

In this chapter, we address the interaction of a classical electromagnetic field with the relativistic Bose gas, using a semiclassical version of scalar quantum electrodynamics at finite temperature and charge density. Using an approach similar to the one discussed in the relativistic electron gas in previous chapters, we derive the effective electric permittivity, the effective magnetic permeability, and the electromagnetic modes of propagation of the gas, both in the normal and condensed phase.

5.2 Field theory treatment

Let us begin by writing the Euclidean grand partition function of the relativistic Bose gas interacting with an external electromagnetic field A_μ as a functional integral over gauge and charged bosonic fields ϕ^* and ϕ

$$\Xi = \oint [dA][d\phi^*][d\phi] \det\left(\frac{\partial F}{\partial \lambda}\right)\delta(F) \times \exp\left(-\int d^4x_E\, \mathscr{L}_{\text{SQED}}\right). \tag{5.1}$$

Here, ϕ is the complex scalar field (ϕ^* its complex conjugate) that represents charged spin-0 bosons with mass m and charge e. The Lagrangian density $\mathscr{L}_{\text{SQED}}$ of Scalar Quantum Electrodynamics (SQED) is written as [22]

$$\mathscr{L}_{\text{SQED}} = \frac{1}{4} F_{\mu\nu} F_{\mu\nu} + \bar{D}_\mu \phi^* \bar{D}_\mu \phi + m^2 \phi \phi^*, \tag{5.2}$$

with $F_{\mu\nu} = \partial_\nu A_\mu - \partial_\mu A_\nu$, the field strength tensor, and $\bar{D}_\mu \phi = (\bar{\partial}_\mu - ieA_\mu)\phi$, the gauge-covariant derivative. Here, we also introduced the chemical potential ξ via $\bar{\partial}_\mu \equiv (\partial_4 - \xi, \partial_i)$. Integrating Eq.(5.1) over the scalar fields with boundary conditions $\phi(0, \vec{x}) = \phi(\beta, \vec{x})$, one obtains a bosonic determinant. This leads to an effective action S_{eff}

$$S_{\text{eff}} = \frac{1}{4} \int_0^\beta d\tau \int d^3x \left(F_{\mu\nu} F_{\mu\nu} \right) + \operatorname{Tr} \ln(-\bar{D}^2 + m^2). \tag{5.3}$$

Since we accounted for the quantum contribution of the bosons by the integration over the scalar fields, by extremizing the effective action in Eq. (5.3)

$$\frac{\delta S_{\text{eff}}}{\delta A_\nu(x)} = 0, \tag{5.4}$$

we obtain the equation of motion

$$-\partial_\mu F_{\mu\nu} + \frac{\delta}{\delta A_\nu(x)} \operatorname{Tr} \ln(-\bar{D}^2 + m^2) = 0, \tag{5.5}$$

that is, Maxwell's equation $\partial_\mu F_{\mu\nu} = J_\nu(x)$, where the total current J_ν is given by

$$J_\nu(x) = \frac{\delta}{\delta A_\nu(x)} \operatorname{Tr} \ln(-\bar{D}^2 + m^2). \tag{5.6}$$

Note that

$$\bar{G}^{-1}(A) \equiv -\bar{D}^2 + m^2 = (\bar{G}_0^{-1} + \Pi) = (1 + \Pi \bar{G}_0) \bar{G}_0^{-1}, \tag{5.7}$$

where $\bar{G}_0^{-1} \equiv \bar{G}^{-1}(A=0) = (-\bar{\partial}^2 + m^2)$ is the inverse of the free boson propagator, and

$$\Pi = 2ieA \cdot \bar{\partial} + ie(\bar{\partial} \cdot A) + e^2 A^2. \tag{5.8}$$

Therefore, Eq.(5.6) reads

$$J_\nu(x) = \frac{\delta}{\delta A_\nu(x)} \operatorname{Tr} \ln(\bar{G}_0^{-1}) + \frac{\delta}{\delta A_\nu(x)} \operatorname{Tr} \ln(1 + \Pi \bar{G}_0^{-1}), \tag{5.9}$$

Note that the dependence on the external gauge field A comes only through $\Pi \equiv \Pi(A)$, thus $\operatorname{Tr} \ln \bar{G}_0^{-1}$ does not contribute to the current density which is given by

$$J_\nu = \frac{\delta}{\delta A_\nu(x)} \operatorname{Tr} \ln(1 + \Pi \bar{G}_0^{-1}). \tag{5.10}$$

We are interested in the linear response to the external gauge field, therefore one may expand Eq.(5.10), and retain terms up to order $O(A^2)$. For weak background A_ν, the current density in linear response is

$$J_\nu(x) = \frac{\delta}{\delta A_\nu(x)}\left(\mathrm{Tr}\ln(\Pi\bar{G}_0) - \frac{1}{2}\mathrm{Tr}\ln(\Pi\bar{G}_0\Pi\bar{G}_0)\right). \tag{5.11}$$

One may Fourier transform Eq.(5.11) (see Appendix I) to obtain

$$J_\nu(q) = \Pi_{\mu\nu}(q)A_\mu(q), \tag{5.12}$$

where $\Pi_{\mu\nu}$ is the field theory polarization tensor for scalar quantum electrodynamics, which contributes two terms to the current: the tadpole and the thermal bubble Feynman graphs

$$\Pi_{\mu\nu}(q) = -\frac{2e^2}{\beta}\sum_{n=-\infty}^{+\infty}\int\frac{d^3p}{(2\pi)^3}\frac{\delta_{\mu\nu}}{\bar{p}^2+m^2} + \frac{e^2}{\beta}\sum_{n=-\infty}^{+\infty}\int\frac{d^3p}{(2\pi)^3}\frac{(2\bar{p}_\mu+q_\mu)(2\bar{p}_\nu+q_\nu)}{(\bar{p}^2+m^2)[(\bar{p}+q)^2+m^2]}. \tag{5.13}$$

The sum is over bosonic Matsubara frequencies $\bar{p}_4 = 2n\pi T + i\xi$, with ξ the chemical potential. Writing $\Pi_{\mu\nu} = \Pi^{(v)}_{\mu\nu} + \Pi^{(m)}_{\mu\nu}$, where the former corresponds to the value at $T = 0$ and $\xi = 0$, we have used symmetry and gauge invariance [21, 23] to derive its tensor form in Appendix C. Here, the scalar functions $\mathscr{A}$ and $\mathscr{B}$ will be a function of the components of the polarization tensor for bosons in (5.13), Π_{44} and $\Pi_{\mu\mu}$. The Matsubara sum and the integral over angles can be done using the same procedure we used for fermions in appendices D and E, to arrive at

$$\begin{aligned}\mathscr{B}(q_4,\vec{q}) &= -\frac{\Pi^{(m)}_{44}}{q^2}\\ &= \frac{e^2}{q^2}\mathrm{Re}\int\frac{d^3p}{(2\pi)^3}\frac{n_B(p)}{\omega_p}\left(\frac{\vec{q}^2+4\omega_p^2-2p_4q_4+2\vec{p}\cdot\vec{q}}{q^2+2p_4q_q+2\vec{p}\cdot\vec{q}}\right),\end{aligned} \tag{5.14}$$

and

$$\begin{aligned}\mathscr{A}(q_4,\vec{q}) &= -\frac{\Pi^{(m)}_{\mu\mu}}{2q^2} + \left(\frac{3}{2|\vec{q}|^2} - \frac{1}{q^2}\right)\Pi^{(m)}_{44}\\ &= \frac{e^2}{2(2\pi)^3q^2}\mathrm{Re}\int\frac{d^3p}{\omega_p}n_B(p)\frac{3q^2+3m^2+4p\cdot q}{q^2+2p\cdot q} + \left(1-\frac{3q^2}{2|\vec{q}|^2}\right)\mathscr{B},\end{aligned} \tag{5.15}$$

where $n_B(p) = n_B^-(p) + n_B^+(p)$ is the Bose-Einstein distribution for bosons and antibosons

$$n_B(p) = \frac{1}{e^{\beta(\omega_p-\xi)}-1} + \frac{1}{e^{\beta(\omega_p+\xi)}-1}. \tag{5.16}$$

The contribution of the antibosons becomes relevant only for relativistic temperatures ($T \gg m$) or relativistic densities ($\eta \gg m^3$). Fig. 5.1 shows the ratio of the density of antibosons and that of bosons, $\rho = N^+/N^-$, as a function of temperature for some values of the total density for an ideal Bose gas, where

$$\rho = \frac{N^+}{N^-} = \frac{\int d^3p \frac{1}{e^{\beta(\omega_p+\xi)}-1}}{\int d^3p \frac{1}{e^{\beta(\omega_p-\xi)}-1}}. \tag{5.17}$$

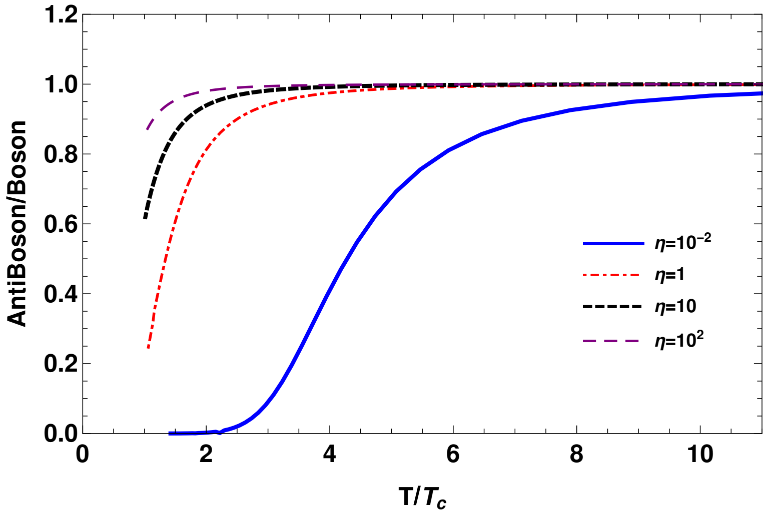

Figure 5.1: The ratio $\eta = N^+/N^-$ of the densities of antibosons and bosons for the ideal relativistic Bose gas as a function of the temperature for some values of total density η (in units of $(mc/\hbar)^3$).

We are now ready to discuss the responses both above and below the critical temperature of Bose-Einstein condensation:

a. For $T > T_c$, the permittivities and inverse permeabilities are determined by the three scalar functions $\mathscr{A}^*$, $\mathscr{B}^*$, and $\mathscr{C}^*$. The asterisk denotes continuation to Minkowski space $q_4 \to i\omega - 0^+$ of the Euclidean scalar functions $\mathscr{A}(|\vec{q}|, q_4)$, $\mathscr{B}(|\vec{q}|, q_4)$ and $\mathscr{C}(\vec{q}^2 + q_4^2)$. From now on, we shall use the Minkowski definition $q^2 = \omega^2 - |\vec{q}|^2$ ($q_E^2 \to -q_M^2$);

b. For $T < T_c$, a part $\eta^{(c)}(T)$ of the density of charge $n^+ - n^-$ condenses in the ground state ($\vec{p} = 0$), as Bose-Einstein condensation sets in for $\xi = m$. To account for the part that condenses, the Bose-Einstein distribution $n(p)$ must be modified to

$$n(p) \to (2\pi)^3 \eta^{(c)}(T) \delta^{(3)}(\vec{p}) + n'(p), \tag{5.18}$$

with

$$n'(p) = \frac{1}{e^{\beta(\omega_p - m)} - 1} + \frac{1}{e^{\beta(\omega_p + m)} - 1}. \tag{5.19}$$

However, the contribution of the antibosons will vanish in condensed phase, $n^+ = 0$. The modification has a contribution due to the charge density in the ground state, and another due to the particles in excited states. The longitudinal responses become

$$\epsilon_L(\omega, |\vec{q}|) = 1 + \mathscr{C}^* - \omega_e^2 \left(\frac{q^2 - 4m^2}{q^4 - 4m^2\omega^2} \right) - \frac{q^2}{|\vec{q}|^2} \mathscr{B}_T^*,$$
$$\nu_L(\omega, |\vec{q}|) = 1 - \frac{2\omega_e^2}{q^2} + 2\mathscr{C}^* + 2\mathscr{A}_T^* - 2\frac{\omega^2}{|\vec{q}|^2}\mathscr{B}_T^*. \tag{5.20}$$

$\omega_e^2 = e^2\eta^{(c)}/m$ is the longitudinal electric plasmon frequency; $\mathscr{A}_T^*$ and $\mathscr{B}_T^*$ are the functions $\mathscr{A}^*$ and $\mathscr{B}^*$ with the modification $n(p) \to n'(p)$.

c. For $T = 0$, all the charge condenses, so $n'_c(p) \to 0$, and the scalar functions $\mathscr{A}_T^*$ and $\mathscr{B}_T^*$ vanish. Neglecting the vacuum contribution ($\mathscr{C}^* << 1$), one obtains

$$\epsilon_L(\omega, |\vec{q}|) = 1 - \omega_e^2 \left(\frac{q^2 - 4m^2}{q^4 - 4m^2\omega^2} \right),$$
$$\nu_L(\omega, |\vec{q}|) = 1 - \frac{2\omega_e^2}{q^2}, \tag{5.21}$$

for $q^2 < 4m^2$. For $q^2 > 4m^2$, as $|\vec{q}| \to 0$, the longitudinal responses at $T = 0$ are the same as those obtained in [17] for the relativistic electron gas, $\epsilon_L = 1 - \omega_e^2/\omega^2$ and $\nu_L = 1 - 2\omega_e^2/\omega^2$.

5.3 Imaginary part of ϵ_L

The imaginary part of the longitudinal permittivity is

$$\mathrm{Im}\epsilon_L = -\frac{q^2}{|\vec{q}|^2}\mathrm{Im}\mathscr{B}^*. \tag{5.22}$$

Note that the scalar function is $\mathscr{B}^* = \Pi_{00}^{(m)}/q^2$. The component $\Pi_{00} = \Pi_{00}^{(m)} + \Pi_{00}^{(v)}$ of the polarization tensor for bosons may be computed in alternative form as

$$\begin{aligned}
\Pi_{00} &= e^2 \int \frac{d^3p}{(2\pi)^3} \frac{1 + n^+(p) + n^-(p)}{\omega_p} \\
&- e^2 \int \frac{d^3p}{(2\pi)^3} \frac{C^*}{4\omega_p\omega_{p+q}} \left[-\frac{1 + n^+(p) + n^-(p+q)}{\omega - \omega_p - \omega_{p+q} + i0^+} + \frac{n^-(p+q) - n^-(p)}{\omega + \omega_p - \omega_{p+q} + i0^+} \right. \\
&- \left. \frac{n^+(p) - n^+(p+q)}{\omega - \omega_p + \omega_{p+q} + i0^+} + \frac{1 + n^-(p) + n^+(p+q)}{\omega + \omega_p + \omega_{p+q} + i0^+} \right],
\end{aligned} \tag{5.23}$$

where $C^* = 2(\omega_p^2 + \omega_{p+q}^2) - \omega^2$. At $T = 0$, a macroscopic charge density condenses in the ground state ($\vec{p} = 0$), so we have $n^-(p) = (2\pi)^3\eta\delta^{(3)}(\vec{p})$ and $n^-(p+q) = (2\pi)^3\eta\delta^{(3)}(\vec{p}+\vec{q})$, with

$n^+(p) = n^+(p+q) = 0$. Thus, substituting the component of the polarization tensor above in the scalar function $\mathscr{B}^*$, we obtain the longitudinal permittivity ϵ_L

$$
\begin{aligned}
\epsilon_L &= 1 - \frac{e^2}{\vec{q}^2}\int \frac{d^3p}{(2\pi)^3}\frac{1}{\omega_p} + \frac{e^2\eta}{m\vec{q}^2} \\
&- \frac{e^2}{\vec{q}^2}\int \frac{d^3p}{(2\pi)^3}\frac{(\omega_p-\omega_{p+q})^2}{4\omega_p\omega_{p+q}}\left[\frac{1}{\omega+\omega_p+\omega_{p+q}+i0^+} - \frac{1}{\omega-\omega_p-\omega_{p+q}+i0^+}\right] \\
&- \frac{e^2}{\vec{q}^2}\eta\frac{(\omega_q-\omega_0)^2}{4\omega_q\omega_0}\left[\frac{1}{\omega-\omega_q-\omega_0} - \frac{1}{\omega+\omega_0+\omega_q}\right] \\
&- \frac{e^2}{\vec{q}^2}\eta\frac{(\omega_q+\omega_0)^2}{4\omega_q\omega_0}\left[\frac{1}{\omega+\omega_0-\omega_q} - \frac{1}{\omega+\omega_q-\omega_0}\right],
\end{aligned}
\tag{5.24}
$$

where $\omega_0 = m$. Note that the first integral has a divergent contribution, which can be suppressed by a minimal subtraction renormalization. The imaginary part of ϵ_L may be obtained using the relation

$$\frac{1}{\omega-\omega_0 \pm i0^+} = P\left(\frac{1}{\omega-\omega_0}\right) \mp i\pi\delta(\omega-\omega_0). \tag{5.25}$$

For $\omega > 0$, we have

$$\mathrm{Im}\epsilon_L = \frac{e^2\pi}{\vec{q}^2}\int \frac{d^3p}{(2\pi)^3}\frac{(\omega_p-\omega_{p+q})^2}{4\omega_p\omega_{p+q}}\delta(\omega+\omega_p+\omega_{p+q}). \tag{5.26}$$

After we integrate the expression above over angles, imaginary parts appear only for frequencies such that $\omega^2 > 4m^2 + |\vec{q}|^2$. Note that, when $|\vec{q}| = 0$, we always have imaginary parts for $\omega > 2m$, which indicates that photons will decay into boson-antiboson pairs of total mass $2m$. Thus, the expression for imaginary part at $T = 0$ is

$$\mathrm{Im}\epsilon_L(\omega, |\vec{q}|) = \frac{e^2}{48\pi}\left(\frac{q^2}{q^2-4m^2}\right)^{3/2}. \tag{5.27}$$

5.4 Nonrelativistic limit for bosons

The nonrelativistic limit of longitudinal responses may be obtained similarly to what was done for the REG in 2.4. The Bose distribution $n_B(p) \to [e^{\beta(\omega_p-\xi)}-1]^{-1} \equiv n(p)$ accounts only the for the boson contributions, since the antibosons contribution will vanish, and the longitudinal responses in that limit become $\epsilon_L \approx 1 + \mathscr{B}$. We obtain

$$\epsilon_L = 1 - \frac{e^2}{|\vec{q}|}\mathrm{Re}\int \frac{d^3p}{(2\pi^3)}\frac{n(\vec{p}-\vec{q}) - n(\vec{p})}{\varepsilon_{p-q} - \varepsilon_p - \omega - i0^+}. \tag{5.28}$$

The result above is the same as the one obtained in [72] for a charged Bose gas in the random-phase approximation, and similar to what was obtained for the REG in the nonrelativistic limit, with the Fermi distribution. Integrating the expression above over angles, one obtains

$$\epsilon_L = 1 + \frac{e^2 m}{4\pi^2 |\vec{q}|^3} \int_0^\infty p\, dp\, n(p) \ln \left[\frac{(|\vec{q}|^2 + 2p|\vec{q}|)^2 - 4m^2\omega^2}{(|\vec{q}|^2 - 2p|\vec{q}|)^2 - 4m^2\omega^2} \right]. \tag{5.29}$$

We may now discuss the Bose-Einstein condensation. For temperatures $T < T_c$, where T_c is the critical temperature of condensation. With the Bose-Einstein distribution modified to include the ground state charged density as defined in 5.19, we obtain in the condensed phase $T < T_c$

$$\epsilon_L = 1 - \frac{\omega_e^2}{\omega^2 - |\vec{q}|^2/4m^2} + \frac{e^2 m}{4\pi^2 |\vec{q}|^3} \int_0^\infty p\, dp\, n'(p) \ln \left[\frac{(|\vec{q}|^2 + 2p|\vec{q}|)^2 - 4m^2\omega^2}{(|\vec{q}|^2 - 2p|\vec{q}|)^2 - 4m^2\omega^2} \right], \tag{5.30}$$

with $\omega_e^2 = e^2\eta^{(c)}/m$, and $n'(p) \equiv [e^{\beta\omega_p} - 1]$, where $\xi = 0$ is the condition for condensation in the nonrelativistic limit. At $T = 0$, all the charge density condenses ($n'(p) \to 0$), and

$$\epsilon_L = 1 - \frac{\omega_e^2}{\omega^2 - \frac{|\vec{q}|^2}{4m^2}}. \tag{5.31}$$

Note that, in the long-wavelength limit ($\vec{q} \to 0$), we obtain a Drude-type expression for the longitudinal response, $\epsilon_L = 1 - \omega_e^2/\omega^2$.

5.5 Propagation

We now turn our attention to the propagation of collective modes in the gas, and evaluate how the medium affects the photon propagator. Just as in the case of the relativistic electron gas, we obtain the photon propagator $\Gamma^{-1}_{\mu\nu}$ in the form

$$\Gamma^{-1}_{\mu\nu} = \frac{\mathscr{P}^L_{\mu\nu}}{-q^2\epsilon_L} + \frac{\mathscr{P}^T_{\mu\nu}}{-q^2(\nu_L + 1)} + \frac{\lambda}{q^2}\frac{q_\mu q_\nu}{q^2}, \tag{5.32}$$

where we have introduced the longitudinal $\mathscr{P}^L_{\mu\nu}$ and transverse $\mathscr{P}^T_{\mu\nu}$ projectors in eq. (3.31). The poles of the photon propagator correspond to collective excitations and yield their dispersion relations.

In the longitudinal propagator, there is a pole whenever the longitudinal electric permittivity vanishes $\epsilon_L(\omega, \vec{q}) = 0$, leading to a longitudinal plasmon mode. For $\epsilon_L(\omega, \vec{q})$ nonzero, Maxwell's equations lead to transverse fields $\vec{q}\cdot\vec{E}=0$ that vanish when contracted with $\mathscr{P}^L_{\mu\nu}$, so that $q^2=0$ is not realized in this case. The transverse propagator has a pole whenever $\mu_L^{-1}(\omega,\vec{q})=\nu_L(\omega,\vec{q})=-1$, which corresponds to collective oscillations of the current density. It has another pole whenever $q^2=\omega^2-|\vec{q}|^2=0$, which corresponds to a photonic mode propagating with the speed of light c in vacuum. Similar modes have already appeared in the relativistic electron gas [43].

At $T=0$, the plasmon modes have longitudinal $\omega_L(|\vec{q}|)$ and transverse $\omega_T(|\vec{q}|)$ dispersion relations, obtained from (5.21), given by

$$\omega^2_{L\pm}=\frac{1}{2}(4m^2+\omega_e^2+2|\vec{q}|^2)\pm\frac{1}{2}\sqrt{(4m^2-\omega_e^2)^2+16m^2|\vec{q}|^2},$$

$$\omega_T^2=\omega_e^2+|\vec{q}|^2. \tag{5.33}$$

The expression for ω_L^2 has two branches: one beginning at $\omega_{L-}=\omega_e$, at $|\vec{q}|=0$; the other, which leads to pair creation, beginning at $\omega_{L+}=2m$, at $|\vec{q}|=0$. For $\omega_e^2<4m^2$, the longitudinal mode will show a local minimum at low values of $|\vec{q}|$, known as *negative dispersion* [71]. This behavior will appear only in the relativistic regime, since in the non-relativistic limit our expression reduces to $\omega_L^2=\omega_e^2+|\vec{q}|^4/4m^2$, the same result obtained in [72] for a charged Bose gas within the random phase approximation. Fig 5.2 shows the normalized longitudinal modes ω_{L-} at zero temperature as a function of wave vector for some value of Bose gas density. Fig. 5.3 shows the dispersion curves of the two possibilities for the longitudinal mode and the transverse modes.

5.6 Negative refraction

We stress that the responses discussed thus far are NOT the ones appearing in Maxwell's equations. In order to find the exact analog of the situation proposed by Veselago [7], we need the effective electric permittivity and effective magnetic permeability that appear in the two equations with sources. Following [44] and eqs. (4.9) and (4.10), we may define the

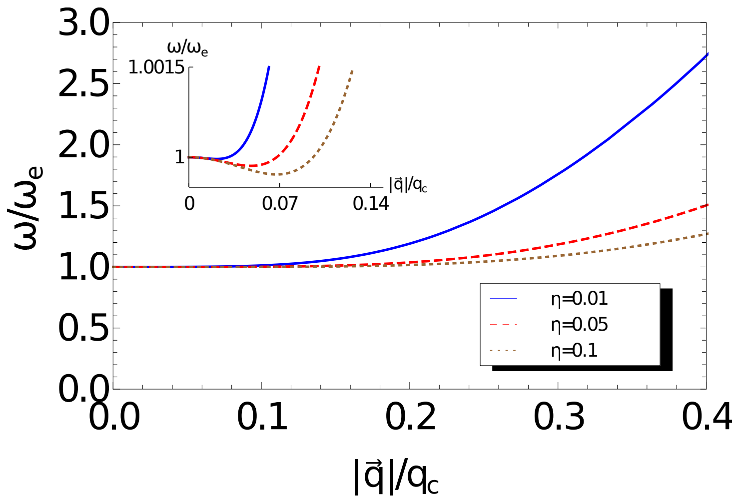

Figure 5.2: Normalized longitudinal plasmon dispersion, ω_{L-}, for $\omega_e^2 < 4m^2$, at zero temperature for some values of boson density η in units of mc$/\hbar)^3$. The region of *negative dispersion* is shown in the inset.

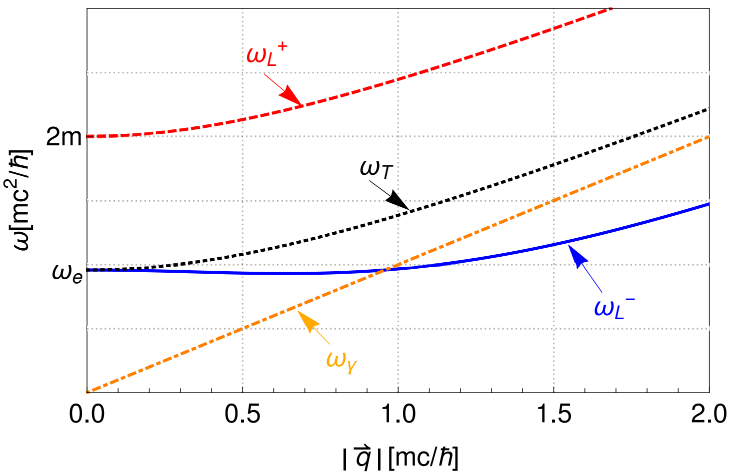

Figure 5.3: Longitudinal (ω_L), transverse (ω_T), and photonic (ω_γ) modes at $T = 0$ and boson density $\eta = 10(\mathrm{mc}/\hbar)^3$.

effective responses as

$$\nu_{\text{eff}} = \nu_T - \frac{\omega\tau}{|\vec{q}|}, \quad \epsilon_{\text{eff}} = \epsilon_T + \frac{|\vec{q}|}{\omega}\tau, \tag{5.34}$$

where $\epsilon_T = \epsilon$ and $\nu_T = \nu$. In terms of $\mathscr{A}^*$ and $\mathscr{B}^*$ ($\mathscr{C}^* << 1$), we have

$$\epsilon_{\text{eff}} = \nu_{\text{eff}} = \mu_{\text{eff}}^{-1} = \frac{\nu_L + 1}{2} = 1 + \mathscr{A}^* - \frac{\omega^2}{|\vec{q}|^2}\mathscr{B}^*. \tag{5.35}$$

Expression (5.35) immediately implies that $|n_{\text{eff}}| = \mu_{\text{eff}}\epsilon_{\text{eff}} = 1$, for any temperature and chemical potential. It also implies $\epsilon_{\text{eff}} = \nu_{\text{eff}} < 0$ as long as $\nu_L < -1$, which means that we will have left-handed behavior for frequencies below the transverse plasmon frequency $\omega_T(|\vec{q}|)$, ($\nu_L = -1$), for any temperature and chemical potential. In particular, for $T = 0$, using (5.21), we obtain

$$\epsilon_{\text{eff}} = \nu_{\text{eff}} = \frac{\nu_L + 1}{2} = \left(1 - \frac{\omega_e^2}{q^2}\right), \tag{5.36}$$

which reduces, in the limit $|\vec{q}| \to 0$, to a Drude expression $\epsilon_{\text{eff}} = \nu_{\text{eff}} = (1 - \omega_e^2/\omega^2)$.

The existence of a photonic mode $\omega_\gamma = |\vec{q}|$ with the speed of light in vacuum is another indication that the modulus of the effective index of refraction of the gas is equal to one. Since, both $\epsilon_{\text{eff}} < 0$ and $\nu_{\text{eff}} < 0$, for $\omega_\gamma(|\vec{q}|) \leq \omega < \omega_T(|\vec{q}|)$, for any temperature and chemical potential, one may use Snell's law to show that $n_{\text{eff}} = -1$ in that region, a negative refraction typical of a left-handed material [7, 44]. The shadowed sections of Fig.5.4 illustrate those regions for both $T = 0$ and $T \neq 0$. Similar behavior was obtained in the analysis of the relativistic electron gas, confirming our hypothesis that the relativistic nature of the gas was the key ingredient to achieve left-handed behavior.

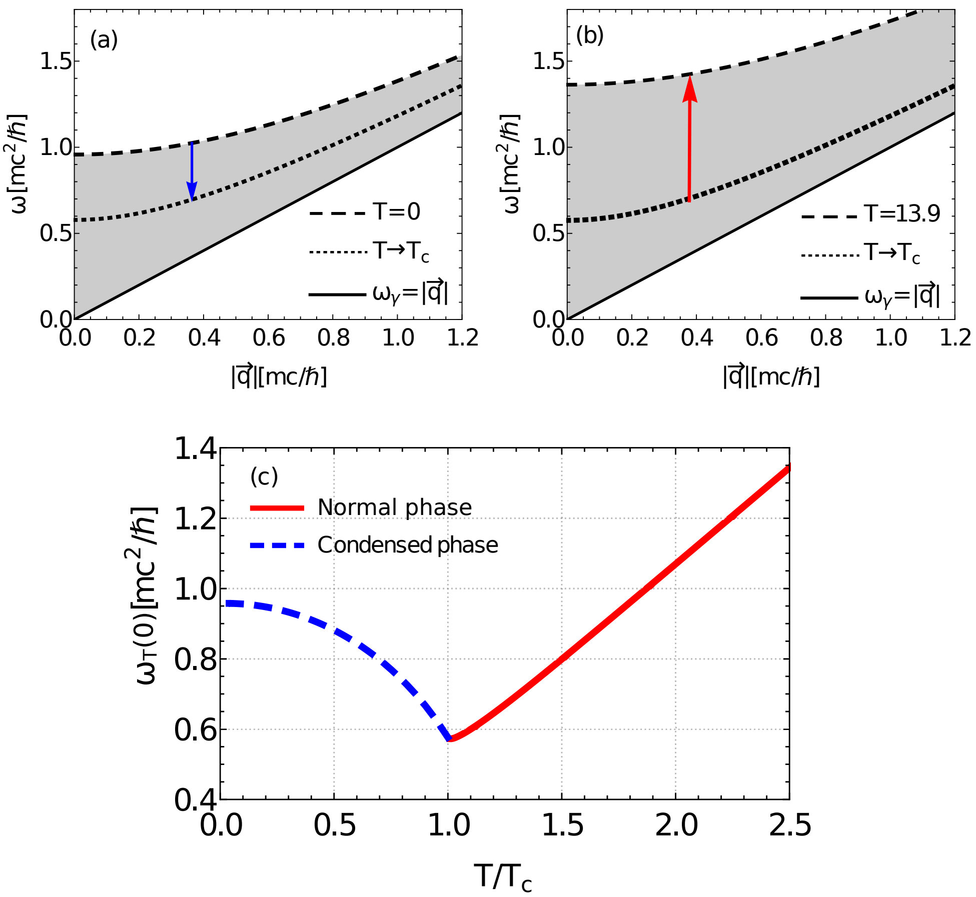

Figure 5.4: The shadowed regions illustrate where the RBG is a LHM: (a) in the condensed phase, the LHM region decreases with the temperature until we reach the critical temperature T_c; (b) above the critical temperature T_c, the LHM region starts to increase with the temperature; (c) transverse plasmon ω_T at $|\vec{q}| = 0$ as a function of the relative temperature. Calculations were performed for $\eta = 10(mc/\hbar)^3$ and $T_c = 5.47mc^2/k_B$.

Fig.5.4(a) shows that, in the condensed phase, the region where the gas exhibits left-handed behavior shrinks with increasing temperature, at least up to T_c. Somewhere above T_c (see Fig.5.4.(b)), the region expands and, for the case of ultra-relativistic densities ($\eta \geq (mc/\hbar)^3$), it begins to expand at the critical temperature $T = T_c$, as illustrated in Fig.5.4(c). Fig.5.5 shows the plasmon energy at $|\vec{q}| = 0$, normalized by its value at $T = 0$, as a function of $T/T_c(\eta)$ for various densities.

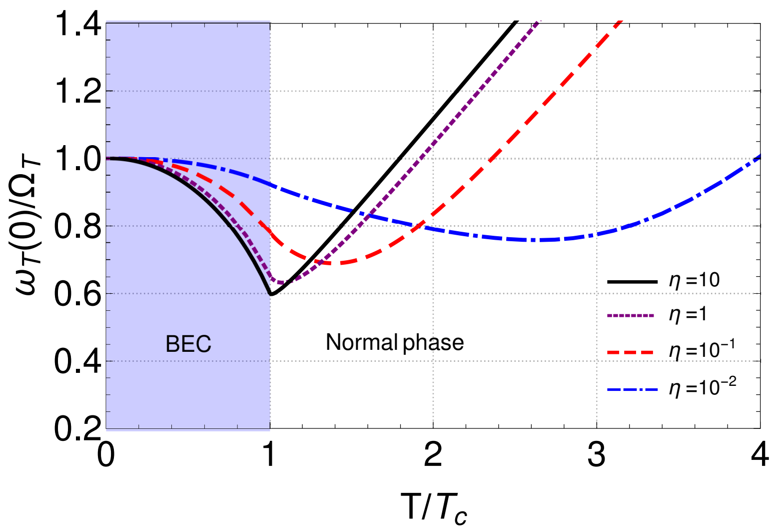

Figure 5.5: Normalized transverse plasmon frequency in the long-wavelength limit ($|\vec{q}| = 0$) as a function of the relative temperature for various densities [in units of $(mc/\hbar)^3$] of the Bose gas in units of $\Omega_T \equiv \omega_T(|\vec{q}| = 0, T = 0)$. In the shadowed region, below the critical temperature T_c, the gas is in the Bose-Einstein condensed phase (BEC). For each density η, the critical temperatures [in units of (mc^2/k_B)] are $T_c = 5.47(\eta = 10)$, $T_c = 1.72(\eta = 1)$, $T_c = 0.53(\eta = 10^{-1})$, and $T_c = 0.14(\eta = 10^{-2})$.

In contrast to the non-relativistic case, the transverse plasmon frequency at $|\vec{q}| = 0$, known as plasmon gap energy, is a function of temperature for relativistic densities. In fact, the two regimes just described correspond to $T < T_t$ and $T \geq T_t$, where T_t is the temperature at which the transverse plasmon gap energy reaches a minimum, and then increases linearly with temperature. The ratio $T_t/T_c(\eta)$ decreases with increasing density until it reaches unity, as can be seen in Fig.5.6.

For ultra-relativistic densities, one may perform a high temperature hard thermal loop expansion [22], and derive analytic solutions for the transverse plasmon frequency $\omega_T(|\vec{q}|)$. At $|\vec{q}| = 0$, we obtain $\omega_T^2(0) = \omega_e^2 + e^2T^2/9$, for $T \leq T_c$, and $\omega_T^2(0) = e^2T^2/9$, for $T \geq T_c$. For $T < T_c$, using $\omega_e^2 = e^2\eta^{(c)}/m$, and the ultra-relativistic expression $\eta^{(c)} = \eta(1 - T^2/T_c^2)$, we obtain

$$\omega_T^2(0) = \frac{e^2\eta}{m}\left[1 - \left(\frac{T}{T_c}\right)^2\right] + \frac{e^2T^2}{9}, \tag{5.37}$$

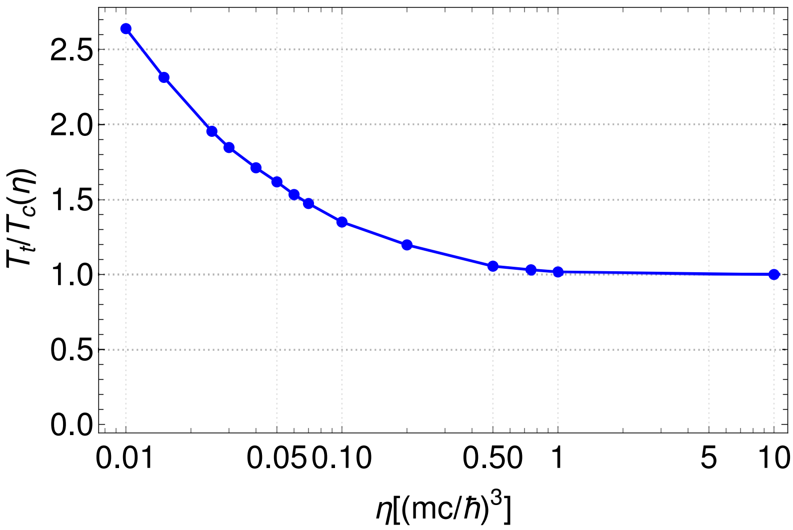

Figure 5.6: The ratio $T_t/T_c(\eta)$ as a function of the total charge density η. For temperatures $T \geq T_t$, the transverse plasmon gap energy, ω_T, increases linearly with the temperature, where $T_c(\eta)$ is the critical temperature where the gas condenses for density η. For densities above $\eta = 1$, we have $T_t \approx T_c$, characterizing the relativistic regime.

which shows that the transverse plasmon frequency decreases with temperature in the condensed phase, whereas it increases linearly in the normal phase, with $\omega_T(0) = eT/3$, for $T \geq T_c$.

5.7 Rotons

We now turn to the longitudinal plasmon mode. For $T > 0$, we have to resort to numerical results. Fig.5.7(a) depicts the longitudinal dispersion relation $\mathrm{Re}[\epsilon_L] = 0$ for temperatures above and below the critical temperature T_c of Bose-Einstein condensation. For $T > T_c$, the dispersion relation is similar to the case of the relativistic electron gas. For $T < T_c$, we observe a new kind of elementary excitation, with a local maximum and a local minimum analogous to the maxons and rotons in the spectrum of *neutral* superfluid ^{4}He described by Landau [58], who proposed the existence of two kinds of elementary excitations in a *neutral* superfluid: phonons, for low wave vectors, associated to acoustic waves; and rotons, gapped excitations at finite momentum $|\vec{q}| = |\vec{q}_{rot}|$, interpreted as vortices in the superfluid.

The existence of roton-like structures has been predicted for condensates of dipolar particles [59, 60, 73, 74, 75], of nonpolar atoms under the action of an intense laser light [76], and for Rydberg-excited condensates [77]. Recently, these vortex-like quasi-particles have

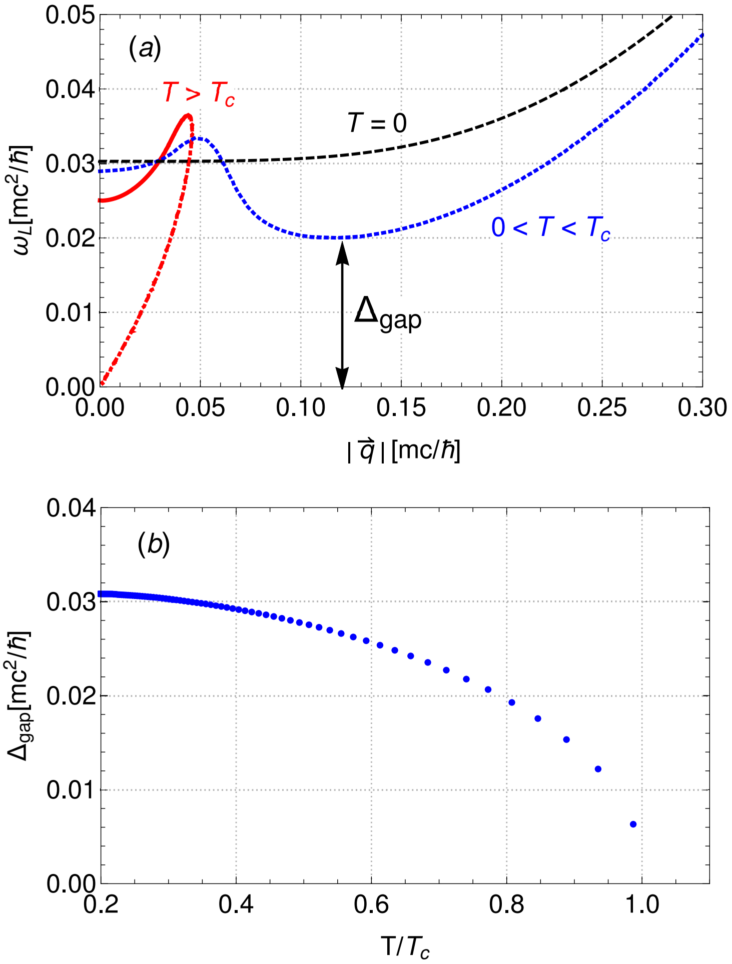

Figure 5.7: (a) Dispersion curves for longitudinal modes for $T > T_c$ (solid and dotted-dashed line), $0 < T < T_c$ (dotted line), and $T = 0$ (dashed line). The dotted-dashed line for $T > T_c$ is discarded because, for high temperatures, the longitudinal plasmon mode will behave similarly to the plasmon excitations in a relativistic electron gas, with a superior and an inferior branch. The latter does not propagate because all its values of frequency $\omega_L(|\vec{q}|)$ lie in the region where $\mathrm{Im}[\epsilon_L(\omega,|\vec{q}|)] \neq 0$, as discussed in [43]; (b) Roton gap energy as a function of the relative temperature. Calculations were performed for $\eta = 10^{-2}(mc/\hbar)^3$, and $T_c = 0.14mc^2/k_b$.

been observed for the first time in a Bose-Einstein condensate of ultra-cold atoms [78, 79]. However, in a *charged* superfluid, it has been shown that the phonon mode of the neutral superfluid is pushed to a finite plasmon frequency ω_p, whereas the roton mode is more or less unaffected [86, 87]. In the charged case, the spectrum of the superfluid field shows a plasmon excitation that turns into a roton excitation, with a gap energy $\Delta(|\vec{q}_{rot}|)$ for higher $|\vec{q}|$.

In the present study of a *charged* relativistic Bose gas, the dispersion relation of the longitudinal plasmon mode shows an *ordinary* plasmon, near $|\vec{q}| = 0$, and a *roton* excitation, near the value of $|\vec{q}|$ that corresponds to the local minimum. As the temperature is increased, the gap energy of the local minimum decreases, and Fig.5.7(b) shows how it depends on the temperature. We may view the gap energy as an order parameter, which vanishes at $T = T_c$. For $0 < T < T_c$, as the temperature is increased, the *ordinary* plasmon near $|\vec{q}| = 0$ turns into an elementary *roton* excitation with a (lower) minimum energy at finite momentum. We further illustrate the presence of rotons by presenting the dispersion curves of the longitudinal mode for various densities at temperatures below the critical temperature T_c in Fig.5.8, for non-relativistic densities [Fig.5.8(a) and (b)], and for relativistic and ultra-relativistic densities [Fig.5.8(c) and (d)]. It should be noted that those results agree remarkably well with the non-relativistic results reported in the literature, obtained via a different route [88].

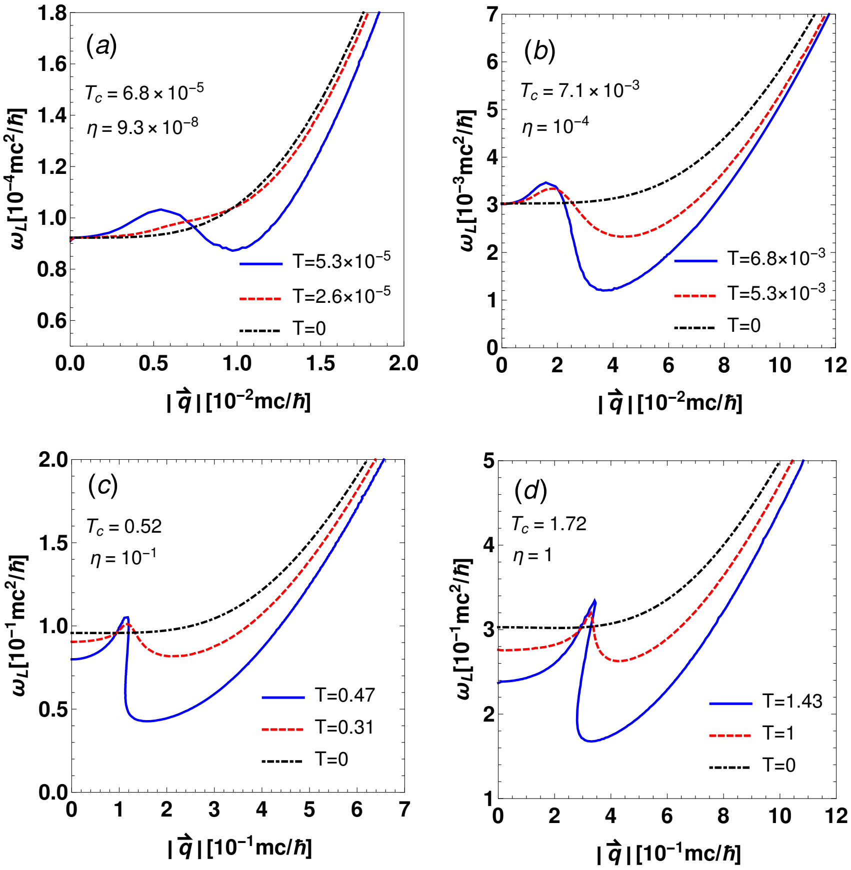

Figure 5.8: Dispersion curves for longitudinal modes for various temperatures below the critical temperature T_c (in units of mc^2/k_B), and various densities η [in units of $(mc/\hbar)^3$]. In (a) and (b), calculations were performed for non-relativistic densities and temperatures; in (c) and (d), for relativistic and ultra-relativistic.

Figures 5.7 and 5.8 suggest that thermal effects induce the rotons that will contribute to disorder the system. Thermally induced rotons were also present in the bosonic spectrum of a two-dimensional dilute Bose gas [89], where it was argued that their emergence is a consequence of the strong phase fluctuation in two dimensions.

We remark that the Lagrangian density in our approach does not include a self-interaction term $\lambda(\phi^*\phi)^2$. The condensate is introduced by performing the substitution (5.18), which yielded $T = 0$ results for the longitudinal plasmon mode in agreement with the literature in both relativistic [54] and nonrelativistic limits [72]. We plan to include self-interactions, either directly or induced by integration over quantum electromagnetic fields, in a future investigation. In the non-relativistic limit, that inclusion will be useful in the description of the superfluidity of liquid Helium at low temperatures [51]. In the relativistic limit, it could possibly help in the study of the relativistic Bose plasma found in astrophysical scenarios such as neutron stars, where the creation of charged pion pairs and pion condensation may take place [54, 55].

Chapter 6

Electromagnetic quantum shifts in relativistic Bose-Einstein condensation

6.1 Introduction

In this chapter, we compute deviations from ideal gas behavior of the pressure, density, and Bose-Einstein condensation (BEC) temperature of a relativistic gas of charged scalar bosons caused by the current-current interaction induced by electromagnetic quantum fluctuations treated via scalar quantum electrodynamics.

Normally, BEC is considered only for free boson gases. The inclusion of interactions, going now from an ideal gas into a real gas, in general is highly non trivial and several procedures have been developed. The influence of an interacting potential on the BEC critical temperature in the non-relativistic case has been discussed by several authors [90],[91]. Here, however, interaction emerges from vacuum fluctuations in scalar electrodynamics. No interacting potential is introduced by hand. The idea is to integrate out the photon degrees of freedom, producing an effective interaction for the charged bosons.

Because of its *electromagnetic* (EM) charge e, the gas will inevitably couple to EM quantum fluctuations that induce a current-current interaction. Thus, it may no longer be treated as ideal - one has to treat it via scalar quantum electrodynamics at finite temperature and charge density, the microscopic theory that naturally incorporates such fluctuations.

Within that framework, we will show that the interaction changes the pressure, density, and critical temperature of condensation of the gas with respect to their ideal gas values by amounts that depend on the fine structure constant $\alpha = e^2/4\pi\hbar c$, and compute the deviations in the ultra-relativistic (UR), relativistic, and nonrelativistic (NR) regimes.

Our calculation starts with the grand partition function of the system $\Xi = \operatorname{Tr} e^{-\beta(\hat{H}-\mu\Delta\hat{N})}$, $\Delta\hat{N} \equiv \hat{N}_+ - \hat{N}_-$, written as a functional integral over EM and scalar fields. Doing the quadratic integration over EM quantum fluctuations, we obtain an effective action for the scalars with an induced current-current interaction proportional to α.

We treat the induced interaction as a perturbation in the remaining integral over the scalars, and compute a Feynman graph that gives the current-current expectation value. Finally, we integrate that expectation value, times the photon propagator, over photonic momenta.

6.2 Formalism

From the thermodynamic potential $\Omega = -T\ln\Xi$, we obtain the pressure $P = -\Omega/V$, and the density $\eta = \Delta N/V = (\partial P/\partial\mu)_{T,V}$. Since, as before, the zero momentum state does not contribute to the sum, the condensation temperature comes from equating the integral over occupation numbers to η.

In natural units, the action for Euclidean scalar quantum electrodynamics at finite temperature and density is

$$S = \int_\Omega d^4x \left[\frac{1}{4}F_{\rho\sigma}F_{\rho\sigma} + \bar{D}_\rho\phi^*\bar{D}_\rho\phi + m^2\phi^*\phi\right], \tag{6.1}$$

where $\int_\Omega d^4x \equiv \int_0^\beta dx_4 \int_V d^3x$, $\bar{D}_\rho\phi = (\bar{\partial}_\rho - ieA_\rho)\phi$, and $\bar{\partial}_\rho \equiv (\partial_i, \partial_4 - \mu)$. The grand partition function of the system may be expressed as a functional integral [22]

$$\Xi = \oint [d\phi^*][d\phi]d\Sigma[A]\, e^{-S[\phi^*,\phi,A]}, \tag{6.2}$$

where $d\Sigma[A]$ is the gauge invariant measure for the EM field, as discussed in chapter 2. The integral symbol denotes a sum over field configurations of A_ρ, ϕ, and ϕ^* whose value at $(\vec{x},0)$ is the same as at $(\vec{x},\beta)$, boundary conditions that implement the trace.

We sum over the quantum fluctuations of the EM field, by doing the quadratic integral over A_ρ, and derive a current-current interaction. The grand partition function becomes

$$\Xi = \oint [d\phi^*][d\phi] e^{-(S_0+S_I)}, \tag{6.3}$$

where S_0 is the free bosonic action, obtained by setting $A_\rho = 0$ in Eq.(6.1), and the interacting part is

$$S_I[\phi] = -e^2 \int_\Omega d^4x \int_\Omega d^4x' J_\rho(x) G^\phi_{\rho\sigma}(x-x') J_\sigma(x'). \tag{6.4}$$

The current $J_\nu = i(\phi^*\partial_\nu\phi - \phi\partial_\nu\phi^*)$ interacts via the photon propagator in the background of the field ϕ, whose inverse is $(G^\phi_{\rho\sigma})^{-1} \equiv \Gamma^\phi_{\rho\sigma} = \Gamma_{\rho\sigma} + 2e^2|\phi|^2\delta_{\rho\sigma}$. For the free propagator, we have $\Gamma_{\rho\sigma} = -\partial^2\delta_{\rho\sigma} + (1-\lambda^{-1})\partial_\rho\partial_\sigma$, with λ a gauge parameter. In momentum space,

$$G_{\rho\sigma}(q) = \Gamma^{-1}_{\rho\sigma}(q) = \frac{\delta_{\rho\sigma}}{q^2} + \frac{(\lambda-1)}{q^2}\frac{q_\rho q_\sigma}{q^2}. \tag{6.5}$$

Note that the term proportional to $e^2|\phi|^2$ is not present in $G_{\rho\sigma}(q)$. It comes from the coupling of two photons with two bosons in the interaction Lagrangian density $\mathscr{L}_{\text{int}} = eJ_\mu A_\mu + e^2A^2|\phi|^2$. However, if we include the term $e^2A^2|\phi|^2$ through $G^\phi_{\rho\sigma}$, instead of using the free propagator, in the expression for the grand partition function Ξ (see below), the order $e^2 \sim \alpha$ extra term will contribute in order $e^4 \sim \alpha^2$, which can be neglected, as we will show in the numerical results.

We expand the grand partition function to first order to find

$$\Xi/\Xi_0 = 1 + \frac{e^2}{2}\int_\Omega d^4x \int_\Omega d^4y\, G_{\rho\sigma}(x-y)\langle J_\rho(x)J_\sigma(y)\rangle, \tag{6.6}$$

where Ξ_0 is the ideal gas grand partition function ($S_I = 0$), and the current-current expectation value is computed from the scalar theory (Appendix J) given by Eq.(6.3)

$$\langle J_\rho(x)J_\sigma(y)\rangle = \langle J_\rho(x)J_\sigma(y)\rangle_c + \langle J_\rho(x)\rangle\langle J_\sigma(y)\rangle, \tag{6.7}$$

with $\langle J_\rho(x)\rangle = \delta_{\rho 4}\eta$. The second term in Eq.(6.7) gives a $(\ln V/V)$ contribution to the pressure that vanishes in the thermodynamic limit. Besides, it does not contribute to the density either, since it is independent of μ. On the other hand, the connected part $\langle J_\rho(x)J_\sigma(y)\rangle_c \equiv \mathscr{J}_{\rho\sigma}(x-y)$ leads to

$$\Xi/\Xi_0 = 1 + \frac{e^2V}{2}\sum_{n_q=-\infty}^{\infty}\int \frac{d^3q}{(2\pi)^3}\mathscr{J}_{\rho\sigma}(q_\mu)G_{\rho\sigma}(-q_\mu). \tag{6.8}$$

$\mathscr{I}_{\rho\sigma}$ is given by the Feynman graph

$$\mathscr{I}_{\rho\sigma} = T \sum_{n_p=-\infty}^{\infty} \int \frac{d^3p}{(2\pi)^3} \frac{(2\bar{p}_\rho + q_\rho)(2\bar{p}_\sigma + q_\sigma)}{(\bar{p}^2 + m^2)[(\bar{p}+q)^2 + m^2]}, \tag{6.9}$$

with $q_4 = 2\pi n_q T$, $\bar{p}_4 = 2\pi n_p T + i\mu$. Due to current conservation, $q_\rho \mathscr{I}_{\rho\sigma} = \mathscr{I}_{\rho\sigma} q_\sigma = 0$, the

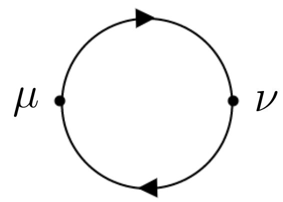

Figure 6.1: Feynman diagram.

gauge-dependent second term of the propagator in Eq.(6.5) will not contribute. Introducing the trace $\mathscr{I}(q_\mu) \equiv \mathscr{I}_{\rho\rho}(q_\mu)$, we have

$$\Xi/\Xi_0 = 1 + \frac{e^2 V}{2} \sum_{n_q=-\infty}^{\infty} \int \frac{d^3q}{(2\pi)^3} \frac{\mathscr{I}(q_\mu)}{q^2}. \tag{6.10}$$

If we perform the Matsubara sum in Eq.(6.9), and subtract the vacuum part $\mathscr{I}_{(0,0)}$, the medium contribution $\mathscr{I}_m = \mathscr{I}_{(T,\mu)} - \mathscr{I}_{(0,0)}$ is given by

$$\mathscr{I}_m(q_\mu) = \mathrm{Re} \int \frac{d^3p}{(2\pi)^3} \frac{\bar{n}(p)}{\omega_p} \left[\frac{q^2 + 4pq - 4m^2}{q^2 + 2pq} \right], \tag{6.11}$$

where $pq = i\omega_p q_4 + \vec{p}\cdot\vec{q}$, $\omega_k = (\vec{k}^2 + m^2)^{1/2}$, and $\bar{n}(k) = n^+(k) + n^-(k)$,

$$n^\pm(k) = \frac{1}{e^{\beta(\omega_k \mp \mu)} - 1}. \tag{6.12}$$

Keeping only the medium contribution, and defining $\Delta\Xi_m \equiv \Xi_m - \Xi_0$,

$$\Delta\Xi_m/\Xi_0 = \frac{e^2 V}{2} \int \frac{d^3q}{(2\pi)^3} \sum_{n_q=-\infty}^{\infty} \frac{\mathscr{I}_m(q_\mu)}{q^2}, \tag{6.13}$$

with $\mathscr{I}_m$ conveniently written as

$$\mathscr{I}_m = \mathrm{Re} \int \frac{d^3p}{(2\pi)^3} \frac{\bar{n}(p)}{\omega_p} \left[2 - \frac{q^2}{q^2 + 2pq} - \frac{4m^2}{q^2 + 2pq} \right]. \tag{6.14}$$

As before, we subtract the $T = 0$ part of Eq.(6.13), and call the result $\Delta\Xi^*/\Xi_0$. We will now compute expressions for pressure, density, and condensation temperature in the UR and NR limits, and present numerical results for those quantities in the relativistic case.

6.3 Ultrarelativistic limit

In the UR limit, $T >> m$ and/or $\eta >> m^3$, the last term in (6.14) does not contribute to the grand partition function in leading order (we have checked this numerically). We perform the sum over n_q in (6.13), and the integral over angles in (6.14), analytically. The real part of the integral over the radial momentum p, and the final radial integral over q may also be computed analytically, yielding

$$\frac{\Delta\Xi^*}{\Xi_0} = \frac{e^2}{60} V T^3. \tag{6.15}$$

The thermodynamic potential is given by

$$\Omega^* = -T\ln\Xi^* = -T\ln\Xi_0 - T\ln\left[1+\frac{\Delta\Xi^*}{\Xi_0}\right]. \tag{6.16}$$

As $\Delta\Xi^*/\Xi_0$ is of order $\alpha = e^2/4\pi$, we expand the log

$$\Delta\Omega^* = \Omega^* - \Omega_0 \cong -T\frac{\Delta\Xi^*}{\Xi_0} = -\frac{\pi\alpha}{15} V T^4. \tag{6.17}$$

In the UR limit, $\Omega_0/VT^4 = -\Gamma(4)\zeta(4)/(3\pi^2) = -\pi^2/45$, so the pressure is

$$P^* = P_0 + \Delta P^* = \frac{\pi^2}{45}T^4 + \frac{\pi\alpha}{15}T^4. \tag{6.18}$$

We go back to Eq. (6.16) to derive the density

$$\eta^* = \left(\frac{\partial P^*}{\partial\mu}\right)_{T,V} = \eta_0 + \Delta\eta^* = \eta_0 - \frac{1}{V}\frac{\partial\Delta\Omega^*}{\partial\mu}, \tag{6.19}$$

where η_0 is the density of the relativistic ideal gas

$$\eta_0 = \left(\frac{\partial P_0}{\partial\mu}\right)_{T,V} = \int\frac{d^3p}{(2\pi)^3}\left[n^+(p) - n^-(p)\right]. \tag{6.20}$$

We then use the *ansatz*

$$\eta^* = \eta_0 + \Delta\eta^* = \frac{1}{3}\mu T^2\left[1 + f(\xi)\,\alpha\tau\right]. \tag{6.21}$$

We define $\tau \equiv T/m$, $\xi \equiv \mu/m$, and the function $f(\xi)$, shown in Fig. (6.2), which is determined numerically. We take its value for $\mu = m$ to be $f(1) = \gamma$. Numerically, $\gamma = 2.14 \cong 2\pi/3$.

In order to obtain T_c, the temperature where Bose-Einstein condensation sets in, we use $\mu = m$ and $\eta = \eta^*$

$$\eta = \eta^* = \frac{1}{3}m^3\tau_c^2\left[1 + \gamma\alpha\tau_c\right], \tag{6.22}$$

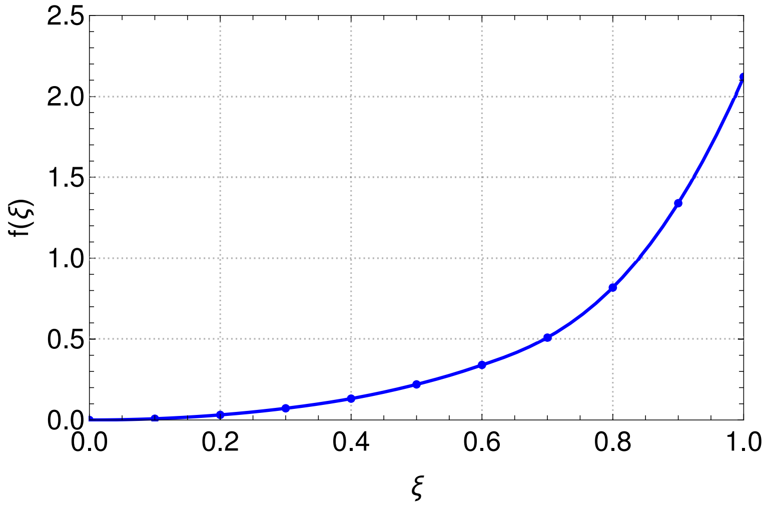

Figure 6.2: Numerical calculation of $f(\xi)$, a function of $\xi = \mu/m$.

which may be written

$$\tau_c^2\left[1+\gamma\alpha\tau_c\right] = 3\eta/m^3 \equiv N_\mathrm{u}. \tag{6.23}$$

Setting $\tau_c = {N_\mathrm{u}}^{1/2} - \Delta\tau$, to first order in α

$$\tau_c = {N_\mathrm{u}}^{1/2} - \frac{\gamma}{2}\alpha N_\mathrm{u}, \tag{6.24}$$

where ${N_\mathrm{u}}^{1/2}$ is the ideal gas value, and $\alpha N_\mathrm{u} = (e/4\pi)Q$, with $Q \equiv e\Delta N$ being the total EM charge.

6.4 Nonrelativistic limit

In the NR limit, $T << m$ and/or $\eta << m^3$, we again perform the sum over n_q and integrate over angles. The leading term is now

$$\frac{\Delta\Xi^*}{\Xi_0} = \frac{\alpha\tau}{3\pi}V\eta_0, \tag{6.25}$$

where η_0 is the nonrelativistic expression for the particle density of the ideal gas (antiparticles are suppressed by $e^{-m/T}$)

$$\eta_0(\nu) = \frac{(mT)^{3/2}}{\sqrt{2}\pi^2}\int_0^\infty dz\frac{z^{1/2}}{e^{z-\nu}-1}, \tag{6.26}$$

with $\nu \equiv (\mu - m)/T < 0$. The shift in the thermodynamic potential with respect to the ideal gas value is

$$\Delta\Omega^* = -T\frac{\Delta\Xi^*}{\Xi_0} = -\frac{\alpha\tau}{3\pi}TV\eta_0. \tag{6.27}$$

However, since $\partial\Omega_0/\partial\nu = -TV\eta_0$,

$$\Omega^*(\nu) = \Omega_0(\nu) + \frac{\alpha\tau}{3\pi}\frac{\partial\Omega_0}{\partial\nu}(\nu) = \Omega_0(\nu_{\rm em}), \tag{6.28}$$

$$\nu_{\rm em}(\nu,\tau) = \nu + \frac{\alpha\tau}{3\pi}. \tag{6.29}$$

Therefore, the effect of the electromagnetic quantum fluctuations is to increase the chemical potential by an amount proportional to $(\alpha\tau)T$. They also lead to an increase in the pressure

$$\Delta P^* = P_0(\nu_{\rm em}) - P_0(\nu) = \frac{\alpha\tau}{3\pi}T\eta_0. \tag{6.30}$$

The nonrelativistic density is

$$\eta^*(\nu,\tau) = \frac{1}{T}\frac{\partial P^*}{\partial\nu} = \frac{1}{T}\frac{\partial P_0}{\partial\nu_{\rm em}} = \eta_0(\nu_{\rm em},\tau). \tag{6.31}$$

Condensation will take place whenever $\nu_{\rm em} = 0$, which means $\nu_c = -(\alpha\tau_c)/3\pi$. Then, the total density is given by $\eta = \eta^*(\nu_c,\tau_c) = \eta_0(0,\tau_c)$. Since $\nu_c << 1$, we follow [92] to compare the condensation temperature T_c with the temperature T_0 of an ideal gas with density η and $\nu = \nu_c$

$$\eta = \zeta(3/2)\left(\frac{mT_0}{2\pi}\right)^{3/2}\left[1 - \frac{\sqrt{4\pi|\nu_c|}}{\zeta(3/2)}\right]. \tag{6.32}$$

Since $\eta = \zeta(3/2)[mT_c/2\pi]^{3/2}$, Eq. (6.32) leads to

$$\tau_c = \tau_0\left[1 - \frac{2}{3}\frac{\sqrt{4\pi|\nu_c|}}{\zeta(3/2)}\right]. \tag{6.33}$$

Introducing $N_{\rm n} = [(2\pi)^{3/2}/\zeta(3/2)](\eta/m^3)$,

$$\tau_c = {N_{\rm n}}^{2/3} - C\alpha^{1/2}N_{\rm n},$$

$$C = \frac{4}{3\sqrt{3}\zeta(3/2)} = 0.295. \tag{6.34}$$

Again, the shift is proportional to the EM charge $\alpha^{1/2}N_{\rm n} = (1/2\sqrt{\pi})Q$.

The critical temperature is always lower than the ideal gas value, an indication that electromagnetic repulsion acts against condensation. In the ultra-relativistic and nonrelativistic cases, this shift is related to an electromagnetic increase in the chemical potential proportional to α

$$\mu_{\rm em} = \mu + g(\xi,\tau)\alpha T. \tag{6.35}$$

We have $g(\xi,\tau) = \tau/3\pi$ for $\tau << 1$ (NR), and $g(\xi,\tau) = \xi f(\xi)$ for $\tau >> 1$ (UR), with $f(\xi)$ defined in Eq.(6.21). Electromagnetic repulsion is also responsible for an increase in pressure when compared to that of the ideal gas. In the UR and NR limits,

$$\Delta P^*_{\rm u}/m^4 = \frac{\pi}{15}\alpha\tau^4, \tag{6.36}$$

$$\Delta P^*_{\rm n}/m^4 = \frac{1}{3\pi}\alpha\tau^2\frac{\eta_0}{m^3} = \frac{\zeta(3/2)}{6\pi^2\sqrt{2\pi}}\alpha\tau^{7/2}. \tag{6.37}$$

As for the increase in density, in the UR limit, we have

$$\Delta\eta^*/m^3 = \frac{\xi f(\xi)}{3}\alpha\tau^3. \tag{6.38}$$

In the NR limit, $\Delta\eta^* = \eta^*(\nu,\tau) - \eta_0(\nu,\tau) = \eta_0(\nu_{\rm em},\tau) - \eta_0(\nu,\tau)$. Using Eq.(6.32), we obtain

$$\Delta\eta^*/m^3 = \frac{1}{6\pi^2\sqrt{2|1-\xi|}} \tag{6.39}$$

6.5 Numerical results

For the relativistic case, the shift in pressure and density as functions of temperature for some values of the chemical potential are shown in Figs.(6.3) and (6.4), respectively. Fig.(6.5) shows the critical temperature as a function of the density. In all the figures, we have taken m to be the charged pion mass $m_{\pi^\pm} = 139.6\text{MeV}/c^2$.

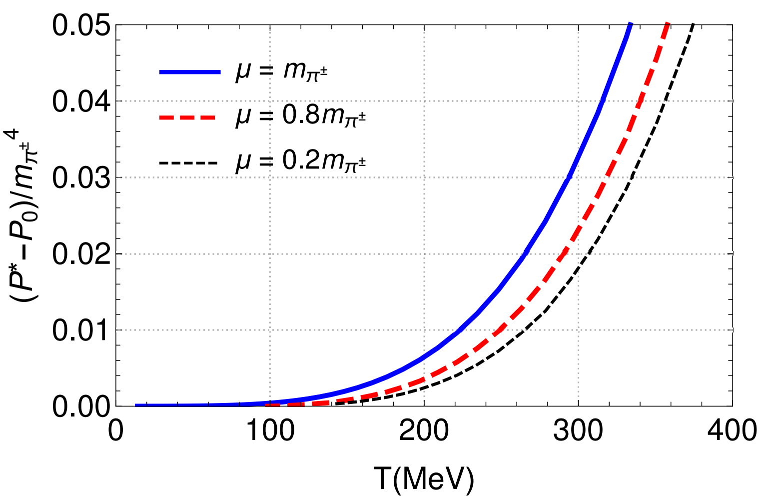

Figure 6.3: Change in the pressure as a function of temperature. The charged pion mass $m_{\pi^\pm} = 139.6$ MeV was used for m.

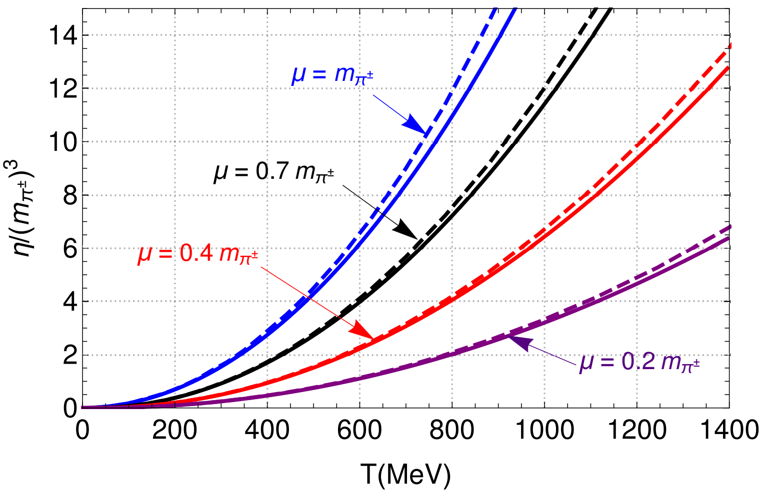

Figure 6.4: Particle density of the ideal gas (full line) and of the gas with electromagnetic interaction (EM gas - dashed line) as a function of temperature for some values of the chemical potential.

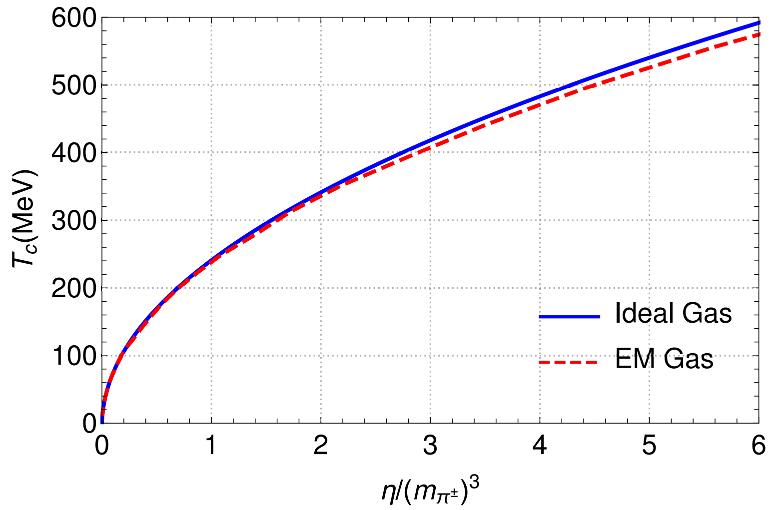

Figure 6.5: Condensation temperature as a function of particle density for the ideal gas and for the gas with electromagnetic interaction.

It is clear from the numerical calculations that the pressure and the density increase with respect to the ideal gas values, whereas the condensation temperature decreases, all this as a consequence of the electromagnetic repulsion that sets in via quantum fluctuations. The increase in pressure and density is expected because the gas will experience a repulsive interaction, since we are fixing the electromagnetic (EM) charge $Q = e\Delta N$, proportional to the number of particles minus the number of antiparticles. For positive chemical potential $\mu > 0$, there are more particles than antiparticles. At low temperatures, no antiparticles will be produced from the vacuum, so that we are left with a system of particles (positive net particle number), all with the same EM charge e, that repel each other. As we increase the temperature above $2mc^2$, zero-charge particle-antiparticle pairs will be continuously created from and annihilated into the vacuum, but this does not change the net charge, and the system still consists of same sign charges that experience a net repulsion. Although the results are order α corrections, as we move into the UR regime, those corrections become more relevant. However, we cannot trust our first order calculation for values of $\tau = T/m$ close to, or larger than, $1/\alpha$.

Since our calculations show that the first order $\mathcal{O}(e^2)$ of the expansion gives a small, yet relevant, contribution in the ultra-relativistic limit, higher order $\mathcal{O}(e^4)$ corrections will lead to even smaller contributions that can be neglected in the calculation of physical quantities such as the pressure, density, and critical temperature of condensation.

We point out that temperatures in the graphs do not exceed $\tau \sim 10 < 137$, spanning a region where our approximations should hold. Note that the increase in pressure already reaches 5% for values of $\tau \sim 2-3$. As for the increase in density, it may reach 9% for $\tau \sim 6$, whereas the decrease in condensation temperature reaches 5% for $\tau \sim 6$. In order to detect changes of the order of $5-10\%$, one would have to search for physical scenarios with temperatures corresponding to $\tau = 2-10$, so that relativistic effects become appreciable still within the validity of our computations.

In the inner core of a neutron star, where pion condensation may occur [93, 94, 95], densities exceed $10^{14}\,\mathrm{g/cm^3}$, with number density $\rho > 0.4\,\mathrm{fm^{-3}}$, and pressure $P > 10^{33}\,\mathrm{dyn/cm^2}$. In our numerical calculations, the shift in condensation temperature shown in Fig.(6.5) becomes appreciable for number densities $\eta/(m_{\pi^\pm})^3 > 2$, or $\eta > 1.4\,\mathrm{fm^{-3}}$, and temperatures where $kT_c > 350\,\mathrm{MeV}$ or $T_c > 4\times 10^{12}\,\mathrm{K}$. Such temperatures $T \sim 10^{12}\,\mathrm{K}$ are found in the center of neutron stars.

In conclusion, we have shown that EM quantum fluctuations increase the pressure and the density of the gas with respect to ideal gas values by amounts proportional to α times a power of τ. The condensation temperature is, however, lowered by a correction proportional to the charge $Q = e\Delta N$. The shifts become more relevant (of the order of a few percent) the more relativistic is the system. The combination of quantum and relativistic effects in dense hot gases leading to deviations from ideal gas behavior should also be present whenever other conserved charges interact via the exchange of their vector boson carriers, as in Quantum Flavordynamics or Quantum Chromodynamics, for example. We plan to investigate this in the near future.

Chapter 7

Conclusions

We have shown that a relativistic quantum gas satisfies the requirement of having $\epsilon < 0$ and $\mu < 0$ simultaneously negative. As the sources of magnetic fields are current densities, in relativistic systems one obtains magnetic responses comparable to electric ones, in opposition to nonrelativistic systems ($v << c$), where magnetic responses are much smaller than electric ones. A relativistic system is then a key ingredient to achieve a natural left-handed behavior.

Summing up, we have presented a theoretical study of the EM propagation and responses of a relativistic electron gas and a relativistic Bose gas, for various temperatures and carrier densities. Using linear response and RPA, we have identified the propagation modes and their dispersion relations from the QED propagators as well as from Maxwell's equations with the added input of the constitutive relations obtained from the QED responses. We have found a longitudinal plasmon mode, two transverse plasmon modes, and a photonic mode which propagates with the speed of light in vacuum, i.e., for which the medium is transparent thanks to the specific form of its relativistic electromagnetic responses. In deriving dispersion relations, we were able to identify stable solutions and regions of instability where the plasmon modes decay. Finally, we have also identified the regions in the $(|\vec{q}|,\omega))$ plane where the longitudinal permittivity ϵ_L and longitudinal inverse permeability ν_L are both simultaneously negative.

For $T = 0$, we have obtained analytic expressions that coincide with those existing in the literature if we neglect the vacuum contributions. The appearance of non-zero imaginary parts indicates that the system is unstable to the decay into electron–hole (lower energies) or electron–positron (higher energies) pairs. The former is well known to occur in the non-relativistic limit. Thus, the region of imaginary parts of longitudinal responses will define a region where the plasmon cannot propagate, that is, there exists a maximum wavevector beyond which (inside the region of imaginary parts) the plasmon excitation disappears. Furthermore, the explicit expressions for longitudinal electric and magnetic responses allow for the calculation of dispersion relations for plasmons.

We have shown, from Maxwell's equations, that the REG has *effective* permittivity and permeability that are both negative at frequencies below the longitudinal electric plasmon frequency in the long wavelength limit (in the study of the relativistic charged Bose gas, we obtained this result for frequencies below the transverse plasmon frequency for any chemical potential and temperature, in the long wavelength limit $|\vec{q}| \to 0$, where both plasmon frequencies are equal, $\omega_L(0) = \omega_T(0)$). We conclude that the REG is a natural realization of a LHM, and this occurs because the gas is relativistic. We have also confirmed that the photonic mode propagates in the REG with the speed of light in vacuum, without losses, by explicitly computing the energy dissipated in the gas and finding that it vanishes, a consequence of the fact the electrons do not self-interact. The REG is thus completely transparent to the photonic mode. Finally, we use Snell's law to argue that the index of refraction for the photonic mode is $n_{\text{eff}} = -1$, and explore the implications of this fact for the reflection and transmission coefficients. We suggest that the REG can act as a perfect waveguide, with no energy dissipation.

In the study of the relativistic Bose gas, we have derived the effective electromagnetic responses and the electromagnetic propagation modes that characterize the gas as a left-handed material with negative effective index of refraction $n_{\text{eff}} = -1$ below the transverse plasmon frequency, that is, the region of LHM behavior is limited to the region $\omega_\gamma < \omega < \omega_T$, where $\omega_\gamma = |\vec{q}|$ is the frequency of photonic mode. In addition, we have obtained analytical expressions for the longitudinal and transverse plasmon modes at $T = 0$, which coincide with the literature in the relativistic [71] and nonrelativistic limits [72], and numerical results for $T \neq 0$ in the condensed phase. We remark that the Lagrangian density in our approach does not include a self-interaction term $\lambda(\phi^*\phi)^2$. The condensate is introduced by the inclusion of the condensed density at zero momentum (ground state) in the Bose-Einstein distribution. We plan to include a self-interaction in a future investigation.

Since the Bose gas is a LHM below the transverse plasmon frequency, we have obtained, for ultra-relativistic densities, analytical solutions for the transverse plasmon frequency $\omega_T(|\vec{q}|)$, and have shown that in the long-wavelength limit, $|\vec{q}| \to 0$, in the condensed phase the transverse plasmon frequency decreases when the temperature is increased to $T \to T_c$, whereas, above the transition critical temperature T_c, $\omega_T(0)$ increases. We suggest that this behavior may be explained by the contribution of antibosons above the critical temperature of condensation. In the condensed phase ($T < T_c$), there are no antibosons in the gas, and particularly for ultra-relativistic densities, the density of antibosons increases rapidly, implying that more energy is needed to obtain a collective excitation such as a transverse plasmon. When we look at relativistic and non-relativistic densities, we have to go beyond the critical temperature of condensation ($T_t > T_c$) for the transverse plasmon frequency to start to increase with the temperature. This is reasonable because only in the ultra-relativistic domain there is a sharp transition at T_c in the density of antibosons (Fig.5.1). For lower densities, the transition is smooth, so that a higher temperature is required for the plasmon frequency to start increasing with temperature.

In particular, for the longitudinal mode, the plasmon dispersion relation exhibits a roton-type local minimum that disappears at the transition temperature. This roton structure agrees remarkable well with the non-relativistic results reported in the literature [88]. There, in a charged superfluid, it has been shown that the phonon mode of the neutral superfluid is pushed to a finite plasmon frequency ω_p, whereas the roton mode is more or less unaffected. In the charged case, the spectrum of the superfluid field shows a plasmon excitation that turns into a roton excitation, with a gap energy $\Delta(|\vec{q}_{\mathrm{rot}}|)$ for higher $|\vec{q}|$. This gap energy $\Delta(T)$ may be interpreted as an order parameter, whose temperature dependence defines the regions of BEC and normal phase. For $T = T_c$, the gap energy disappears, and we obtain a normal phase. We believe that in the vicinity of the critical temperature of BEC ($T \to T_c$) we may extract a critical exponent of the phase transition. We also hope to obtain an analytic solution for the spectrum gap energy $\Delta(T)$ in the non-relativistic limit to compare with the result obtained in [88], where the authors studied the dynamical properties of a weakly coupled charged Bose gas at finite temperature by means of the dielectric formalism. With all this, we hope to obtain an energy spectrum that behaves like $E_p^2 = \omega_L^2 + \Delta(T)^2 + C(\eta - \eta_c)$, where C is a parameter which may depend on the temperature and charge density, to better understand how the roton excitation is thermally induced.

Finally, we have computed deviations from ideal gas behavior of the pressure, density, and Bose-Einstein condensation temperature of a relativistic gas of charged scalar bosons caused by the current-current interaction induced by electromagnetic quantum fluctuations treated via Scalar Quantum Electrodynamics. We have obtained expressions for those quantities in the ultra-relativistic and nonrelativistic limits, and presented numerical results for the relativistic case. We have shown that EM quantum fluctuations increase the pressure and the density of the gas with respect to ideal gas values by amounts proportional to α times a power of T. The condensation temperature is, however, lowered by a correction proportional to the charge $Q = e\Delta N$, all this as a consequence of the electromagnetic repulsion that sets in via quantum fluctuations. The increase in pressure and density is expected because the gas will experience a repulsive interaction, since we are fixing the electromagnetic (EM) charge. The shifts become more relevant (of the order of a few percent) the more relativistic is the system.

Thus, we notice that the inclusion of electromagnetic interactions in the non-relativistic charge Bose gas gives small corrections that can be neglected, compared with the ideal Bose gas. However, for relativistic densities such as in astrophysical scenarios as neutrons stars and white dwarfs, the correction of the critical temperature has a small relevant contribution that shows we cannot neglected the electromagnetic quantum fluctuations of a charged system. We must to emphasize that our calculations are limited in first order in α, thus we cannot trust in corrections beyond $\alpha = 1/137$, because for densities $\eta \to \infty$, the critical temperature $T_c \to 0$.

The combination of quantum and relativistic effects in dense hot gases leading to deviations from ideal gas behavior should also be present whenever other conserved charges interact via the exchange of their vector boson carriers, as in Quantum Flavordynamics or Quantum Chromodynamics, for example. We plan to investigate this in the near future.

We also plan to investigate the role of strong magnetic fields in scenarios like pion condensation. A condensed pion phase inside a magnetar (neutron star with a intense magnetic field) is a very important topic today. Thus, considering how an external strong magnetic field affects our results is certainly a line of research to be pursued.

Another development that we contemplate is the extension of our results to 2+1 dimensions, where experiments with graphene may provide accessible testing grounds for our findings. Relativistic dispersion relations emerge naturally in the discussion of graphene, so that we hope to investigate electromagnetic responses in such systems, in a systematic way, by using our formalism.

Bibliography

[1] A. Priou, et al., *Advances in complex electromagnetic materials* **28** (Springer Science and Business Media, 2012).

[2] D. R. Smith, et al. Applied Physics Letters **77**, 14 (2000).

[3] R. A. Shelby, D. R. Smith, and S. Schultz, Science **292**, 77 (2001)

[4] J. B. Pendry, A. J. Holden, W. J. Steward, and I. Youngs, Physical Review Letters **76**, 4773 (1996);

[5] D. R. Smith, W. J. Padilla, D. C. Vier, S. C. Nemat-Nasser, and S. Schultz, Physical Review Letters **84**, 4184 (2000).

[6] S. A. Cummer, J. Christensen, A. Alù, Nature Reviews Materials **1**, 3, 1 (2016).

[7] V. G. Veselago, Soviet Physics Uspekhi **10**, 509 (1968).

[8] M. Born and E. Wolf. *Principles of Optics.* (Cambridge University Press, Cambridge UK, 7th edition, 1999).

[9] N. Fang, H. Lee, C. Sun, and X. Zhang, Science **308**, 5721 (2005).

[10] J. Chen, et al, Nature Photonics **5**, 4 (2011).

[11] J. D. Jackson, *Classical Electrodynamics* (Wiley, 1998).

[12] L. Landau and E. Lifshitz, *Electrodynamics of Continuous Media* (Pergamon, 1960).

[13] A. D. Boardman, N. King, and L. Velasco, Electromagnetics **25** 5 (2005).

[14] L. I. Mandelshtam, Zhurnal Experimentalnoi i Teoreticheskoi FizikiJournal of Experimental and Theoretical Physics (JETP) **15** 475, (1945).

[15] S. A. Ramakrishna, and T. M. Grzegorczyk. *Physics and applications of negative refractive index materials* (CRC press, 2008).

[16] P. W. Milonni, *Fast light, slow light and left-handed light* (CRC Press, 2004).

[17] C. A. A. de Carvalho, Physical Review D **93**, 105005 (2016).

[18] E. Reyes-Gómez, L. E. Oliveira and C. A. A. de Carvalho, Europhys. Lett **114**, 17009, (2016).

[19] E. T. Jensen, R. E. Palmer, W. Allison and J. F. Annett, Phys. Rev. Lett **66**, 492, (1991).

[20] M. Portail, M. Carrere and J. M. Layet, Surf. Sci **433**, 863, (1999).

[21] C. Itzykson and J. B. Zuber, *Quantum Field Theory* (McGraw-Hill, New-York, 1980).

[22] J. I. Kapusta and C. Gale, *Finite-Temperature Field Theory*, (Cambridge University Press, Cambridge, England (2006)).

[23] I. A. Akhiezer and S. V. Peletminskii, Soviet Physics JETP **11**, 1316 (1969).

[24] E. S. Fradkin, *Proceedings of the P. N. Lebedev Physics Institute* **29**, Consultants Bureau (1967).

[25] C. A. A. de Carvalho and D. M. Reis, Journal of Plasma Physics **84**, 905840112 (2018).

[26] A. A. Abrikosov, L. P. Gorkov and I. E. Dzyaloshinski, *Methods of Quantum Field Theory in Statistical Physics* (Dover, 1975)

[27] N. W. Ashcroft and N. D. Mermin, *Solid State Physics* (Holt, Rinehart and Winston 2005).

[28] A. L. Fetter and J. D. Walecka, *Quantum Theory of Many-particle Systems* (Courier Corporation, 2012).

[29] M. Le Bellac, *Thermal field theory* (Cambridge university press, 2000).

[30] B. Jancovici, Il Nuovo Cimento **25**, 2, 428 (1962).

[31] D. B. Melrose and L. M. Hayes, Austral. J. Phys. **37**, 6, 639 (1984)

[32] G. Barton, Ann. Phys. **200**, 2, 271 (1990).

[33] P. Pulsifer and G. Kalman, Phys. Rev. A **45**, 8, 5820 (1992).

[34] M. B. Barbaro, R. Cenni and M. R. Quaglia, Eur. Phys. J. A. **25**, 2, 299 (2005).

[35] J. McOrist, D. B. Melroes and J. I. Weise, J. Plasma Phys. **73**, 4, 49 (2007).

[36] B. Eliasson and P. K. Shukla, Phys. Rev. E **83**, 4, 046407 (2011).

[37] W.-Y. Tsai and T. Erber, Phys. Rev. D **10**, 2, 492 (1974).

[38] H. Pérez Rojas and A. E. Shabad, Ann. Phys. **138**, 1, 1 (1982).

[39] H. A. Weldon, Phys. Rev. D **26**, 6, 1394 (1982).

[40] J. F. Donoghue, B. R. Holstein and R. W. Robinett, Ann. Phys. **164**, 2, 233 (1985).

[41] K. Ahmed and S. Masood, Ann. Phys. **207**, 2, 460 (1991).

[42] S. Masood and I. Saleem Intl J. Mod. Phys. A, 1750081 (2016).

[43] D. M. Reis, E. Reyes-Gómez, L. E. Oliveira, and C. A. A. de Carvalho, Annalen der Physik **530**, 1700443 (2018).

[44] C. A. A. de Carvalho, D. M. Reis, and D. Szilard, J. Opt. Soc. Am. B **37**, 3542 (2020).

[45] D. M. Reis, S. B. Cavalcanti, and C. A. A. de Carvalho, Physics Letters B, **812**, 136003 (2021).

[46] D. M. Reis, and C. A. A. de Carvalho, Physics Letters B, **823**, 136715 (2021).

[47] M. Grether, M. de Lanno, and G. A. Baker, Physical Review Letters **99**, 200406 (2007);

[48] A. Haber and H. Weldon, Physical Review Letters **46**, 1947 (1981);

[49] C. A. A. de Carvalho and S.G. Rosa, Journal of Physics A **13**, 3233 (1980).

[50] M. R. Schafroth, Physical Review **100**, 463 (1955).

[51] A. Schmitt, *Lecture Notes in Physics* **888**, Springer (2015).

[52] M. G. Alford, S. K. Mallavarapu, A. Schmitt and S. Stetina, Phys. Rev. D **87**, 065001 (2013).

[53] G. Baym, and C. Pethick, Annual Review of Nuclear Science **25**, 1, 27 (1975).

[54] V. Kowalenko, N. E. Frankel, and K. C. Hines, Physics Reports **126**, 109 (1985).

[55] P. Moitra, Y. Yang, Z. Anderson, I. I. Kravchenko, D. P. Briggs, and J. Valentine, Nature Photonics **7**, 791 (2013).

[56] V. L. Ginzburg, Journal of Statistical Physics **1**, 3 (1969).

[57] D. G. Henshaw and A. D. B. Woods, Phys. Rev. **121** 1266 (1961).

[58] L. D. Landau, USSR Journal of Physics **11**, 91 (1947).

[59] U. R. Fischer, Physical Review A **73**, 031602(R) (2006).

[60] R. M. Wilson, S. Ronen, J.L. Bohn, and H. Pu, Physical Review Letters **100**, 245302 (2008).

[61] C. Kittel and P. McEuen, *Introduction to solid state physics* **8**, New York: Wiley (1996).

[62] J. Lindhard, K. Dan. Vidensk. Selsk., Mat. Fys. Medd., **28**, 8 (1954).

[63] K. Sturm, Adv. Phys. **31**, 1, 1. (1982).

[64] K. Sturm and L. E. Oliveira, Phys. Rev. B **22**, 12, 6268 (1980).

[65] K. Sturm and L. E. Oliveira, Phys. Rev. B **24**, 6, 3054 (1981).

[66] J. Stiebling, Zeitschrift für Physik B Condensed Matter **31**, 4 355 (1978).

[67] V. I. Berezhiani, N. L. Shatashvili and N. L. Tsintsadze, Phys. Scr. **90**, 068005 (2015).

[68] A. G. Aksenov, R. Ruffini and G. V. Vereshchagin, Phys. Rev. E **81** 046401 (2010).

[69] Y. Wang, P. K. Shukla, and B. Eliasson, Phys. Plasmas **20**, 013103 (2013).

[70] J. D. Mazo-Vasques, L. M. Hicpaie-Zuluaga, and E. Reyes-Gómez, J. Opt. Soc. Am. B **37**, 211 (2020).

[71] D. Melrose, *Quantum Plasmadynamics: Unmagnetized Plasmas* (Springer, 2008).

[72] S. R. Hore and N. E. Frankel, Physical Review B **12**, 2619 (1975).

[73] L. Santos, G. V. Shlyapnikov, and M. Lewenstein, Physical Review Letters **90**, 250403 (2003).

[74] T. Lahaye, C. Menotti, L. Santos, M. Lewenstein, and T. Pfau, Reports of Progress in Physics **72**, 126401 (2009).

[75] R.N. Bisset and P.B. Blakie, Physical Review Letters **110**, 265302 (2013).

[76] D.H.J. O'Dell, S. Giovanazzi, and G.Kurizki, Physical Review Letters **90**, 110402 (2003).

[77] N. Henkel, R. Nath, and T. Pohl, Physical Review Letters **104**, 195302 (2010).

[78] L. Chomaz, R. M. van Bijnen, D. Petter, G. Faraoni, S. Baier, J.H. Becher, and F. Ferlaino, Nature Physics **14**, 442 (2018).

[79] D. Petter, G. Natale, R.M.W. van Bijnen, A. Patscheider, M. J. Mark, L. Chomaz, and F. Ferlaino, Physical Review Letters **122**, 183401 (2019).

[80] N. Engheta and R.W. Ziolkowski, *Metamaterials: Physics and Engineering Explorations* (IEEE Wiley, New York 2006).

[81] *Metamaterials Handbook: Vol. I. Phenomena and Theory of Metamaterials*, ed. F. Capolino, Taylor and Francis, Boca Raton (2009).

[82] D. G. Henshaw and A. D. B. Woods, Physical Review **121**, 1266 (1961).

[83] H. R. Glyde, *Excitations in Liquid and Solid Helium* **9** (Oxford University Press 1994).

[84] M. V. Berry, Proc. R. Soc. Lond. A **461**, 2059, 2071 (2005).

[85] X.-Q. Gu, S.-Y. Wang and W.-Y. Yin, Opt. Commun. **313**, 9 (2014).

[86] S. Dai, Hirashima and H. Namaizawa, Progress of Theoretical Physics **74**, 400 (1985).

[87] S. C. Zhang, *Low-Dimensional Quantum Field Theories for Condensed Matter* Physicists, 191 (1995).

[88] B. Davoudi and M. P. Tosi, Phys. Rev. B **72**, 134520 (2005).

[89] F. S. Nogueira and H. Kleinert, Physical Review B **73**, 104515 (2006).

[90] G. Baym, J. , M. Holzmann, F. P Blaizot, F. Lalöe, and D. Vautherin, Phys. Rev. Lett. **83**, 1703 (1999)

[91] C. J. Pethick, and H. Smith, *Bose–Einstein condensation in dilute gases* (Cambridge university press 2008).

[92] L.D. Landau, E. Lifchitz, *Physique Statistique* (Éditions Mir, Moscow, 1970).

[93] M. Loewe and C. Villavicencio, Phys. Rev. D **67**, 074034 (2003).

[94] J. O. Andersen, Phys. Rev. D **75**, 065011 (2007).

[95] B. B. Brandt, G. Endrõdi, E. S. Fraga, M. Hippert, J. Schaffner-Bielich, and S. Schmalzbauer, Phys. Rev. D, **98**, 094510 (2018).

[96] F. Karbstein and R. Shaisultanov, Phys. Rev. D **91**, 113002 (2015).

Appendix A

Minkowski to Euclidean

Most of the calculations in this thesis were performed with Euclidean metric, and to obtain the final results we performed an analytic continuation to Minkowski metric. For this, we defined the temporal coordinate in Euclidean metric as $x_4 \equiv \tau = it$, with $t = x^0$.

A.1 Fourier Transforms

In Minkowski space, the Fourier transform of a function $f(x)$ is

$$\begin{aligned} \tilde{f}(q) &= \int d^4x\, e^{iqx} f(x), \\ f(x) &= \int \frac{d^4q}{(2\pi)^4} e^{-iqx} \tilde{f}(q), \end{aligned} \tag{A.1}$$

with $q = (\omega, \vec{q})$, $x = (t, \vec{x})$, and $\int d^4x = \int dx^0 \int d^3x$. The product $q \cdot x = q^0 x^0 - \vec{q} \cdot \vec{x} = \omega t - \vec{q} \cdot \vec{x}$. In Euclidean space we have $q^0 \to i q_4 \equiv i\omega_n$, where ω_n is the Matsubara frequencies for bosons or fermions, so that

$$(q \cdot x)_M \to -(q \cdot x)_E = -\omega_n \tau - \vec{q} \cdot \vec{x} \tag{A.2}$$

or $(q \cdot x)_E = \omega_n \tau + \vec{q} \cdot \vec{x}$. The subscript M denotes Minkowski and E Euclidean. The Fourier transforms in Euclidean metric are

$$\tilde{f}(\omega_n, \vec{q}) = \int_0^\beta d\tau \int d^3x e^{-i\omega_n \tau - i\vec{q}\cdot\vec{x}} f(\tau, \vec{x}), \tag{A.3}$$

$$f(\tau, \vec{x}) = T \sum_n \int \frac{d^3q}{(2\pi)^3} e^{i\omega_n \tau + i\vec{q}\cdot\vec{x}} \tilde{f}(\omega_n, \vec{q}), \tag{A.4}$$

and the Euclidean derivatives are

$$\partial_\mu f(\tau,\vec{x}) = T\sum_n \int \frac{d^3q}{(2\pi)^3}(iq_\mu)e^{iqx}\tilde{f}(\omega_n,\vec{q}), \tag{A.5}$$

so $\partial_\mu \to iq_\mu$. In Minkowski metric, we have

$$\partial_\mu f(x) = T\sum_n \int \frac{d^3q}{(2\pi)^3}(-iq_\mu)e^{-iqx}\tilde{f}(q), \tag{A.6}$$

so we identify $\partial_\mu \to -iq_\mu$.

A.2 Electromagnetic field

In Minkowski space, we write the four-vector potential as $A \equiv (A^0, A^i) = (\phi, A^i)$, where $A^0 = \phi$ is the time component and A^1, A^2, A^3 the space components, with contravariant components $A_i = -A^i$. In Euclidean metric, we have $A_E \equiv (A_4, A_i^E)$, with $A_4 = i\phi = iA^0$. The spatial coordinantes are $x_i^E = x_M^i$ and $A_i^E = A_M^i$, where the superscript E is for Euclidean and M for Minkowski.

The components of electromagnetic tensor $F_{\mu\nu}$ in Minkowski metric are

$$F_{ij}^M = \partial_i A_j^M - \partial_j A_i^M = -(\partial_i A_M^j - \partial_j A_M^i), \tag{A.7}$$

$$= -\left(\frac{\partial A_j^E}{\partial x_i^E} - \frac{\partial A_i^E}{\partial x_j^E}\right) = -F_{ij}^E. \tag{A.8}$$

Thus, from Minkowski to Euclidean, $F_{ij}^M = -F_{ij}^E$. The temporal coordinate F_{0j}^M is

$$\begin{aligned} F_{0j}^M &= \partial_0 A_j^M - \partial_j A_0^M = -\partial_0 A_M^j - \partial_j A_M^0, \\ &= -i\left(\frac{\partial A_j^E}{\partial x_4^E} - \frac{\partial A_4^E}{\partial x_j^E}\right) = -iF_{4j}^E. \end{aligned} \tag{A.9}$$

We obtain $F_{0j}^M = -iF_{4j}^E$, and the components of electric and magnetic fields are

$$F_{ij}^E = -F_{ij}^M = B_M^k, \tag{A.10}$$

$$F_{4j}^E = iF_{0j}^M = iE_M^j, \tag{A.11}$$

and $F_{0i}F^{0i} \to -F_{4_i}F_{4i}$ and $F_{ij}^M F_M^{ij} \to -F_{ij}^E F_{ij}^E$. Therefore, the Maxwell Lagrangian density transforms as

$$\mathscr{L}_M = -\frac{1}{4}F_{\mu\nu}^M F_M^{\mu\nu} \to \frac{1}{4}F_{\mu\nu}^E F_{\mu\nu}^E, \tag{A.12}$$

or

$$\mathscr{L}_E = \frac{1}{4} F_{\mu\nu} F_{\mu\nu}. \tag{A.13}$$

A.3 Dirac field

The fermion Lagrangian density with the inclusion of chemical potential ξ, is

$$\mathscr{L}_F = \bar{\psi}(i\gamma^0 \partial_t + i\vec{\gamma}\cdot\vec{\nabla} + m - \xi\gamma^0)\psi, \tag{A.14}$$

where $\bar{\psi} = \psi^\dagger \gamma^0$ and $\gamma_\mu = (\gamma^0, \vec{\gamma})$ are the Dirac matrices. In Quantum Electrodynamics, the interacting Lagrangian in $\mathscr{L}_{\text{int}} = e\bar{\psi}\not{A}\psi = e\bar{\psi}\gamma^0 A^0 \psi - e\bar{\psi}\vec{\gamma}\cdot\vec{A}\psi$. Writing the temporal coordinate as $\partial_t = i\partial_4$, and $A_4 = iA^0$, we obtain

$$\mathscr{L}_F + \mathscr{L}_{\text{int}} = i\psi^\dagger \left[-iD_4 - \gamma^0\vec{\gamma}\cdot\vec{D} - im\gamma^0 - \xi\right]\psi, \tag{A.15}$$

where $D_4 \equiv (\partial_4 - ieA_4)$ and $\vec{D} \equiv (\vec{\nabla} - ie\vec{A})$. Thus, if we perform the functional integral over the fermion fields in Euclidean metric, we have

$$\begin{aligned} Z_e &= \oint [id\psi^\dagger][d\psi] \exp\left(\oint d^4x_E \, i\psi^\dagger \left[iD_4 + \gamma^0\vec{\gamma}\cdot\vec{D} + im\gamma^0 - i\xi\right]\psi\right) \\ &= \det\left[\beta\left(iD_4 + \gamma^0\vec{\gamma}\cdot\vec{D} - im\gamma^0 - i\xi\right)\right]. \end{aligned} \tag{A.16}$$

We may rewrite the determinant using $\gamma_4 = i\gamma^0$, $\gamma_i = \gamma^i$. Then, we obtain eq.(2.5)

$$\begin{aligned} \det\left[\beta\left(iD_4 + \gamma^0\vec{\gamma}\vec{D} - im\gamma^0 - i\xi\right)\right] &= \det\left[-\beta\gamma_4\left(-i\gamma_4 iD_4 - i\vec{\gamma}\vec{D} + m + i\xi\gamma_4\right)\right] \\ &= \det\left[-\beta\gamma_4\left(i\not{D} - m - i\xi\gamma_4\right)\right]. \end{aligned} \tag{A.17}$$

Appendix B

Semiclassical expansion of Z

The action of Quantum Electrodynamics in Euclidean metric is

$$S[A,\bar{\psi},\psi] = \int d^4x \left(\frac{1}{4} F_{\mu\nu}F_{\mu\nu} + \bar{\psi}(\partial_\mu \gamma_\mu - m - i\xi)\psi + e\bar{\psi}\gamma_\mu A_\mu \psi \right), \tag{B.1}$$

where $F_{\mu\nu} = \partial_\mu A_\nu - \partial_\nu A_\mu$, and we have used the shorthand $\int dx \equiv \int_0^\beta dx_4 \int d^3x$. Considering the electromagnetic field $A_\mu = A_\mu^{(c)} + \hbar a_\mu$ as the sum of an external classical field plus quantum fluctuations, the electromagnetic action $S[A] = S[A^{(c)} + \hbar a]$ may be expanded around the classical part

$$S[A] = S[A^{(c)}] + \hbar \int d^4x \frac{\delta S_A}{\delta A_\mu}\bigg|_{A^{(c)}} a_\mu(x) + \frac{\hbar^2}{2!} \int d^4x d^4y \; a_\mu(x) \frac{\delta^2 S}{\delta A_\mu(x) \delta A_\nu(y)}\bigg|_{A^{(c)}} a_\nu(y) + \mathcal{O}(\hbar^4). \tag{B.2}$$

The first integral is zero because the classical field $A_\mu^{(c)}$ is a solution of the equation of motion, and

$$\frac{\delta^2 S}{\delta A_\mu(x) \delta A_\nu(y)}\bigg|_{A^{(c)}} = (\partial^2 \delta_{\mu\nu} - \partial_\mu \partial_\nu)\delta(y-x). \tag{B.3}$$

Thus, to second order in the Planck constant, we obtain

$$S[A,\bar{\psi},\psi] = S[A^{(c)},\bar{\psi},\psi] + \hbar^2 S_a[a,\bar{\psi},\psi], \tag{B.4}$$

and the functional integral over a_μ is given by the quadratic form

$$S_a = \frac{1}{2} \int d^4x d^4y a_\mu^x [G_{\mu\nu}^\gamma]_{xy}^{-1} a_\nu^y + e \int d^4x (\bar{\psi}\gamma_\nu\psi) a_\mu^x, \tag{B.5}$$

where $G_{\mu\nu}^\gamma$ is the photon propagator in the chosen gauge. The quadratic integral may be performed. Taking minus its logarithm

$$S_e^{\text{int}} = -\frac{e^2}{2} \int d^4x \, d^4y \, (\bar{\psi}\gamma_\mu\psi)_x G_{\mu\nu}^\gamma (x-y) (\bar{\psi}\gamma_\nu\psi)_y. \tag{B.6}$$

The integral over quantum fluctuations of the gauge field leads to electron-electron interactions mediated by the photon propagator. The remaining fermionic integral is given by

$$Z_e^{(sc)}[A^{(c)}] = \oint [id\psi^\dagger][d\psi] e^{-S_e^{(sc)}[\psi^\dagger,\psi,A^{(c)}]}, \tag{B.7}$$

where the fermionic semiclassical action is $S_e^{(sc)} = S_e + S_e^{\rm int}$. Expanding $\exp(-S_e^{\rm int})$, the fermion integral reads

$$Z_e^{(sc)}[A^{(c)}] \approx \oint [id\psi^\dagger][d\psi] e^{-S_e[\psi^\dagger,\psi,A^{(c)}]}[1 - S_e^{\rm int}], \tag{B.8}$$

where we have neglected a term $\mathcal{O}(\alpha^4)$. The approximation in (2.5) only kept the leading term in (B.8). There, we dropped the superscript c with the understanding that A is a classical field. The fermion determinant which results from the integration involves the electron propagator in the presence of the background field. That propagator can be expanded in the background, 2.1, so that $\mathrm{Tr}\ln\left[-\beta\gamma_4 G[A]\right] - \mathrm{Tr}\ln\left[-\beta\gamma_4 G_0^{-1}\right]$, with $G_0 \equiv G[A=0]$, is given as an infinite sum of one-loop graphs: a fermion loop with an even number (due to Furry's theorem) of insertions of the classical field

$$\frac{1}{2}\mathrm{Tr}\,(G_0 \not{A} G_0 \not{A}) + \frac{1}{4}\mathrm{Tr}\,(G_0 \not{A} G_0 \not{A} G_0 \not{A} G_0 \not{A}) + \ldots \tag{B.9}$$

The first term of the series is just

$$\frac{1}{\beta}\sum_n \int \frac{d^3q}{(2\pi)^3} A_\mu(q)\Pi_{\mu\nu}(q)A_\nu(-q), \tag{B.10}$$

with $\Pi_{\mu\nu}(q)$ given by (5.13), the one-loop vacuum polarization tensor. The next term, with four insertions, is still one-loop, nonlinear in the fields, depending on (T,ξ), and typically of order $\alpha(\alpha E^2/m^4)$ or $\alpha(\alpha B^2/m^4)$.

If we consider the first contribution from the electron-electron interaction, we have to contract the four-fermion term in $S_e^{\rm int}$ with the electron propagator in the external field. The resulting graph (Fig. B.1) is a two-loop contribution. When we expand in the external field, the first contribution that depends on the field is quadratic and of order α^2, and contributes in linear response. The next terms in the expansion in the external field are nonlinear, (T,ξ)- dependent contributions of order $\alpha(\alpha E^2/m^4)$, $\alpha(\alpha B^2/m^4)$.

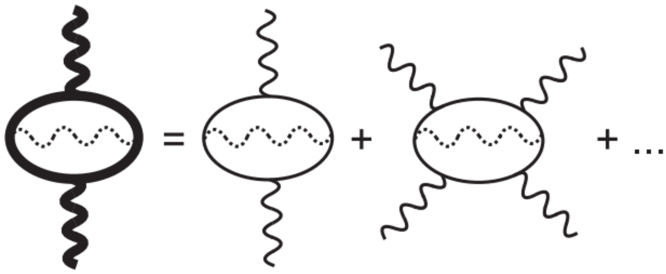

Figure B.1: Graph for the electron-electron interaction expanded in the external field (wiggly lines). The dashed wiggly lines represent the photon propagator.

Thus, restricting our attention to formula (2.5) is equivalent to neglecting one-loop contributions that are nonlinear, as well as a two-loop contribution to linear response of order α^2, and nonlinear ones that also come with electron-electron interactions. Although non-linear terms might bring interesting effects [96], we restrict our analysis to fields that are not strong enough to invalidate the linear response approximation.

Appendix C

Three-dimensional rotation and gauge invarianve of $\Pi_{\mu\nu}$

The gauge invariance of the polarization tensor $\Pi_{\mu\nu}$ allows us to write

$$q_\mu \Pi_{\mu\nu} = \begin{cases} \nu = 4 \quad q_4\Pi_{44} + q_i\Pi_{i4} = 0, \\ \nu = j \quad q_4\Pi_{44} + q_i\Pi_{i4} = 0. \end{cases} \tag{C.1}$$

Multiplying the first equation by q_4 and the second by q_j, we obtain

$$q_4^2\Pi_{44} + q_4 q_i \Pi_{i4} = 0, \tag{C.2}$$

$$q_j q_4 \Pi_{44} + q_i q_j \Pi_{i4} = 0. \tag{C.3}$$

Since $\Pi_{i4} = \Pi_{4i}$, subtracting the equations, we have

$$\Pi_{44} = \frac{q_i q_i}{q_4^2}\Pi_{ij}. \tag{C.4}$$

One may write the tensor as $\Pi_{\mu\nu} = \Pi^{(v)}_{\mu\nu} + \Pi^{(m)}_{\mu\nu}$, to split the vacuum ($T = \xi = 0$) and medium contributions. The vacuum contribution may be written in a fully covariant form

$$-\frac{\Pi^{(v)}_{\mu\nu}}{q^2} = \left(\delta_{\mu\nu} - \frac{q_\mu q_\nu}{q^2}\right)\mathscr{C}(q^2), \tag{C.5}$$

where the scalar function $\mathscr{C}(q^2)$ may be obtained from standard calculation at $T = \xi = 0$ [21]. However, one cannot write the medium contribution tensor $\Pi^{(m)}_{\nu\sigma}$ in a fully covariant form due the fact that the center of mass of the medium introduces a preferred reference.

The symmetry is then reduced to three-dimensional rotation and gauge invariance, leading to [23]

$$-\frac{\Pi^{(m)}_{ij}}{q^2}=\left(\delta_{ij}-\frac{q_iq_j}{|\vec{q}|^2}\right)\mathscr{A}+\delta_{ij}\frac{q_4^2}{|\vec{q}|^2}\mathscr{B}, \tag{C.6}$$

where $\mathscr{A}(q_4,\vec{q})$ e $\mathscr{B}(q_4,\vec{q})$ are scalar functions. We write (C.4) as

$$\Pi_{44}=(-q^2)\left[\frac{q_iq_j}{q_4^2}\left(\delta_{ij}-\frac{q_iq_j}{|\vec{q}|^2}\right)\mathscr{A}+\frac{q_iq_j}{q_4^2}\delta_{ij}\frac{q_4^2}{|\vec{q}|^2}\mathscr{B}\right], \tag{C.7}$$

and obtain

$$\mathscr{B}(q_4,\vec{q})=-\frac{\Pi^{(m)}_{44}(q)}{q^2}. \tag{C.8}$$

From (C.1), we have $\tilde{\Pi}^{(m)}_{4j}$

$$\begin{aligned}\Pi^{(m)}_{4j} &= -\frac{q_i}{q_4}\Pi^{(m)}_{ij}\\ &= -\frac{q_i}{q_4}(-q^2)\left((\delta_{ij}-\frac{q_iq_j}{\vec{q}^2})\mathscr{A}+\delta_{ij}\frac{q_4^2}{\vec{q}^2}\mathscr{B}\right)\\ &= q_4\frac{q^2}{\vec{q}^2}q_jB.\end{aligned} \tag{C.9}$$

The scalar function $\mathscr{B}(q_4,\vec{q})$ allows us to define the tensors $\Pi^{(m)}_{44}$ and $\Pi^{(m)}_{4j}$. Finally, the function $\mathscr{A}(q_4,\vec{q})$, may be obtained taking the trace $\Pi^{(m)}_{ij}$

$$\begin{aligned}\Pi^{(m)}_{ii} &= -q^2\left[(\delta_{ii}-1)\mathscr{A}+\delta_{ii}\frac{q_4^2}{\vec{q}^2}\mathscr{B}\right]\\ &= -2q^2\mathscr{A}+3\frac{q_4^2}{|\vec{q}|^2}\Pi^{(m)}_{44}.\end{aligned} \tag{C.10}$$

Adding $\Pi^{(m)}_{44}$ on both sides of the equation above, with $\Pi^{(m)}_{\mu\mu}=\Pi^{(m)}_{ii}+\Pi^{(m)}_{44}$, we obtain

$$\Pi^{(m)}_{ii}+\Pi^{(m)}_{44}=-2q^2\mathscr{A}+\frac{3q_4^2}{\vec{q}^2}\Pi^{(m)}_{44}+\Pi^{(m)}_{44}. \tag{C.11}$$

Thus, we obtain the scalar functions $\mathscr{A}$ and $\mathscr{B}$ in terms of $\Pi^{(m)}_{44}$ and the trace $\Pi^{(m)}_{\mu\mu}$ from the medium contribution to the polarization tensor

$$\mathscr{A}(q_4,\vec{q})=-\frac{1}{2q^2}\Pi^{(m)}_{\mu\mu}+\left(\frac{3}{2|\vec{q}|^2}-\frac{1}{q^2}\right)\Pi^{(m)}_{44}, \tag{C.12}$$

$$\mathscr{B}(q_4,\vec{q})=-\frac{\Pi^{(m)}_{44}}{q^2}. \tag{C.13}$$

We define $\Delta\Pi_{\mu\nu}=\Pi_{\mu\nu}(T,\mu)-\Pi_{\mu\nu}(0,0)$ by subtracting the vacuum contribution.

Appendix D

Calculation of the Matsubara sums of $\Pi_{44}^{(m)}$ and $\Pi_{\mu\mu}^{(m)}$ for fermions

D.1 Computation of $\Pi_{44}^{(m)}$

The component Π_{44}^{m} of the polarization tensor 5.13 is

$$\Pi_{44} = -e^2 T \sum_{n=-\infty}^{\infty} \int \frac{d^3 p}{(2\pi)^3} \mathrm{Sp}\left[\gamma_4 G_F(p) \gamma_4 G_F(p-q)\right], \tag{D.1}$$

where $G_F(p) = -(\gamma_\mu \bar{p}_\mu + m)^{-1}$ is the fermion propagator in momenta space, $\bar{p}_\mu \equiv (\bar{p}_4, p_j) = (p_4 + i\xi, p_j)$, with $p_4 = 2\pi T\left(n + \frac{1}{2}\right)$, and $q_\mu = (q_4, \vec{q})$. The fermion propagator may be written as

$$G_F(p) = -\frac{\bar{\not{p}} - m}{\bar{p}^2 - m^2}, \tag{D.2}$$

where $\not{p} = \bar{\gamma}_\mu p_\mu$. Calculating the spin trace in D.1 we have

$$\mathrm{Sp}\left[\gamma_4 G_F(p) \gamma_4 G_F(p-q)\right] = \frac{\mathrm{Sp}\left[\gamma_4 (\bar{\not{p}} - m) \gamma_4 (\bar{\not{p}} - \not{q} - m)\right]}{(\bar{p}^2 + m^2)[(\bar{p} - \bar{q})^2 + m^2]}. \tag{D.3}$$

The numerator may be computed using the algebra of Dirac matrices[1], eq. D.1 reads

$$\Pi_{44} - 4e^2 T \sum_{n=-\infty}^{\infty} \int \frac{d^3 p}{(2\pi)^3} \frac{\bar{p}_4(\bar{p}_4 - q_4) - \vec{p}\cdot(\vec{p} - \vec{q}) - m^2}{(\bar{p}^2 + m^2)[(\bar{p} - \bar{q})^2 + m^2]}. \tag{D.4}$$

[1]

$$\begin{aligned}
\mathrm{Sp}[\gamma_4\gamma_\mu\gamma_4\gamma_\nu] &= 4(\delta_{4\mu}\delta_{4\nu} + \delta_{4\nu}\delta_{4\mu} - \delta_{\mu\nu}\delta_{44}) \\
\mathrm{Sp}[\gamma_4\gamma_\mu\gamma_4] &= 0 \\
\mathrm{Sp}[\gamma_4^2 m^2] &= -m^2\mathrm{Sp}[I] = -4m^2
\end{aligned}$$

Writing the numerator of (D.1) as

$$\bar{p}_4(\bar{p}_4 - q_4) - \vec{p}\cdot(\vec{p}-\vec{q}) - m^2 = \frac{1}{2}(\bar{p}_4^2 + \omega_p^2) + \frac{1}{2}[(\bar{p}_4 - q_4)^2 + \omega_{p-q}^2] - \frac{C}{2}, \tag{D.5}$$

where $\omega_p^2 = \vec{p}^2 + m^2$, and

$$C = q^2 + 4\omega_p^2 - 4\vec{p}\cdot\vec{q}, \tag{D.6}$$

with $q^2 = q_4^2 + \vec{q}^2$, eq. D.4 reads

$$\Pi_{44} = -2e^2 T \int \frac{d^3p}{(2\pi)^3}\left\{\sum_{n=-\infty}^{\infty}\frac{1}{\bar{p}_4^2+\omega_p^2} + \sum_{n=-\infty}^{\infty}\frac{1}{(\bar{p}_4-q_4)^2+\omega_{p-q}^2} - C\sum_{n=-\infty}^{\infty}\frac{1}{(\bar{p}_4^2+\omega_p^2)[(\bar{p}_4-q_4)^2+\omega_{p-q}^2]}\right\} \tag{D.7}$$

The problem reduces to solving the three Matsubara sums in the equation above. Solving the first sum, we have

$$\sum_{n=-\infty}^{\infty}\frac{1}{\bar{p}_4^2+\omega_p^2} = \frac{1}{(2\pi T)^2}\sum_{n=-\infty}^{\infty}\frac{1}{(n+\frac{1}{2}+i\xi)^2+\omega_p^2}, \tag{D.8}$$

where $\xi \equiv \frac{\beta\xi}{2\pi}$ and $\omega_p \equiv \frac{\beta\omega_p}{2\pi}$. We may identify the term $(n+\frac{1}{2}+i\xi)^2+\omega_p^2 = (n-x_+)(n-x_-)$, and using the result

$$\sum_{n=-\infty}^{\infty}\frac{1}{(n-x_+)(n-x_-)} = \pi\frac{\cot\pi x_+ - \cot\pi x_-}{x_- - x_+} \tag{D.9}$$

with $x_\pm = -\frac{1}{2} \pm i(\omega_p \mp \xi)$, we have $\cot\pi x_\pm = \cot\left[\pi\left(-\frac{1}{2}\pm i(\omega_p-\xi)\right)\right]$. Noting that

$$\cot\left[\pi\left(l\pm\frac{1}{2}+ib\right)\right] = i\frac{1+e^{2\pi b}e^{-2\pi i l}e^{\mp\pi i}}{1-e^{2\pi b}e^{-2\pi i l}e^{\mp\pi i}}, \tag{D.10}$$

if $l = \pm1, \pm2, \ldots$, we obtain

$$\cot\left[\pi\left(l\pm\frac{1}{2}+ib\right)\right] = i\frac{e^{-\pi b}-e^{\pi b}}{e^{-\pi b}+e^{\pi b}} = -i\tanh\pi b. \tag{D.11}$$

We may identify $\tanh(\pi b) = 1 - 2n_F(2\pi b)$, where

$$n_F(\theta) = \frac{1}{e^\theta+1}, \tag{D.12}$$

thus

$$\cot\pi x_\pm = \mp i\left[1-2n_F\left(\beta(\omega_p\mp\xi)\right)\right]. \tag{D.13}$$

Therefore, the sum (D.14) is

$$\sum_{n=-\infty}^{\infty}\frac{1}{\bar{p}_4^2+\omega_p^2} = \frac{1}{2T\omega_p}[1-n_F^-(p)-n_F^+(p)], \tag{D.14}$$

where $n_F^{\pm}(p) \equiv n_F(\beta\omega_p - \beta\xi)$. The second sum in D.4 may be evaluated directly if we write the term $\bar{p}_4 - q_4 = (2n+i)\pi T + i(\mu + iq_4)$. Thus, if we let $\mu \to \mu + iq_4$, where, $q_4 = 2\pi l T$, and $\omega_p \to \omega_{p-q}$, we can use the same result of the first sum (D.14). We have

$$\sum_{n=-\infty}^{\infty} \frac{1}{(\bar{p}_4 - q_4)^2 + \omega_{p-q}^2} = \frac{1}{2\omega_{p-q}T}\left[1 - n_F^-(p-q) - n_F^+(p-q)\right]. \tag{D.15}$$

This result is identical to the first sum, because one may let $\vec{p} \to \vec{p} - \vec{q}$ in the $\int d^3p$ and obtain $n_F^{\pm}(p) \to n_F^{\pm}(p-q)$. It remains to calculate the last sum

$$S = \sum_{n=-\infty}^{\infty} \frac{1}{(\bar{p}_4^2 + \omega_p^2)[(\bar{p}_4 - q_4)^2 + \omega_{p-q}^2]}. \tag{D.16}$$

Splitting in partial fractions, we obtain

$$S = \sum_{n=-\infty}^{\infty} \left\{ \frac{a_1}{\bar{p}_4 - \alpha_1} + \frac{a_2}{\bar{p}_4 - \alpha_2} + \frac{a_3}{\bar{p}_4 - \alpha_3} + \frac{a_4}{\bar{p}_4 - \alpha_4} \right\}, \tag{D.17}$$

where, $\alpha_1 = i\omega_p$, $\alpha_2 = -i\omega_p$, $\alpha_3 = q_4 + i\omega_{p-q}$ and $\alpha_4 = q_4 - i\omega_{p-q}$. We must calculate the factors a_i. From the partial fraction decomposition, we obtain

$$\begin{aligned} a_1 &= a_2^* = \frac{1}{2i\omega_p\left[(i\omega_p - q_4)^2 + \omega_{p-q}^2\right]} \\ &= \frac{1}{2i\omega_p\left(q^2 - 2pq\right)}, \end{aligned} \tag{D.18}$$

where $p \cdot q = i\omega_p q_4 + \vec{p} \cdot \vec{q}$, and

$$a_3 = a_4^* = \frac{1}{2i\omega_{p-q}\left[(q_4 + i\omega_{p-q})^2 + \omega_p^2\right]}, \tag{D.19}$$

where a_i^* is the complex conjugate of a_i. Now we need to compute the sum

$$S_i' = \sum_{n=-\infty}^{\infty} \frac{1}{\bar{p}_4 - \alpha_i} = \sum_{n=-\infty}^{\infty} \frac{1}{2\pi T\left(n + \frac{1}{2} + i\xi - \alpha_i\right)} \tag{D.20}$$

where $\alpha_i = \frac{\beta\alpha_i}{2\pi}$. The sum may be written as

$$S_i' = \frac{\beta}{2\pi} \sum_{n=-\infty}^{\infty} \frac{1}{n - x_i}, \tag{D.21}$$

where $x_i = -\frac{1}{2} + \alpha_i - i\xi$. The sum above may be rewritten in the form

$$\begin{aligned} S_i' &= \frac{\beta}{2\pi}\left[-\frac{1}{x_i} + \sum_{n=1}^{\infty}\left(\frac{1}{n - x_i} + \frac{1}{-n - x_i}\right)\right] \\ &= \frac{\beta x}{\pi}\left(-\frac{1}{2x_i^2} + \sum_{n=1}^{\infty} \frac{1}{(n - x_i)(n + x_i)}\right). \end{aligned}$$

From eq. (D.14), we already know how to evaluate the last sum

$$\begin{aligned}\sum_{n=-\infty}^{\infty}\frac{1}{(n-x_i)(n+x_i)} &= -\frac{1}{x_i^2}+2\sum_{n=1}^{\infty}\frac{1}{(n-x_i)(n+x_i)}\\ &= i\frac{\pi}{x_i},\end{aligned}\tag{D.22}$$

where $\mathrm{Im}\alpha_i$ is the imaginary part of α_i. We obtain

$$S_i' = \frac{i\beta}{2}\left[1-2n_F\left(\beta(\mathrm{Im}\alpha_i-\xi)\right)\right].\tag{D.23}$$

The complete sum is $S = a_1S_1' + a_2S_2' + a_3S_3' + a_4S_4'$. Since $a_1 = a_2^*$ and $a_3 = a_4^*$, and writing $a_i \equiv \mathrm{Re}a_i + i\mathrm{Im}a_i$, we obtain

$$\begin{aligned}S &= 2i\beta\Big\{\mathrm{Re}a_1\left[n_F^+(p)-n_F^-(p)\right]+i\mathrm{Im}a_1\left[1-n_F^+(p)-n_F^-(p)\right]\\ &+ \mathrm{Re}a_3\left[n_F^+(p-q)-n_F^-(p-q)\right]+i\mathrm{Im}a_3\left[1-n_F^+(p-q)-n_F^-(p-q)\right]\Big\}.\end{aligned}\tag{D.24}$$

The sum above will be integrated over $\int d^3p$. Thus, if we let $\vec{p}\to\vec{p}-\vec{q}$, this implies $\omega_p\to\omega_{p-q}$, and we obtain $a_1\to -a_3^*$. The first and third terms above will cancel in the $\int d^3p$, and we obtain

$$S = -2\beta\mathrm{Im}a_1\left[1-n_F(p)\right],\tag{D.25}$$

where,

$$\begin{aligned}n_F(p) &= n_F^-(p)+n_F^+(p)\\ &= \frac{1}{e^{\beta(\omega_p-\xi)}-1}+\frac{1}{e^{\beta(\omega_p+\xi)}-1},\end{aligned}\tag{D.26}$$

and the polarization tensor Π_{44} is

$$\Pi_{44} = -2e^2\int\frac{d^3p}{(2\pi)^3}\frac{1}{\omega_p}[1-n_F(p)][1+2C\mathrm{Im}a_1\omega_p].\tag{D.27}$$

The term $C = q^2-4\vec{p}\cdot\vec{q}-2p_4^2\in\mathbb{R}$. Thus, substituting a_1 we write

$$\begin{aligned}\Pi_{44} &= -2e^2\int\frac{d^3p}{(2\pi)^3}\frac{1}{\omega_p}[1-n_F(p)]\mathrm{Re}\left(1-\frac{C}{q^2-2p\cdot q}\right)\\ &= -\frac{e^2}{2\pi^3}\mathrm{Re}\int\frac{d^3p}{\omega_p}\left[1-n_F(p)\right]\frac{p\cdot q-2p_4(q_4-p_4)}{q^2-2p\cdot q}.\end{aligned}\tag{D.28}$$

Here, we redefine $p_4 = i\omega_p$. We are interested in the medium contribution to the polarization tensor, which can be obtained by subtracting the vacuum contribution $\Pi_{44}(T=0,\xi=0)\equiv\Pi_{44}^{(v)}$, of (D.28), where $\Pi_{44}^{(m)} = \Pi_{44}(T,\xi)-\Pi_{44}(0,0)$. We obtain

$$\Pi_{44}^{(m)} = \frac{e^2}{2\pi^3}\mathrm{Re}\int\frac{d^3p}{\omega_p}n_F(p)\frac{p\cdot q-2p_4(q_4-p_4)}{q^2-2p\cdot q}.\tag{D.29}$$

D.2 Computation of $\Pi_{\mu\mu}^{(m)}$

To calculate the Matsubara sum of the trace $\Pi_{\mu\mu}^{(m)}$ we will apply a similar procedure to the one used for $\Pi_{44}^{(m)}$. We have

$$\begin{aligned}\Pi_{\mu\mu} &= -e^2 T \sum_{n=-\infty}^{\infty} \int \frac{d^3 p}{(2\pi)^3} \mathrm{Sp}\left[\gamma_\mu G_F(p)\gamma_\mu G_F(p-q)\right] \\ &= -e^2 T \sum_{n=-\infty}^{\infty} \int \frac{d^3 p}{(2\pi)^3} \frac{\mathrm{Sp}\left[\gamma_\mu(\bar{\not p}-m)_\nu\gamma_\mu(\bar{\not p}-\not q-m)_\sigma\right]}{(\bar p^2+m^2)[(\bar p-\bar q)^2+m^2]}.\end{aligned} \tag{D.30}$$

The spin trace in the numerator is

$$\mathrm{Sp}\left[\gamma_\mu\left(\gamma_\nu\bar p_\nu - m\right)\gamma_\mu\left(\gamma_\sigma(\bar p_\sigma - q_\sigma)-m\right)\right] = \mathrm{Sp}[\gamma_\mu\gamma_\nu\gamma_\mu\gamma_\sigma](\bar p_\nu(\bar p-q)_\sigma) + \mathrm{Sp}[\gamma_\mu\gamma_\mu]m^2. \tag{D.31}$$

One may show that $\mathrm{Sp}[\gamma_\mu\gamma_\nu\gamma_\mu\gamma_\sigma] = -8\nu\sigma$, and $\mathrm{Sp}[\gamma_\mu\gamma_\mu] = -16$. We then obtain

$$\Pi_{\mu\mu} = -\frac{e^2 T}{\pi^3}\sum_{n=-\infty}^{\infty}\int \frac{d^3p}{(2\pi)^3}\frac{-\bar p\cdot(\bar p - q) - 2m^2}{(\bar p^2+m^2)[(\bar p-q)^2+m^2]}. \tag{D.32}$$

Writing the numerator as

$$-\bar p\cdot(\bar p-q) - 2m^2 = -\frac{1}{2}\left[(\bar p^2+m^2) + \left((\bar p-q)^2 - m^2\right) - D\right], \tag{D.33}$$

where $D \equiv q^2 - 2m^2 \in \mathbf{R}$, we have

$$\Pi_{\mu\mu} = \frac{e^2 T}{2\pi^3}\int d^3p\left\{\sum_{n=-\infty}^{\infty}\frac{1}{\bar p_4^2+\omega_p^2} + \sum_{n=-\infty}^{\infty}\frac{1}{(\bar p_4 - q_4)^2+\omega_{p-q}^2} - D\sum_{n=-\infty}^{\infty}\frac{1}{(\bar p_4^2+\omega_p^2)[(\bar p_4-q_4)^2+\omega_{p-q}^2]}\right\}.$$

The result above is analogous to eq. (D.7), therefore we may apply the same results obtained before to solve the sums in Π_{44}. We have

$$\begin{aligned}\Pi_{\mu\mu} &= \frac{e^2}{2\pi^3}\int\frac{d^3p}{\omega_p}[1-n_F(p)][1+2D\mathrm{Im}a_1\omega_p] \\ &= -\frac{e^2}{\pi^3}\mathrm{Re}\int\frac{d^3p}{\omega_p}[1-n_F(p)]\frac{p\cdot(p+q)}{q^2-2p\cdot q},\end{aligned} \tag{D.34}$$

and finally, subtracting the vacuum contribution from the equation above, we arrive at the medium contribution $\Pi_{\mu\mu}^{(m)}$

$$\Pi_{\mu\mu}^{(m)} = \frac{e^2}{\pi^3}\mathrm{Re}\int\frac{d^3p}{\omega_p}n_F(p)\frac{p\cdot(p+q)}{q^2-2p\cdot q}. \tag{D.35}$$

Appendix E

Integral over angles of $\mathscr{A}$ and $\mathscr{B}$ for fermions

We may write eq. (2.23) as

$$\mathscr{A}+\frac{1}{2}\left(1+\frac{3q_4^2}{|\vec{q}|^2}\right)\mathscr{B}=-\frac{e^2}{2\pi^3 q^2}\mathrm{Re}\int_0^\infty \frac{2\pi p^2 dp}{\omega_p}n_F(p)\int_0^\pi \sin\theta d\theta \frac{p^2+p\cdot q}{q^2-2p\cdot q}, \tag{E.1}$$

where θ is the angle between the vectors $\vec{p}$ e $\vec{q}$. We may write

$$\begin{aligned}\frac{p^2+p\cdot q}{q^2-2p\cdot q} &= \frac{-m^2+i\omega_p q_4+|\vec{p}||\vec{q}|\cos\theta}{q^2-2i\omega_p q_4-2|\vec{p}||\vec{q}|\cos\theta}\\ &= -\frac{\alpha_1+x}{\lambda_1+2x},\end{aligned} \tag{E.2}$$

where $x=\cos\theta$, and

$$\alpha_1=\frac{-m^2+i\omega_p q_4}{|\vec{p}||\vec{q}|},\quad \lambda_1=\frac{2i\omega_p q_4-q^2}{|\vec{p}||\vec{q}|}. \tag{E.3}$$

The integral over angles will be of the form

$$\int_{-1}^1 dx\frac{\alpha+x}{\lambda+2x}=1+\frac{1}{2}\left(\alpha-\frac{\lambda}{2}\right)\ln\frac{\lambda+2}{\lambda-2}. \tag{E.4}$$

Performing it in (E.1) yields

$$\int_0^\pi \sin\theta d\theta\frac{p^2+p\cdot q}{q^2-2p\cdot q}=-\left[1+\frac{q^2-2m^2}{4|\vec{p}||\vec{q}|}\ln\left(\frac{q^2-2|\vec{p}||\vec{q}|-2i\omega_p q_4}{q^2+2|\vec{p}||\vec{q}|-2i\omega_p q_4}\right)\right] \tag{E.5}$$

We may split the logarithm into real and imaginary parts in order to retain only the real part in (E.1). Since $\ln z=\ln|z|+i\phi$, we have

$$\ln\left(q^2\pm 2|\vec{p}||\vec{q}|-2i\omega_p q_4\right)=\frac{1}{2}\ln\left[(q^2\pm 2|\vec{p}||\vec{q}|)^2+4\omega_p^2 q_4^2\right]-i\arctan\left(\frac{2\omega_p q_4}{q^2\pm 2|\vec{p}||\vec{q}|}\right). \tag{E.6}$$

Defining $|\vec{p}| \equiv p$, eq. (E.1) becomes

$$\mathscr{A} + \frac{1}{2}\left(1+\frac{3q_4^2}{|\vec{q}|^2}\right)\mathscr{B} = \frac{e^2}{\pi^2 q^2}\int_0^\infty \frac{p^2 dp}{\omega_p} n_F(p)\left\{1+\frac{2m^2-q^2}{8p|\vec{q}|}\ln\frac{(q^2+2p|\vec{q}|)^2+4\omega_p^2 q_4^2}{(q^2-2p|\vec{q}|)^2+4\omega_p^2 q_4^2}\right\}. \quad \text{(E.7)}$$

A similar procedure may be used to obtain the integral over angles of (2.24)

$$\mathscr{B} = \frac{-e^2}{2\pi^3 q^3}\mathrm{Re}\int \frac{d^3 p}{\omega_p} n_F(p)\frac{p\cdot q - 2p_4(q_4-p_4)}{q^2-2p\cdot q}. \quad \text{(E.8)}$$

We may write

$$\frac{p\cdot q - 2p_4(p_4+q_4)}{q^2-2p\cdot q} = -\frac{\alpha_2+x}{\lambda_2+2x}, \quad \text{(E.9)}$$

where

$$\alpha_2 = \frac{-2\omega_p^2 - i\omega_p q_4}{p|\vec{q}|}, \quad \lambda_2 = \frac{2i\omega_p q_4 - q^2}{p|\vec{q}|}. \quad \text{(E.10)}$$

Then,

$$\begin{aligned}
\mathscr{B} &= \frac{e^2}{2\pi^3 q^3}\mathrm{Re}\int_0^\infty \frac{2\pi p^2 dp}{\omega_p} n_F(p)\int_{-1}^1 dx\frac{\alpha_2+x}{\lambda_2+2x} \\
&= -\frac{e^2}{2\pi^3 q^3}\mathrm{Re}\int_0^\infty \frac{2\pi p^2 dp}{\omega_p} n_F(p)\left\{1+\frac{q^2-4\omega_p^2-4i\omega_p q_4}{4p\vec{q}}\ln\left(\frac{2i\omega_p q_4 - q^2+2p|\vec{q}|}{2i\omega_p q_4 - q^2 - 2p|\vec{q}|}\right)\right\}.
\end{aligned}$$

Extracting the real part, comes

$$\begin{aligned}
\mathscr{B} &= \frac{e^2}{\pi^2}\int_0^\infty \frac{p^2 dp}{\omega_p} n_F(p)\left[1+\frac{4\omega_p^2-q^2}{8p\vec{q}|}\ln\left(\frac{(q^2+2p|\vec{q}|)^2+4\omega_p^2 q_4^2}{(q^2-2p|\vec{q}|)^2+4\omega_p^2 q_4^2}\right)\right. \\
&- \left.\frac{\omega_p q_4}{p|\vec{q}|}\arctan\left(\frac{8p|\vec{q}|\omega_p q_4}{4\omega_p^2 q_4^2 - 4p^2|\vec{q}|^2+q^4}\right)\right]. \quad \text{(E.11)}
\end{aligned}$$

The results for $\mathscr{A}$ and $\mathscr{B}$ may be continued to Minkowski metric by letting $q_4 \to i\omega$ and $q^2 \to -q_M^2$, with $q_M^2 = \omega^2 - |\vec{q}|^2$, and using the relation

$$\arctan(ix) = i\,\mathrm{arctanh}(x) \equiv -\frac{i}{2}\ln\left(\frac{1+z}{1-z}\right), \quad \text{(E.12)}$$

the scalar functions $\mathscr{A} \to \mathscr{A}^*$ and $\mathscr{B} \to \mathscr{B}^*$ in Minkoswki metric are

$$\mathscr{A}^* - \left(1+\frac{3q_M^2}{2|\vec{q}|^2}\right)\mathscr{B}^* = -\frac{e^2}{\pi^2 q_M^2}\int_0^\infty \frac{p^2 dp}{\omega_p} n_F(p)\left[1+\frac{2m^2+q_M^2}{8p|\vec{q}|}f_1\right], \quad \text{(E.13)}$$

$$\mathscr{B}^* = -\frac{e^2}{\pi^2 q_M^2}\int_0^\infty \frac{p^2 dp}{\omega_p} n_F(p)\left[1+\frac{4\omega_p^2+q_M^2}{8p|\vec{q}|}f_1 - \frac{\omega_p\omega}{2p|\vec{q}|}f_2\right], \quad \text{(E.14)}$$

where

$$f_1 = \ln\left(\frac{(q_M^2 - 2p|\vec{q}|)^2 - 4\omega_p^2\omega^2}{(q_M^2 + 2p|\vec{q}|)^2 - 4\omega_p^2\omega^2}\right), \tag{E.15}$$

$$f_2 = \ln\left(\frac{q_M^4 - 4(p|\vec{q}| - \omega_p\omega)^2}{q_M^4 - 4(p|\vec{q}| + \omega_p\omega)^2}\right). \tag{E.16}$$

Appendix F

Limiting behavior, $(|\vec{q}| \to 0)$, of ϵ and μ^{-1} for relativistic Fermi gas

In order to access the long-wavelength limit of the relativistic electromagnetic responses, for $\omega \neq 0$ and $\omega = 0$ (static case), one takes $|\vec{q}| \to 0$ and expands the expressions $\mathscr{A}^*$ and $\mathscr{B}^*$ after doing the angular integrals. Introducing the dimensionless variables $x \equiv \omega_m/m$, $a \equiv \omega/2m$, and $b \equiv |\vec{q}|/2m$, and the functions

$$L_1(a,b) \equiv \ln\left(ax + b\sqrt{x^2-1} + a^2 - b^2\right), \tag{F.1}$$

$$L_2(a,b) \equiv \ln\left(ax + b\sqrt{x^2-1} + a^2\right), \tag{F.2}$$

we may rewrite the functions f_1 and f_2 in (2.28) and (2.29) as

$$f_1 = -L_1(a,b) - L_1(-a,b) + L_1(a,-b) + L_1(-a,-b), \tag{F.3}$$

$$f_2 = +L_2(a,b) + L_2(-a,-b) - L_1(a,-b) - L_2(-a,b). \tag{F.4}$$

Expanding f_1 and f_2 in powers of b, we derive

$$\frac{f_1}{\sqrt{x^2-1}} = -\frac{2b}{a}F_-^{(1)} - \frac{2b^3}{3a^3}\left[F_-^{(1)} + aF_+^{(2)} + (a^2-1)F_-^{(3)}\right], \tag{F.5}$$

$$\frac{f_2}{\sqrt{x^2-1}} = \frac{2b}{a}F_+^{(1)} + \frac{2b^3}{3a^3}\left[F_+^{(1)} - aF_-^{(2)} + (a^2-1)F_+^{(3)}\right], \tag{F.6}$$

where we have used

$$F_\pm^{(j)} \equiv \frac{1}{(x+a)^j} \pm \frac{1}{(x-a)^j}. \tag{F.7}$$

In terms of the dimensionless variables introduced above, we have

$$\mathscr{B}^* = -\frac{e^2}{4\pi^2}\frac{1}{a^2-b^2}\int_1^\infty dx n_F(x)\left[\sqrt{x^2-1}+\frac{(x^2+a^2-b^2)}{4b}f_1-\frac{a}{2b}f_2\right], \tag{F.8}$$

$$\mathscr{D}^* = -\frac{e^2}{4\pi^2}\frac{1}{a^2-b^2}\int_1^\infty dx n_F(x)\left[\sqrt{x^2-1}+\frac{(1+2a^2-2b^2}{8b}f_1\right]. \tag{F.9}$$

Using (F.3) and (F.4), we obtain

$$\frac{a^2}{b^2}\mathscr{B}^* = \frac{e^2}{4\pi^2}\left[\frac{2}{3a^2}I^{(0)}+\frac{1+14a^2}{3a^2}I^{(1)}+4a^2I^{(2)}\right], \tag{F.10}$$

$$a^2\mathscr{D}^* = -\frac{e^2}{4\pi^2}\left[I^{(0)}+\frac{1+2a^2}{2}I^{(1)}\right], \tag{F.11}$$

which lead to

$$\mathscr{A}^* = \frac{3e^2}{2\pi^2}[I^{(1)}+a^2I^{(2)}], \tag{F.12}$$

where the integrals $I^{(j)}$ are given by

$$I^{(j)} \equiv \int_1^\infty dx n_F(x)\frac{\sqrt{x^2-1}}{(x^2-a^2)^j}, \tag{F.13}$$

with $I^{(2)} = \partial I^{(1)}/\partial a^2$. We may compute these integrals exactly at $T = 0$, when $n_F(x) = \Theta(\zeta - x)$. We use the Euler substitutions $\sqrt{(x-1)(x+1)} = t(x+1)$ and decomposition in partial fractions to derive

$$I^{(0)} = \frac{1}{2}\left[\zeta\sqrt{\zeta^2-1}-\ln\left(\zeta+\sqrt{\zeta^2-1}\right)\right], \tag{F.14}$$

$$I^{(1)} = \ln\left(\zeta+\sqrt{\zeta^2-1}\right)-\frac{1}{\sigma(a)}\arctan\left(\frac{\sigma(a)}{\sigma(\zeta)}\right), \tag{F.15}$$

where $\sigma(y) \equiv y/\sqrt{|1-y^2|}$. We have used $q_M^2 \to \omega^2 > 0$. Since we are interested in $\omega \to 0$, we have also taken $a \ll 1$. Using the expressions

$$\epsilon = 1+\mathscr{C}^*+\mathscr{A}^*+\left(1-\frac{a^2}{b^2}\right)\mathscr{B}^*, \tag{F.16}$$

$$\mu^{-1} = 1+2\mathscr{C}^*+\mathscr{A}^*+-2\frac{a^2}{b^2}\mathscr{B}^*, \tag{F.17}$$

and expanding (F.10) and (F.11) for $a \ll 1$ [$\mathscr{C}^*$ is $\mathscr{O}(a^2)$], we obtain

$$\epsilon = 1-\frac{a_e^2}{a^2}+\frac{e^2}{3\pi^2}g_e(\zeta)+\mathscr{O}(a^2) \tag{F.18}$$

$$\mu^{-1} = 1 - \frac{a_m^2}{a^2} - \frac{5e^2}{6\pi^2} g_m(\zeta) + \mathcal{O}(a^2), \tag{F.19}$$

where $a_m^2 = 2a_e^2$,

$$a_e^2 = \frac{\omega_e^2}{4m^2} = \frac{e^2}{12\pi^2} \frac{(\zeta^2-1)^{3/2}}{\zeta}, \tag{F.20}$$

and the $\mathcal{O}(\alpha)$ corrections are given by

$$g_e(\zeta) = \ln\left(\zeta + \sqrt{\zeta^2-1}\right) - \frac{1}{\sigma(\zeta)} - \frac{7}{6\sigma^3(\zeta)}, \tag{F.21}$$

$$g_m(\zeta) = \ln\left(\zeta + \sqrt{\zeta^2-1}\right) - \frac{1}{\sigma(\zeta)} - \frac{14}{15\sigma^3(\zeta)}. \tag{F.22}$$

Appendix G

Imaginary and Real parts at $T = 0$

G.1 Imaginary parts at $T = 0$

Again, the vacuum contribution does not have an imaginary part. We then refer to the three cases described in subsection 3.2, which correspond to different regions in the (a, b) plane.

In case (i), $\chi^2 < 0$, $\eta > 1$, $a < b < b\eta$, the lower integration limit of (3.10), (3.11) is $x_l = -a + b\eta$ whereas the upper one is $x_u = a + b\eta$. For a nonvanishing result, we need $x_l = -a + b\eta < x_F$. This will occur if $b_- < b < b_+$, where

$$b_\pm = \pm\frac{y_F}{2} + \sqrt{\frac{y_F^2}{4} + a(x_F + a)}. \tag{G.1}$$

Depending on whether $x_u < x_F$ or $x_u > x_F$, results for the imaginary part will differ. For $x_u = a + b\eta < x_F$, one needs $a < x_F$ and

$$b^2 - y_F b + a(x_F - a) < 0, \tag{G.2}$$

$$b^2 + y_F b + a(x_F - a) > 0. \tag{G.3}$$

To satisfy (G.2), the argument of the square-root appearing in the roots of the associated equation has to be positive, so that $0 < a < (x_F - 1)/2$ and $(x_F + 1)/2 < a < x_F$. Then, (G.3) will always be satisfied whereas (G.2) implies $\bar{b}_- < b < \bar{b}_+$, where

$$\bar{b}_\pm = \frac{y_F}{2} \pm \sqrt{\frac{y_F^2}{4} - a(x_F - a)}. \tag{G.4}$$

As a result, the integrals in (3.10) and (3.11), with the definition $[f(x)]_{x_l}^{x_u} \equiv f(x_u) - f(x_l)$, define regions (A) and (B) in subsection 3.2.

In case (iii) [$\chi^2 > 1$, $\eta < 1$ ($a > b > b\eta$)], the lower integration limit of (3.10), (3.11) is $x_l = a - b\eta$ whereas the upper one is $x_u = a + b\eta$. For a nonvanishing result, $x_l = a - b\eta < x_F$. This will always occur if $a < x_F$ whereas for $a > x_F$, $b'_- < b < b'_+$, where

$$b'_\pm = \pm\frac{y_F}{2} + \sqrt{\frac{y_F^2}{4} - a(x_F - a)}. \tag{G.5}$$

Again, depending on whether $x_u < x_F$ or $x_u > x_F$, results for the imaginary part will differ. For $x_u = a + b\eta < x_F$, $a < x_F$ and

$$b^2 - y_F b + a(x_F - a) > 0, \tag{G.6}$$

$$b^2 + y_F b + a(x_F - a) > 0. \tag{G.7}$$

To satisfy (G.6), the argument of the square-root appearing in the roots of the associated equation has to be positive, so that $0 < a < (x_F - 1)/2$ and $(x_F + 1)/2 < a < x_F$. Then, (G.7) will always be satisfied whereas (G.6) implies $\bar{b}'_- < b < \bar{b}'_+$, with

$$\bar{b}'_\pm = \frac{y_F}{2} \pm \sqrt{\frac{y_F^2}{4} - a(x_F - a)}. \tag{G.8}$$

We may then define regions (C) and (D) in subsection 3.2.

G.2 Real parts at $T = 0$

The first integral in expressions (3.5) and (3.6) is simply

$$\frac{1}{2}\left[x_F y_F - \ln(x_F + y_F)\right], \tag{G.9}$$

whereas the last ones may be integrated by parts, using $R_1(1) = R_2(1) = 0$, to yield

$$\frac{x_F}{12b}[(x_F^2 + 3\chi^2)R_1(x_F) + 6ax_F R_2(x_F)] - \frac{1}{12b}\int_1^{x_F} dx\,[(x^3 + 3\chi^2 x)R'_1 + 6ax^2 R'_2], \tag{G.10}$$

for (3.5), and

$$\frac{x_F}{8b}(1 + 2\chi^2)R_1(x_F) - \frac{1}{8b}\int_1^{x_F} dx(1 + 2\chi^2)xR'_1, \tag{G.11}$$

for (3.6). It is convenient to introduce

$$L_{\pm}(x) \equiv \ln\left(\frac{|\pm ax + by + \chi^2|}{|\pm ax - by + \chi^2|}\right), \tag{G.12}$$

so that $R_1 = -(L_+ + L_-)$, $R_2 = -(L_+ + L_-)/2$. Taking derivatives, dividing out the resulting polynomials, and adding the $\pm$ contributions leads to

$$\frac{x_F}{12b}[(x_F^2 + 3\chi^2)R_1(x_F) + 6ax_F R_2(x_F)] + \frac{1}{6}\left[x_F y_F + \left(3 - 4b^2\right)\ln(x_F + y_F)\right] + Z_B, \tag{G.13}$$

for (3.5) and

$$\frac{x_F}{8b}(1 + 2\chi^2)R_1(x_F) + \frac{1}{2}\left(1 + 2\chi^2\right)\ln(x_F + y_F) + Z_D, \tag{G.14}$$

for (3.6), with Z_B and Z_D defined and calculated in section below

Definition and calculation of Z_B and Z_D

The explicit expressions of $Z_{B,D}$ are

$$Z_{B,D} = C_{B,D}\int_1^{x_F}\frac{dx}{\sqrt{x^2-1}}\frac{M_{B,D}\,x^2 + N_{B,D}}{(x^2+\zeta^2)^2 - 4a^2x^2}, \tag{G.15}$$

where $\zeta^2 \equiv a^2 - \eta^2 b^2$, $C_B = 1/3$ and $C_D = (1 + 2\chi^2)/2$. The expressions for $M_{B,D}$ and $N_{B,D}$ depend solely on a and b,

$$M_B = -2a^2(1 + 4b^2) - [1 - 2b^2 - 2a^2(2 - \eta^2)]\zeta^2,$$
$$N_B = -\zeta^4(1 - 2b^2),$$
$$M_D = 2a^2(1 + \eta^2) - \zeta^2,$$
$$N_D = -\zeta^4.$$

Defining $t = \sqrt{(x^2-1)/x^2} = y/x$, (G.15) reduces to

$$Z_{B,D} = C_{B,D}[(M_{B,D} + N_{B,D})\mathfrak{I}_0 - N_{B,D}\mathfrak{I}_2], \tag{G.16}$$

where $\mathfrak{I}_j$ is

$$\mathfrak{I}_j = \int_0^{t_F}\frac{dt\,t^j}{\mathfrak{C}t^4 + \mathfrak{B}t^2 + \mathfrak{A}}, \tag{G.17}$$

and the coefficients are $\mathfrak{C} = \zeta^4$, $\mathfrak{B} = -2[\zeta^2(\zeta^2+1) - 2a^2]$, and $\mathfrak{A} = (\zeta^2+1)^2 - 4a^2$. There are two cases to be considered, depending on the roots of the biquadratic equation $\mathfrak{C}t^4 + \mathfrak{B}t^2 + \mathfrak{A} = 0$:

(i) For $\eta^2 > 0$, the roots are real

$$t_\pm^2 = \frac{\zeta^2(\zeta^2+1) - 2a^2 \pm 2ab|\eta|}{\zeta^4}, \tag{G.18}$$

so that the integrals become

$$\mathfrak{I}_j = \frac{1}{4ab|\eta|}\left[t_+^j \int_0^{t_F} \frac{dt}{t^2 - t_+^2} - t_-^j \int_0^{t_F} \frac{dt}{t^2 - t_-^2} \right]. \tag{G.19}$$

One may show that $t_\pm^2 > 0$, therefore

$$\int_0^{t_F} \frac{dt}{t^2 - t_\pm^2} = \frac{1}{2t_\pm} \ln\left| \frac{t_F - t_\pm}{t_F + t_\pm} \right|, \tag{G.20}$$

where, from (G.18), we may write $t_\pm = (y_\pm/|x_\pm|)$, with $x_\pm = a \pm b\eta$ and $y_\pm = \sqrt{x_\pm^2 - 1}$. Then,

$$\mathfrak{I}_0 = \frac{1}{4ab|\eta|}\left[\frac{1}{2t_+} \ln\left| \frac{t_F - t_+}{t_F + t_+} \right| - (t_+ \to t_-) \right], \tag{G.21}$$

$$\mathfrak{I}_2 = \frac{1}{4ab|\eta|}\left[\frac{t_+}{2} \ln\left| \frac{t_F - t_+}{t_F + t_+} \right| - (t_+ \to t_-) \right]. \tag{G.22}$$

(ii) For $\eta^2 < 0$, the roots are complex conjugate $(t_c^2, \bar{t}_c^2)$, with

$$t_c^2 = \frac{[\zeta^2(\zeta^2+1) - 2a^2] + i[2ab|\eta|]}{\zeta^4}. \tag{G.23}$$

We may decompose into partial fractions to obtain $\mathfrak{I}_j = \mathfrak{I}_j^+ - \mathfrak{I}_j^-$ ($t_r \equiv \mathrm{Re}\, t_c$; $t_i \equiv \mathrm{Im}\, t_c$)

$$\mathfrak{I}_j^\pm = \frac{1}{4\zeta^4 t_r |t_c|^2} \int_0^{t_F} \left[\frac{dt\, t^j (t \pm 2t_r)}{t^2 \pm 2t_r t + |t_c|^2} \right], \tag{G.24}$$

and write

$$\begin{aligned} \mathfrak{I}_0 = \frac{1}{8\zeta^4 t_r |t_c|^2} \Bigg\{ \ln\left| \frac{t_F^2 + 2t_r t_F + |t_c|^2}{t_F^2 - 2t_r t_F + |t_c|^2} \right| + \\ \frac{2t_r}{|t_i|}[\arctan(\frac{t_F + t_r}{|t_i|}) + \arctan(\frac{t_F - t_r}{|t_i|})] \Bigg\}, \end{aligned} \tag{G.25}$$

as well as

$$\begin{aligned} \mathfrak{I}_2 = \frac{1}{8\zeta^4 t_r} \Bigg\{ -\ln\left| \frac{t_F^2 + 2t_r t_F + |t_c|^2}{t_F^2 - 2t_r t_F + |t_c|^2} \right| + \\ \frac{2t_r}{|t_i|}[\arctan(\frac{t_F + t_r}{|t_i|}) + \arctan(\frac{t_F - t_r}{|t_i|})] \Bigg\}, \end{aligned} \tag{G.26}$$

where, from (G.23), one may show that $t_c = (y_c/x_c)$, with $x_c = a + ib|\eta|$ and $y_c = \sqrt{x_c^2 - 1}$.

Appendix H

Polarization and magnetization vectors

Although the REG may be bianisotropic, since its polarization and magnetization depend on both $\vec{E}$ and $\vec{B}$ in eqs. (4.1) and (4.2), for the EM wave characteristic of the photonic mode this is NOT the case.

For the photonic mode, Maxwell's equations $q_i D_i = 0$ and $q_i B_i = 0$ lead to $E_L = B_L = 0$, where we have used $D_i = \epsilon_{ij} E_j + \tau_{ij} B_j$, with $\epsilon_{ij} = \epsilon \delta_{ij} + \epsilon' \hat{q}_i \hat{q}_j$, and the fact that $\epsilon_L = \epsilon + \epsilon' \neq 0$. From $\vec{q} \times \vec{H} = -\omega \vec{D}$, and using the constitutive relations of H_i and D_i, we derive

$$\hat{q} \times \vec{B}_T = -[(\epsilon + \tau)/(\nu - \tau)]\vec{E}_T. \tag{H.1}$$

Using the equations (4.26)-(4.28), we obtain

$$\epsilon + \tau = \nu - \tau = 1 + 2\mathscr{C}^* + \mathscr{A}^* - \mathscr{B}^*, \tag{H.2}$$

which yields

$$\hat{q} \times \vec{B}_T = -\vec{E}_T. \tag{H.3}$$

Eqs.(4.1) and (4.2), with $E_L = B_L = 0$ read

$$\vec{P} = (\epsilon - 1)\vec{E}_T - \tau(\hat{q} \times \vec{B}_T), \tag{H.4}$$

$$\vec{M} = (1 - \nu)\vec{B}_T + \tau(\hat{q} \times \vec{E}_T). \tag{H.5}$$

For the photonic mode, $\hat{q} \times \vec{B}_T = -\vec{E}_T$ and $\hat{q} \times \vec{E}_T = \vec{B}_T$, leading to

$$\vec{P} = (\epsilon - 1 + \tau)\vec{E}_T, \tag{H.6}$$

$$\vec{M} = (1 - \nu + \tau)\vec{B}_T. \tag{H.7}$$

Since $\vec{D} = \vec{E} + \vec{P}$ and $\vec{H} = \vec{B} - \vec{M}$, we end up with

$$\vec{D} = (\epsilon + \tau)\vec{E}_T, \tag{H.8}$$

$$\vec{H} = (\nu - \tau)\vec{B}_T. \tag{H.9}$$

Thus, for $|\vec{q}| = \omega$, the effective responses in (4.10) and (4.9) read $\epsilon_{\text{eff}} = \epsilon + \tau$, $\nu_{\text{eff}} = \nu - \tau$, and furthermore $\epsilon_{\text{eff}} = \nu_{\text{eff}}$. This leaves us with the usual expressions

$$\vec{D} = \epsilon_{\text{eff}}\vec{E}, \tag{H.10}$$

and

$$\vec{H} = \nu_{\text{eff}}\vec{B}. \tag{H.11}$$

Therefore, $\vec{P}$ and $\vec{D}$ lie along the direction of the electric field, whereas $\vec{M}$ and $\vec{H}$ lie along the direction of the magnetic field. Thus, the bianisotropy does not occur for an EM wave typical of the photonic mode, and we are justified in using this to calculate the reflection and transmission coefficients in section 4.5.

Appendix I

Current J_μ for relativistic Bose gas

The current density in linear response may be split in two parts

$$
\begin{aligned}
J_\mu(x) &= \frac{\delta}{\delta A_\mu(x)}\left\{\mathrm{Tr}\,(\Pi\bar{G}_0) - \frac{1}{2}\mathrm{Tr}\,(\Pi\bar{G}_0\Pi\bar{G}_0)\right\} \\
&= J_\mu^{(a)}(x) + J_\mu^{(b)}(x).
\end{aligned} \tag{I.1}
$$

Let us calculate each term explicitly.

I.1 Calculation of $J_\mu^{(a)}$

We have

$$
J_\mu^{(a)}(x) = \frac{\delta}{\delta A_\mu(x)}\int d^4y d^4z \underbrace{\langle y|\Pi|z\rangle}_{\langle y|z\rangle\Pi(z)}\underbrace{\langle z|\bar{G}_0|y\rangle}_{\bar{G}_0(z,y)}. \tag{I.2}
$$

Substituting $\Pi(z)$ defined in 5.8, and using the definition of the Dirac delta function,

$$
\begin{aligned}
J_\mu^{(a)}(x) &= \frac{\delta}{\delta A_\mu(x)}\int d^4y\, d^4z\, \delta^{(4)}(y-z)\left\{2ieA_\nu(z)\bar{\partial}_\nu^z + ie(\bar{\partial}\cdot A)_z\right\}\bar{G}_0(z,y) \\
&+ \frac{\delta}{\delta A_\mu(x)}\int d^4y\, d^4z\, \delta^{(4)}(y-z)e^2A^2(z)\bar{G}_0(z,y).
\end{aligned} \tag{I.3}
$$

Taking the functional derivative in $A_\mu(x)$, and integrating over d^4z, we obtain

$$
J_\mu^{(a)}(x) = \int d^4y\, \delta^{(4)}(y-z)\left\{2ie\bar{\partial}_\mu^x - ie\bar{\partial}_\mu^x\right\}\bar{G}_0(z,y) + 2e^2\int d^4y\, \delta^{(4)}(y-z)A_\mu(x)\bar{G}_0(x,y), \tag{I.4}
$$

therefore,

$$J_\mu^{(a)}(x) = \int d^4y\, \delta^{(4)}(y-x)\left\{ie\bar{\partial}_\mu^x \bar{G}_0(x,y)\right\} + 2e^2 A_\mu(x)\bar{G}_0(x,x). \tag{I.5}$$

In momentum space, the current density and the free boson propagator are written in Euclidean metric as

$$J_\mu^{(a)}(q) = \oint d^4x\, e^{-iq\cdot x} J_\mu(x), \tag{I.6}$$

$$\bar{G}_0(x,y) = \oint \frac{d^4p}{(2\pi)^4}\frac{e^{ip\cdot(x-y)}}{\bar{p}^2+m^2}, \tag{I.7}$$

with $\bar{p}_4 \equiv -i(\partial_4 - \xi)$. The current density $J_\mu^{(a)}(x)$ becomes

$$J_\mu^{(a)}(x) = -e\oint \frac{d^4p}{(2\pi)^4}\frac{\bar{p}_\mu}{\bar{p}^2+m^2} + 2e^2 A_\mu(x)\bar{G}_0(x,x). \tag{I.8}$$

The first term in (I.8) is the free current density in the gas, since it is a constant independent of the background field A_μ. The second term contributes to the total current density in first order in A_μ. We may write this term as

$$\left[J_\mu^{(a)}(x)\right]_{\text{ind}} = \oint \frac{d^4q}{(2\pi)^4} e^{iqx} \underbrace{A_\mu(q)(2e^2)\oint \frac{d^4p}{(2\pi)^4}\frac{1}{\bar{p}^2+m^2}}_{\left[J_\mu^{(a)}(q)\right]_{\text{ind}}}. \tag{I.9}$$

We have

$$\left[J_\mu^{(a)}(q)\right]_{\text{ind}} = \Pi_{\mu\nu}^{\text{tad}}(q)A_\mu(q). \tag{I.10}$$

We identify the tensor $\Pi_{\mu\nu}^{\text{tad}}$ as the contribution from the *tadpole* diagram in the current density

$$\Pi_{\mu\nu}^{\text{tad}}(q) = 2e^2\oint \frac{d^4p}{(2\pi)^4}\frac{\delta_{\mu\nu}}{\bar{p}^2+m^2}. \tag{I.11}$$

I.2 Calculation of $J_\mu^{(b)}$

The contribution $J_\mu^{(b)}$ to the induced current is

$$J_\mu^{(b)} = \frac{\delta}{\delta A_\mu(x)}\left\{-\frac{1}{2}\text{Tr}\,(\Pi\bar{G}_0\Pi\bar{G}_0)\right\}. \tag{I.12}$$

Computing the trace,

$$-\frac{1}{2}\text{Tr}\left(\Pi\bar{G}_0\Pi\bar{G}_0\right) = -\frac{1}{2}\int d^4x\, d^4y\, d^4z\, d^4w \langle x|\Pi|\rangle y \underbrace{\langle y|\bar{G}_0|\rangle z}_{\bar{G}_0(y,z)}\langle z|\Pi|\rangle w \underbrace{\langle w|\bar{G}_0|\rangle x}_{\bar{G}_0(w,x)}, \tag{I.13}$$

and substituting 5.8, we have

$$-\frac{1}{2}\mathrm{Tr}\left(\Pi\bar{G}_0\Pi\bar{G}_0\right) = -\frac{1}{2}\int d^4x\, d^4y\, d^4z\, d^4w \delta^{(4)}(x-y)\left\{2ieA\cdot\bar{\partial}^y + ie\left[\bar{\partial}\cdot A\right]_y + e^2A^2(y)\right\}\bar{G}_0(y,z)$$

$$\times \quad \delta^{(4)}(z-w)\left\{2ieA\cdot\bar{\partial}^w + ie\left[\bar{\partial}\cdot A\right]_w + e^2A^2(w)\right\}\bar{G}_0(w,x). \tag{I.14}$$

Keeping the second order terms in A_μ, and writing them in Fourier space,

$$-\frac{1}{2}\mathrm{Tr}\left(\Pi\bar{G}_0\Pi\bar{G}_0\right) = -\frac{1}{2}\int d^4x\, d^4y\, d^4z\, d^4w\, \delta^{(4)}(x-y)\delta^{(4)}(z-w)\left\{2ie\oint\frac{d^4q}{(2\pi)^4}A_\mu(q)e^{iqy}\right.$$

$$\times \quad \oint\frac{d^4p}{(2\pi)^4}\frac{i\bar{p}_\mu e^{ip(y-z)}}{\bar{p}^2+m^2} + ie\oint\frac{d^4q}{(2\pi)^4}iq_\mu A_\mu(q)e^{iqy}\oint\frac{d^4p}{(2\pi)^4}\left.\frac{e^{ip(y-z)}}{\bar{p}^2+m^2}\right\}$$

$$\times \quad \left\{2ie\oint\frac{d^4q'}{(2\pi)^4}A_\rho(q')e^{iq'w}\oint\frac{d^4p'}{(2\pi)^4}\frac{i\bar{p}_\rho e^{ip'(w-x)}}{\bar{p}'^2+m^2} + ie\oint\frac{d^4q'}{(2\pi)^4}iq'_\rho A_\rho(q')e^{iq'w}\oint\frac{d^4p'}{(2\pi)^4}\frac{e^{ip'(w-x)}}{\bar{p}'^2+m^2}\right\},$$

we obtain

$$-\frac{1}{2}\mathrm{Tr}\left(\Pi\bar{G}_0\Pi\bar{G}_0\right) = -\frac{e^2}{2}\oint\frac{d^4q}{(2\pi)^4}\frac{d^4p}{(2\pi)^4}\frac{d^4q'}{(2\pi)^4}\frac{d^4p'}{(2\pi)^4}(2\pi)^4\delta^{(4)}(q+p-p')(2\pi)^4\delta^{(4)}(-p+q'+p')$$

$$\times \quad \left[A_\mu(q)\frac{(2\bar{p}_\mu+q_\mu)}{\bar{p}^2+m^2}\frac{(2\bar{p}'_\rho+q'_\rho)}{\bar{p}'^2+m^2}A_\rho(q')\right]. \tag{I.15}$$

Integrating over d^4q' and d^4p',

$$-\frac{1}{2}\mathrm{Tr}\left(\Pi\bar{G}_0\Pi\bar{G}_0\right) = -\frac{e^2}{2}\oint\frac{d^4q}{(2\pi)^4}\frac{d^4p}{(2\pi)^4}A_\mu(q)\frac{(2\bar{p}_\mu+q_\mu)(2\bar{p}_\rho+q_\rho)}{(\bar{p}^2+m^2)([\bar{p}+q]^2+m^2)}A_\rho(-q)$$

$$= \frac{e^2}{2}\oint\frac{d^4q}{(2\pi)^4}A_\mu(q)\Pi^{\text{loop}}_{\mu\rho}A_\rho(-q), \tag{I.16}$$

where $\Pi^{\text{loop}}_{\mu\rho}$, is the 1-*loop* contribution to the polarization diagram in the medium, given by

$$\Pi^{\text{loop}}_{\mu\rho} = -e^2\oint\frac{d^4p}{(2\pi)^4}\frac{(2\bar{p}_\mu+q_\mu)(2\bar{p}_\rho+q_\rho)}{(\bar{p}^2+m^2)([\bar{p}+q]^2+m^2)}. \tag{I.17}$$

Therefore, for the current density, we write

$$\begin{aligned} J^{(b)}_\mu(x) &= \frac{\delta}{\delta A_\mu(x)}\left[\frac{1}{2}\oint d^4x\, d^4y\, A_\mu(x)\Pi^{\text{loop}}_{\mu\nu}(x-y)A_\nu(y)\right] \\ &= \oint d^4y\, \Pi^{\text{loop}}_{\mu\nu}(x-y)A_\nu(y) \\ &= \oint\frac{d^4q}{(2\pi)^4}\Pi^{\text{loop}}_{\mu\nu}(q)A_\nu(q). \end{aligned} \tag{I.18}$$

In momentum space, we have $J^{(b)}_\mu(q) = \Pi^{\text{loop}}_{\mu\nu}(q)A_\nu(q)$, and the total current density $J_\mu = J^{(a)}_\mu + J^{(b)}_\mu$ is

$$J_\mu(q) = \Pi_{\mu\nu}(q)A_\nu(q) \tag{I.19}$$

with $\Pi_{\mu\nu} = \Pi^{\text{tad}}_{\mu\nu} + \Pi^{\text{loop}}_{\mu\nu}$ being the full polarization tensor in the medium

$$\Pi_{\mu\nu}(q) = -2e^2 \oint \frac{d^4p}{(2\pi)^4}\frac{\delta_{\mu\nu}}{\bar{p}^2+m^2} + e^2 \oint \frac{d^4p}{(2\pi)^4}\frac{(2\bar{p}_\mu+q_\mu)(2\bar{p}_\nu+q_\nu)}{(\bar{p}^2+m^2)([\bar{p}+q]^2+m^2)}. \tag{I.20}$$

Appendix J

Derivation of $\langle J_\mu(x) J_\nu(y)\rangle$.

The expectation value $\langle J_\mu(x) J_\nu(y)\rangle$ is

$$\langle J_\mu(x) J_\nu(y)\rangle = \frac{1}{\Xi_0}\oint [d\phi^*][d\phi] J_\mu(x) J_\nu(y) e^{-S_0[\phi]}, \tag{J.1}$$

where $S_0[\phi] = \int_\Omega d^4z\, d^4z'\, \phi^*(z) G^{-1}(z-z')\phi(z')$, is the free scalar action, with $G^{-1} \equiv (-\partial^2 + m^2)$ the free scalar propagator, and $J_\mu = \phi^* i\partial_\mu\phi - \phi i\partial_\mu\phi^*$ the scalar current density. Here, Ξ_0 is the ideal gas grand partition function which acts as a normalization factor. To obtain the expectation value in (J.1), we may write Ξ in the presence of an external current, and take its functional derivatives

$$\Xi[j^*, j] = \oint [d\phi^*][d\phi] e^{-\int_\Omega d^4z [\phi^* G^{-1}\phi - j^*\phi - \phi j]}. \tag{J.2}$$

Writing $\mathscr{L}_j[\phi] = \phi'^* G^{-1}\phi' - j^* G j$, with $\phi' = \phi - Gj$ and $\phi'^* = \phi^* - j^* G$, then

$$\begin{aligned}\Xi[j^*, j] &= \left[\oint [d\phi^*][d\phi] e^{-\int_\Omega d^4x \phi'^* G^{-1}\phi'}\right] e^{\int_\Omega d^4z d^4z' j^*(z) G(z-z') j(z')} \\ &= \Xi_0 e^{\langle j^* G j\rangle}.\end{aligned} \tag{J.3}$$

Defining the normalized partition function $\Xi_N =\equiv \Xi[j^*, j]/\Xi_0$, and taking the functional derivatives

$$\left.\frac{\delta \Xi_N}{\delta j^*(x)}\right|_{j=0} = \langle\phi(x)\rangle, \quad \left.\frac{\delta \Xi_N}{\delta j(x)}\right|_{j=0} = \langle\phi^*(x)\rangle, \tag{J.4}$$

and the second functional derivative

$$\begin{aligned}\frac{\delta}{\delta j(x)}\left[i\partial_\mu \frac{\delta \Xi_N}{\delta j^*(x)}\right]_{j=0} &= \frac{1}{\Xi_0}\oint [d\phi *][d\phi] \phi^* i\partial_\mu \phi(x) e^{-S_0[\phi]} \\ &= \langle \phi^*(x) i\partial_\mu \phi(x)\rangle,\end{aligned} \tag{J.5}$$

one may obtain the expectation value $\langle J_\mu(x)\rangle = \langle \phi^*(x) i\partial_\mu \phi(x) - \phi(x) i\partial_\mu \phi^*(x)\rangle$ as

$$\langle J_\mu(x)\rangle = \left\{ \left[\frac{\delta}{\delta j(x)} \left(i\partial_\mu \frac{\delta}{\delta j^*(x)} \right) - \frac{\delta}{\delta j^*(x)} \left(i\partial_\mu \frac{\delta}{\delta j(x)} \right) \right] \Xi_N \right\}_{j=0}, \tag{J.6}$$

and the expectation value $\langle J_\mu(x)J_\nu(y)\rangle$

$$\begin{aligned} \langle J_\mu(x)J_\nu(y)\rangle &= \left\{ \left[\frac{\delta}{\delta j(x)} \left(i\partial^x_\mu \frac{\delta}{\delta j^*(x)} \right) - \frac{\delta}{\delta j^*(x)} \left(i\partial^x_\mu \frac{\delta}{\delta j(x)} \right) \right] \right. \\ &\times \left. \left[\frac{\delta}{\delta j(y)} \left(i\partial^y_\nu \frac{\delta}{\delta j^*(y)} \right) - \frac{\delta}{\delta j^*(y)} \left(i\partial^y_\nu \frac{\delta}{\delta j(y)} \right) \right] \Xi_N \right\}_{j=0}. \end{aligned} \tag{J.7}$$

Note that the expression above will have four functional derivative in j. Thus, when we take $j = 0$, only terms in Ξ_N with four currents j will contribute. Therefore, expanding Ξ_N

$$\Xi_N = 1 + \langle j^* G^{-1} J\rangle + \frac{1}{2!}\langle j^* G^{-1} J\rangle\langle j^* G^{-1} J\rangle + \dots \tag{J.8}$$

the term that will contribute to the expectation value in J.7 is

$$\Xi \equiv \Xi_N^{(4)} = \frac{1}{2!}\int d^4z_1 d^4z_2 d^4z_3 d^4z_4\, j^*(z_1)G(z_1 - z_2)j(z_2)j^*(z_3)G(z_3 - z_4)j(z_4). \tag{J.9}$$

Taking the functional derivative in J.7, we have $\langle J_\mu(x)J_\nu(y)\rangle = \Omega_1 + \Omega_2 + \Omega_3 + \Omega_4$, where

$$\begin{aligned} \Omega_1 &= \left\{ \left[\frac{\delta}{\delta j(x)} \left(i\partial^x_\mu \frac{\delta}{\delta j^*(x)} \right) \frac{\delta}{\delta j(y)} \left(i\partial^y_\nu \frac{\delta}{\delta j^*(y)} \right) \right] \Xi_N^{(4)} \right\}_{j=0} \\ &= i\partial^x_\mu G(x - x^+) i\partial^y_\nu G(y - y^+) + i\partial^x_\mu G(x - y) i\partial^y_\nu G(y - x). \end{aligned} \tag{J.10}$$

$$\begin{aligned} \Omega_2 &= \left\{ -\left[\frac{\delta}{\delta j^*(x)} \left(i\partial^x_\mu \frac{\delta}{\delta j(x)} \right) \frac{\delta}{\delta j(y)} \left(i\partial^y_\nu \frac{\delta}{\delta j^*(y)} \right) \right] \Xi_N^{(4)} \right\}_{j=0} \\ &= -i\partial^x_\mu G(x^+ - x) i\partial^y_\nu G(y - y^+) - G(x - y) i\partial^x_\mu i\partial^y_\nu G(y - x). \end{aligned} \tag{J.11}$$

The term Ω_3 is obtained from Ω_2 by taking $x \to y$, and $\mu \to \nu$

$$\Omega_3 = -i\partial^y_\nu G(y^+ - y) i\partial^x_\mu G(x - x^+) - G(y - x) i\partial^y_\nu i\partial^x_\mu G(x - y). \tag{J.12}$$

Since $G(y - x) = G(x - y)$, and $i\partial^x_\mu G(x - x^+) = -i\partial^x_\mu G(x^+ - x)$, we have $\Omega_3 = \Omega_2$. The term Ω_4 is the complex conjugate of Ω_1, which is real, thus $\Omega_1 = \Omega_3$, and

$$\langle J_\mu(x)J_\nu(y)\rangle = 4\left[i\partial^x_\mu G(x - x^+) i\partial^y_\nu G(y - y^+) + \frac{1}{2} i\partial^x_\mu G(x - y) i\partial^y_\nu G(y - x) - \frac{1}{2} G(x - y) i\partial^x_\mu i\partial^y_\nu G(y - x) \right]. \tag{J.13}$$

The propagator is

$$G(x-y) = \oint \frac{d^4p}{(2\pi)^4}\frac{e^{ip(x-y)}}{p^2+m^2}, \tag{J.14}$$

and

$$\langle J_\mu(k)J_\nu(k')\rangle = \int_\Omega d^4x d^4y e^{-ikx}e^{-iky}\langle J_\mu(x)J_\nu(y)\rangle. \tag{J.15}$$

Substituting (J.13), we obtain

$$\begin{aligned}\langle J_\mu(k)J_\nu(k')\rangle &= 4\Big\{(2\pi)^8\delta^{(4)}(k)\delta^{(4)}(k')\left[\oint \frac{d^4p}{(2\pi^4)}\frac{(-p_\mu)}{p^2+m^2}\right]\left[\oint \frac{d^4p}{(2\pi^4)}\frac{(-p'_\nu)}{p'^2+m^2}\right]\Big\} \\ &+ \frac{1}{4}(2\pi)^4\delta(k+k')\oint \frac{d^4p}{(2\pi)^4}\frac{(2p-k)_\mu(2p-k)_\nu}{(p^2+m^2)[(p-k)^2+m^2)]}.\end{aligned} \tag{J.16}$$

Note that,

$$\langle J_\mu(x)\rangle = \frac{\delta}{\delta j(x)}\left[i\partial_\mu \frac{\delta \Xi_N}{\delta j^*(x)}\right]. \tag{J.17}$$

Here, only terms with two factors of the current in $\Xi_N = \Xi_N^{(2)} = \langle j^* G^{-1} j\rangle\langle j^* G^{-1} j\rangle$ will contribute. We have

$$\langle J_\mu(x)\rangle = 2i\partial_\mu^x G(x-x^+) = 2\oint \frac{d^4p}{(2\pi)^4}\frac{(-p_\mu)}{p^2+m^2}. \tag{J.18}$$

So, eq. (J.13) may be written as

$$\langle J_\mu(k)J_\nu(k')\rangle = (2\pi)^8\delta^{(4)}(k)\delta^{(4)}(k')\langle J_\mu(x)\rangle\langle J_\nu(y)\rangle + \langle J_\mu(k)J_\nu(k')\rangle_c, \tag{J.19}$$

where the subscript "c" means *connected*. Taking the Fourier transform to compute $\langle J_\mu(x)J_\nu(y)\rangle$, then

$$\langle J_\mu(x)J_\nu(y)\rangle = \oint \frac{d^4k}{(2\pi)^4}\frac{d^4k'}{(2\pi)^4}e^{ikx}e^{ik'y}\langle J_\mu(k)J_\nu(k')\rangle. \tag{J.20}$$

Substituting (J.19), we obtain $\langle J_\mu(x)J_\nu(y)\rangle = \langle J_\mu(x)\rangle\langle J_\nu(y)\rangle + \langle J_\mu(x)J_\nu(y)\rangle_c$, where

$$\langle J_\mu(x)J_\nu(y)\rangle_c = \oint \frac{d^4k}{(2\pi)^4}e^{ik(x-y)}\mathscr{I}_{\mu\nu}, \tag{J.21}$$

with

$$\mathscr{I}_{\mu\nu} = \oint \frac{d^4p}{(2\pi)^4}\frac{(2p+k)_\mu(2p+k)_\nu}{(p^2-m^2)[(p+k)^2+m^2]}. \tag{J.22}$$

We may use the previous results to compute the grand partition function in first order

$$\frac{\Xi}{\Xi_0} = 1 + \frac{e^2}{2}\int_\Omega d^4x d^4y \langle J_\mu(x)J_\nu(y)\rangle G^\gamma_{\mu\nu}(x-y). \tag{J.23}$$

We derive

$$\frac{\Xi}{\Xi_0} = 1 + \frac{e^2}{2}\int_\Omega d^4x d^4y \langle J_\mu(x)\rangle G^\gamma_{\mu\nu}(x-y)\langle J_\nu(y)\rangle + \frac{e^2}{2} V \oint \frac{d^4q}{(2\pi)^4}\frac{\mathscr{J}_{\mu\mu}(q)}{q^2}. \tag{J.24}$$

We have obtained two contributions to the current-current expectation value: a disconnected $\langle J_\mu(x)\rangle\langle J_\nu(y)\rangle$; and a connected $\langle J_\mu(x) J_\nu(x)\rangle$ term. However, in the grand partition function Ξ, the disconnected part will vanish in the thermodynamic limit, since it will give a $(\ln V/V)$ contribution to the pressure. Besides, it does not contribute to the density either, since it is independent of the chemical potential μ.

The finite T free photon propagator, for $r = |\vec{x} - \vec{y}|$, $r_4 = |x_4 - y_4|$, is

$$G(r, r_4) = \frac{T}{8\pi r}\frac{\sinh(2\pi T r)}{\sin^2(\pi T r_4) + \sinh^2(\pi T r)}, \tag{J.25}$$

using this result in the disconnected term, we obtain $\sim Q^2/RT$, $V = \frac{4\pi}{3}R^2$, with $Q = \Delta N$. Note that, at $T = 0$, the expression for the propagator properly reduces to $G(x-y) = 1/4\pi^2(x-y)^2$.